Electrocatalytic CO2 reduction toward liquid fuels : on heterogeneous electrocatalysts and heterogenized molecular catalysts

Birdja, Y.Y.

Electrocatalytic CO_2 Reduction toward Liquid Fuels

On heterogeneous electrocatalysts and heterogenized molecular catalysts

Proefschrift

ter verkrijging van
de graad van Doctor aan de Universiteit Leiden,
op gezag van Rector Magnificus prof. mr. C. J. J. M. Stolker
volgens besluit van het College voor Promoties
te verdedigen op donderdag 19 april 2018
klokke 13:45 uur

door

Yuvraj Yashvant Birdja

geboren te Voorburg in 1988

Promotiecommissie

Promotor: Prof. dr. M. T. M. Koper

Co-promotor: Dr. D. G. H. Hetterscheid

Overige leden: Prof. dr. E. Bouwman (Leiden University)
Prof. dr. G. Mul (University of Twente)
Prof. dr. H. S. Overkleeft (Leiden University)
Prof. dr. M. Robert (Université Paris Diderot)

ISBN 978-94-6182-880-4

Printed by Off Page with financial support of Shimadzu Corporation

Voor mijn ouders en tweelingzus

Voor Sangeeta

Contents

List of Abbreviations

BDD	-	Boron Doped Diamond
CE	-	Counter Electrode
CHE	-	Computational Hydrogen Electrode
CN	-	Coordination number
CO_2RR	-	Electrochemical Carbon Dioxide reduction reaction
CoPP	-	Cobalt protoporphyrin IX
CPET	-	Concerted proton-electron transfer
CrPP	-	Chromium protoporphyrin IX
CuPP	-	Copper protoporphyrin IX
CV	-	Cyclic Voltammetry / Cyclic Voltammogram
DDAB	-	Didodecyldimethylammonium bromide
DFT	-	Density Functional Theory
ET	-	Electron transfer
FE	-	Faradaic Efficiency
FePP	-	Iron protoporphyrin IX
GaPP	-	Gallium protoporphyrin IX
GC	-	Glassy Carbon
GHG	-	Greenhouse gas
HER	-	Hydrogen evolution reaction
HPLC	-	High Performance Liquid Chromatography
InPP	-	Indium protoporphyrin IX
j	-	Current density
j_x	-	Partial current density for x
MnPP	-	Manganese protoporphyrin IX
MPP	-	Metalloprotoporphyrin

NHE	-	Normal Hydrogen Electrode
NiPP	-	Nickel protoporphyrin IX
OD	-	Oxide-derived
OHP	-	Outer Helmholtz plane
OLEMS	-	Online Electrochemical Mass Spectrometry
P4VP	-	Poly(4-vinylpyridine)
PCET	-	Proton coupled electron transfer
PdPP	-	Palladium protoporphyrin IX
PEDOT:PSS	-	Poly(3,4-ethylenedioxythiophene) polystyrene sulfonate
PG	-	Pyrolytic Graphite
PP	-	Protoporphyrin
PT	-	Proton transfer
RE	-	Reference Electrode
RHE	-	Reversible Hydrogen Electrode
RhPP	-	Rhodium protoporphyrin IX
SnPP	-	Tin protoporphyrin IX
WE	-	Working Electrode
XPS	-	X-ray photoelectron spectroscopy
XRD	-	X-ray diffractometry

CHAPTER 1

General Introduction

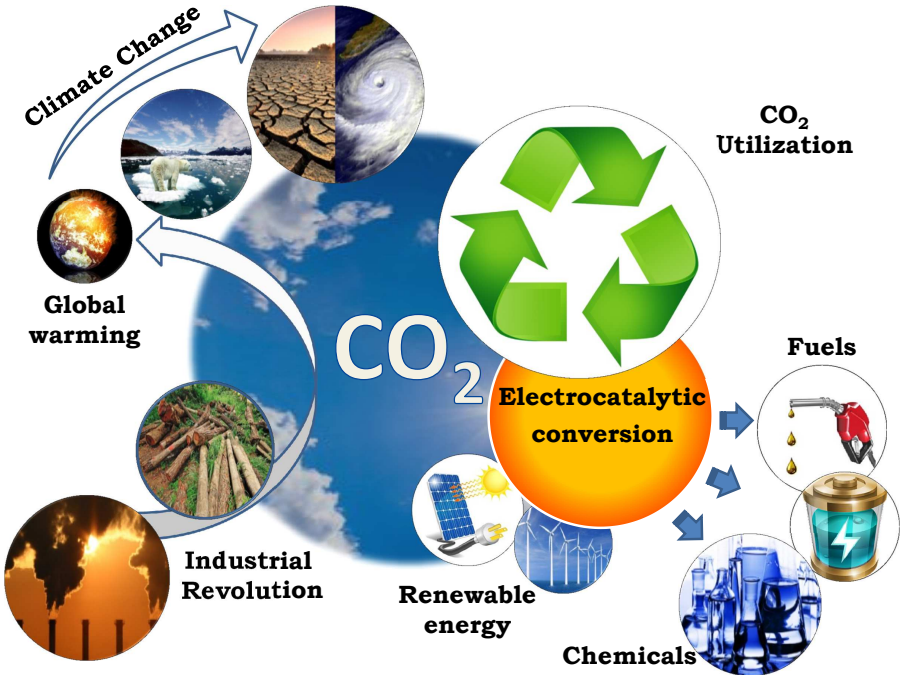

1.1 The *status quo* of the global carbon cycle

The earth is the only planet known to date that can sustain life. The ability to make life possible, is related to the composition of the Earth's atmosphere, which enables a relatively constant temperature. The gases responsible for maintaining this temperature are the so-called greenhouse gases (e.g. water vapor, carbon dioxide, methane and nitrous oxide). The concentration of greenhouse gases (GHGs) are influenced by the interplay of (a)biotic processes on Earth, which are represented by global biogeochemical cycles of the related elements. The scope of this thesis is associated with the carbon cycle (Figure 1.1), which consists of smaller cycles with different time scales, wherein carbon is exchanged between the atmosphere, lithosphere, hydrosphere and biosphere by several processes of which photosynthesis is the most important natural process for living organisms.[1]

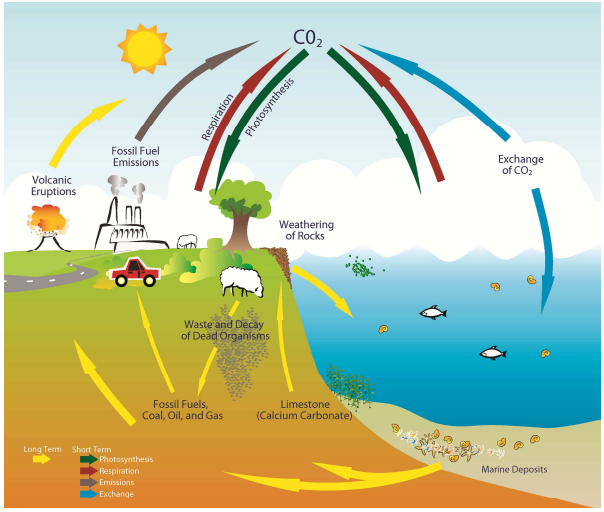

Figure 1.1 Schematic representation of the carbon cycle.[2]

Starting from the Industrial Era around 1750, the carbon cycle has been perturbed significantly by human activities such as fossil fuel combustion, industrial processes and deforestation, leading to substantial emission of CO_2 in the atmosphere. Atmospheric CO_2 levels have increased from 278 ppm to 390.5 ppm in the timespan of 1750 - 2011, with an alarming rate of 2.0 $\pm$ 0.1 ppm/year during 2002 - 2011.[3] To reach the target set by *The International Energy Agency* of $<$ 2° rise in global temperature by 2050, CO_2 emissions should be reduced by at least 50 % compared to 2011.[4] Other factors such as the higher energy demand of mankind and their fossil fuel dependence, the economic growth and the increase in world population indirectly contribute to this anthropogenic CO_2 accumulation in the atmosphere. Consequences of these influences to the carbon cycle are: global

warming, climate change, acidification of oceans, increased seawater levels, etc.[5] Climate change is even envisaged to be one of the most challenging problems of the 21^{st} century.[6] Not entirely coincidental, at the time of writing this section, the record of warmest October day in the Netherlands since the start of the temperature measurements in 1901, has been broken.[7]

1.2 Anthropogenic CO_2 emissions; *quo vadis?*

Over the past few decades, much attention has been given to the mitigation of GHG emissions, and various political policies have covered these topics, aimed at reducing climate change (e.g. Montreal protocol, Kyoto protocol, Copenhagen Accord, Paris agreement).[8] Several strategies have been proposed to remove CO_2 from the atmosphere, or to alleviate anthropogenic CO_2 emissions.

Utilization of CO_2 is preferred above carbon storage methods, since CO_2 can be used as sustainable feedstock for other processes, which simultaneously addresses important issues such as the sustainable energy production, increasing world population, food production, etc.[9,10] CO_2 utilization can be carried out without CO_2 conversion such as in enhanced oil recovery applications, or with conversion of CO_2 by means of thermal, chemical, biological, electrochemical, and photochemical methods.[6,11,12]

In order to curb the CO_2 emissions, decarbonization of the energy system is required. Furthermore, the electricity sector is projected to undergo a transition toward renewable sources, where solar power is likely to become the dominant energy source by 2050.[4] Several researchers proposed solar energy utilization as a key route to meet the targets for 2050 regarding anthropogenic CO_2 mitigation and climate change.[6,13] In a process similar to photosynthesis, we are able to use sunlight and a catalyst to store solar energy in chemical bonds. In this respect, the electrochemical conversion of CO_2 is very attractive for the production of so-called "solar fuels". In this thesis we elaborate on the electrochemical CO_2 conversion toward "electrofuels", which is the broader term used when electricity from different renewable sources are stored in chemical bonds. This process has been shown to be very promising as its effects are multi-fold, *viz.* reduction of CO_2 emissions, production of commodity chemicals, and storage of renewable energy in fuels, which is important due to the intermittent character of renewable energy sources (e.g. solar- and wind energy).[14]

1.3 Electrocatalytic conversion of Carbon Dioxide toward Electrofuels

Carbon dioxide is the most stable form of carbon, and therefore abundantly present in the atmosphere. Conversion of CO_2 is an endothermic process, and a catalyst is needed to obtain reasonable rates of conversion. Electrocatalytic conversion

of CO_2 and electrocatalysis in general have several advantages: we are able to control the reaction by the applied potential, use water as proton donor, and work under ambient conditions.[15] Bottlenecks are the high overpotentials, the broad product spectrum, and competitive hydrogen evolution (in aqueous media), which are thoroughly discussed and reviewed by many researchers in the field.[6,14,16,17] An extended discussion about the recent advances and challenges in the electrocatalytic reduction of CO_2 is given in chapter 2.

Depending on the electrocatalyst, different products can be formed, which leads to a selectivity issue.[16,18,19] Several electrofuels have been discussed in the past for a sustainable society (e.g. the hydrogen economy and methanol economy).[20–22] Although many of the products from CO_2 reduction can be used for further processing, from a renewable energy perspective, the formation of liquid products is preferred, since the existing energy infrastructure is based on liquid fuels. Additionally, liquid products such as formic acid, methanol and ethanol can be employed directly in fuel cells.

Except for formic acid, the formation of liquid products which are higher electron transfer products from electrocatalytic CO_2 reduction, is generally more complex compared to the production of 2-electron transfer products, and the electrocatalyst is more difficult to optimize.[23] We still lack significant mechanistic insight in these electrochemical processes in order to improve the electrocatalytic CO_2 reduction performance. These are the main reasons for the increasing research activity on the topic of electrocatalytic CO_2 reduction toward liquid products, to which the work described in this thesis is devoted.

1.4 Outline of this thesis

The focus throughout this thesis will be on the electrocatalytic reduction of carbon dioxide in aqueous media toward liquid products. The thesis can be divided in two parts. The first part (chapters 2 and 3) is about heterogeneous electrocatalysis of CO_2 reduction, and the second part (chapters 4 - 7) concerns electroreduction of CO_2 on heterogenized molecular catalysts.

In chapter 2, we review the recent advances and challenges in the field of electrocatalytic CO_2 reduction mainly on heterogeneous catalysts. Important topics will be highlighted and discussed such as initial activation of CO_2, the influence of reaction- and process conditions, the electrode morphology, and carbon-carbon bond formation. Moreover, we will discuss two important techniques often used in CO_2 electroreduction research: in situ spectroelectrochemical techniques and computational approaches for CO_2 reduction. This chapter will be concluded with our perspectives for future research of electrochemical CO_2 reduction.

Chapter 3 presents the crucial importance of the effect of local pH changes during CO_2 reduction on the product distribution. We demonstrate the involvement of disproportionation reactions leading to product distributions which should be distinguished from direct CO_2 reduction. These reactions are promoted by the

local pH (changes) during CO_2 reduction, as a result of the simultaneous hydrogen evolution reaction. The importance of this phenomenon is illustrated by generalizing to other reactants and to different electrode materials.

The remaining chapters are related to molecular catalysts, which we introduce with a brief review into the field of molecular catalysis of CO_2 reduction in chapter 4. Moreover, we give an overview of catalysts and recent developments related to heterogenized (molecular) catalysts, with special attention to metalloporphyrins, which are the catalysts under study in the remainder of this thesis.

In chapter 5, we report on the influence of the metal center of immobilized metalloprotoporphyrins on the electrocatalytic CO_2 reduction toward formic acid. We show that rhodium, tin, and indium metal centers are active for formic acid production in the order Rh < Sn < In. We discuss the coupling with the hydrogen evolution reaction, which plays an important role for the selectivity toward formic acid. Additionally, we demonstrate that the faradaic efficiency toward formic acid is strongly dependent on the bulk pH of the electrolyte and applied potential.

In chapter 6, we build upon the findings obtained in the previous chapter, by studying the immobilized indium(III) protoporphyrin for CO_2 electroreduction toward formic acid in more detail. We show the significant influence of the nature of the substrate on the selectivity, reactivity, and stability of CO_2 reduction toward formic acid. Moreover, we study the influence of the surface chemical functionality, and catalyst's chemical environment by respectively electrochemical and plasma treatment of the substrate, and by immobilization of the indium(III) protoporphyrin in polymer membranes. The findings in this work allow for design and optimization of heterogenized molecular systems for CO_2 electroreduction beyond empirical considerations.

We continue with the investigation of immobilized indium protoporphyrin catalyst in chapter 7. Herein we optimize CO_2 reduction performance by modification of the electrolyte composition. We demonstrate the impact of the electrolyte and the buffer strength on the selectivity and activity of CO_2 reduction. Moreover, we discuss factors affecting the stability of the system.

1.5 References

[1] National Research Council of The National Academies, *Ocean Acidification. Starting with the Science*, National Academies Press, Washington DC, **2013**.

[2] National Research Council of The National Academies, *Ocean Acidification. Starting with the Science,* **2013**, accessed: 13-10-2017, `http://dels.nas.edu/Materials/Special-Products/Carbon-Cycle-Image`.

[3] P. Ciais, C. Sabine, G. Bala, L. Bopp, V. Brovkin, J. Canadell, A. Chhabra, R. DeFries, J. Galloway, M. Heimann, C. Jones, C. L. Quéré, R. Myneni, S. Piao, P. Thornton in *Climate Change 2013: The Physical Science Basis. Contribution of Working Group I to the Fifth Assessment Report of the*

Intergovernmental Panel on Climate Change, (Eds.: T. F. Stocker, D. Qin, G.-K. Plattner, M. Tignor, S. Allen, J. Boschung, A. Nauels, Y. Xia, V. Bex, P. Midgley), Cambridge University Press, Cambridge, United Kingdom and New York, NY, USA, **2013**, Chapter 6: Carbon and Other Biogeochemical Cycles, pp. 465–570.

[4] International Energy Agency, *Energy Technology Perspectives 2014*, International Energy Agency, Paris Cedex, France, **2014**.

[5] IPCC in *Climate Change 2014: Synthesis Report. Contribution of Working Groups I, II and III to the Fifth Assessment Report of the Intergovernmental Panel on Climate Change*, (Eds.: Core Writing Team, R. K. Pachauri, L. A. Meyer), IPCC, Geneva, Switzerland, **2014**, 151 pp.

[6] E. V. Kondratenko, G. Mul, J. Baltrusaitis, G. O. Larrazábal, J. Pérez-Ramírez, *Energy Environ. Sci.* **2013**, *6*, 3112–3135.

[7] Weerplaza, *Warmste 16 oktober,* **Oct. 2017**, accessed: 17-10-2017, `https://www.weerplaza.nl/weerinhetnieuws/warmste-16-oktober/3669/`.

[8] United Nations Framework Convention on Climate Change, *Publications,* **Oct. 2017**, accessed: 13-10-2017, `http://newsroom.unfccc.int`.

[9] R. Lal, *Energy Environ. Sci.* **2008**, *1*, 86–100.

[10] A. A. Olajire, *J. CO_2 Utilization* **2013**, *3-4*, 74–92.

[11] B. Hu, C. Guild, S. L. Suib, *J. CO_2 Utilization* **2013**, *1*, 18–27.

[12] E. Alper, O. Y. Orhan, *Petroleum* **2017**, *3*, 109–126.

[13] N. S. Lewis, D. G. Nocera, *Proc. Natl. Acad. Sci.* **2006**, *103*, 15729–15735.

[14] D. T. Whipple, P. J. A. Kenis, *J. Phys. Chem. Lett.* **2010**, *1*, 3451–3458.

[15] D. A. Tryk, A. Fujishima, *The Electrochemical Society INTERFACE* **2011**, *10*, 32–36.

[16] J. Qiao, Y. Liu, F. Hong, J. Zhang, *Chem. Soc. Rev.* **2014**, *43*, 631–675.

[17] Q. Lu, F. Jiao, *Nano Energy* **2016**, *29*, 439–456.

[18] Y. Hori, *In Modern Aspects of Electrochemistry Vol. 42*, Springer, New York, **2008**.

[19] B. Kumar, J. P. Brian, V. Atla, S. Kumari, K. A. Bertram, R. T. White, J. M. Spurgeon, *Catal. Today* **2016**, *270*, 19–30.

[20] J. O. Bockris, *Science* **1972**, *176*, 1323–1323.

[21] G. A. Olah, *Angew. Chem. Int. Ed.* **2005**, *44*, 2636–2639.

[22] G. A. Olah, A. Goeppert, G. K. S. Prakash, *Beyond Oil and Gas: The Methanol Economy*, Wiley-VCH: Weinheim, Weinheim, Germany, **2006**.

[23] M. T. M. Koper, *J. Electroanal. Chem.* **2011**, *660*, 254–260.

CHAPTER 2

Advances and Challenges in the Electrocatalytic conversion of Carbon Dioxide to Fuels

This chapter is based on the article:
Yuvraj Y. Birdja, Elena Pérez-Gallent, Marta C. Figueiredo, Adrien J. Göttle, Federico Calle-Vallejo and Marc T. M. Koper, Nat. Energy, in preparation

Abstract

In this chapter, we critically review recent advances and relevant hurdles in the field of electrochemical CO_2 reduction. We start the discussion with the initial activation of CO_2 on the electrocatalyst, and its importance for the selectivity. Another mechanistic subject covered by this review, is the carbon-carbon bond formation from a mechanistic point of view. Additionally we discuss process- and reaction conditions, electrode mesoscale morphology, mass transport, and their influence on the electrocatalytic CO_2 reduction. Lastly, we discuss progress in two methodologies often used in CO_2 reduction research: in situ spectroscopic techniques and computational techniques.

2.1 Introduction

With the growing importance and falling prices of renewable electricity, the issue of electricity storage to deal with the intermittent nature of renewable energy sources is becoming urgent. The idea of storing renewable electricity into chemical bonds ("electrofuels") is particularly attractive, as it allows for high energy density and potentially high flexibility. While hydrogen is the most likely and realistic candidate for electricity storage in electrofuels, research into the electrochemical conversion of carbon dioxide and water into carbon-based fuels has intrigued electrochemists for many decades, and is currently undergoing a significant renaissance.[1–4] In contrast to hydrogen production by water electrolysis, carbon dioxide electrolysis is still far from a mature technology. Significant hurdles regarding energy efficiency, reaction selectivity and overall conversion rate will need to be overcome if electrochemical carbon dioxide reduction is to become a viable option for storing (a part of) renewable electricity.

Several electrocatalysts have been reported for the production of different products from the electrocatalytic carbon dioxide reduction reaction (CO_2RR). Table 2.1 gives a selective overview of some of the most active and selective metal or metal-derived electrocatalysts towards specific products in aqueous media. The two-electron transfer products, CO and HCOOH, can be produced with low overpotential and high Faradaic efficiency (FE) on suitable electrocatalysts, but substantially higher overpotentials and lower selectivities are observed to multi-electron transfer products such as methane, ethylene and alcohols. For the ultimate goal of a high performance CO_2-electrolyzer in which CO_2 is being reduced to an electrofuel, only CO and HCOOH are currently potentially economically viable options to compete with the current (non-electrochemical) production processes.[2]

There is no lack of reviews on the electrochemical reduction of CO_2; our own group has recently published an overview of the mechanistic aspects of CO_2RR electrocatalysts.[5] The aim of this short review is not to be exhaustive, but rather to critically discuss some recent advances and pertinent challenges in this field, focusing on a few themes that have witnessed important progress in the recent literature.[2,3,5,6] We have selected two mechanistic aspects to discuss. The initial activation of CO_2 on the electrocatalyst is key in determining the selectivity towards the first product, i.e. CO vs. $HCOOH/HCOO^-$. Carbon-carbon bond formation is another mechanistic theme in CO_2RR which has received ample recent attention, especially on copper electrodes. It has also become increasingly clear from recent work that process and reaction conditions influence the CO_2RR significantly. While traditionally catalytic studies emphasize catalyst properties, CO_2RR activity and selectivity are very sensitive to electrolyte properties such as pH, cations, anions and solvent, as well as to mass transport conditions. Electrode morphology, especially on the mesoscale, is another topical theme in CO_2RR. Besides the themes mentioned, we will also discuss progress in two important methodologies, which are often used

to increase fundamental understanding of CO_2RR: in situ spectroscopic techniques and computational techniques.

Table 2.1 Some state-of-the-art electrocatalysts for specific CO_2RR products

CO_2RR product	**Electrocatalyst**	**FE (%)**	**η (V)***	**j_{total} (mA cm^{-2})**	**Electrolyte (CO_2 sat.)**	**Ref.**
HCOOH	Pb	99.4	-1.19 V	5.0	0.1 M $KHCO_3$ $^{\nabla}$	[7]
	Sn	88.4	-1.04 V	5.0	0.1 M $KHCO_3$ $^{\nabla}$	[7]
	$Pd_{nanopart.}$\C	99	-0.15 V	2.4-7	2.8 M $KHCO_3$ $^{\perp}$	[8]
	$Pd_{70}Pt_{30,nanopart.}$\C	90	-0.36 V	4-7.5	0.2 M PO_4^{3-} buffer†	[9]
CO	Au	87.1	-0.64 V	5.0	0.1 M $KHCO_3$ $^{\nabla}$	[7]
	$Au_{nanopart.}$	97	-0.58 V	3.49±0.61	0.1 M $KHCO_3$ $^{\nabla}$	[10]
	OD-$Au_{nanopart.}$	>96	-0.25 V	2-4	0.5 M $NaHCO_3$ $^{\diamond}$	[11]
	Ag	94	-0.99 V	≈5.0	0.1 M $KHCO_3$ $^{\nabla}$	[12]
CH_4	Cu poly	40.4	-1.34 V	≈7	0.1 M $KHCO_3$ $^{\nabla}$	[13]
	Cu(210)	64	-1.29 V	5	0.1 M $KHCO_3$ $^{\nabla}$	[14]
C_2H_4	Cu poly	26.0	-1.13 V	1-2	0.1 M $KHCO_3$ $^{\nabla}$	[13]
	Cu (*O_2 plasma tr.*)	60	-0.98 V	≈15	0.1 M $KHCO_3$ $^{\nabla}$	[15]
	Cu-halide	60.5-79.5	-2.11 V	46.1-39.2	3 M KBr $^{\angle}$	[16]
CH_3OH	Cu_2O	38	-0.34 V	1-2	0.5 M $KHCO_3$ ‡	[17]
	HCl-pretreated Mo	84	-0.33 V	0.12	0.2 M Na_2SO_4 $^{\top}$	[18]
C_2H_5OH	Cu poly	9.8	-1.14 V	≈0.6	0.1 M $KHCO_3$ $^{\nabla}$	[13]
	Cu_2O	9-16	-1.08 V	30-35	0.1 M $KHCO_3$ $^{\nabla}$	[19]
	$CuO_{nanopart.}$	36.1	N/A^{+}	≈11.7	0.2 M KI	[20]
	Cu/CNS	63	-1.29 V	2	0.1 M $KHCO_3$ $^{\nabla}$	[21]

* E_0 vs. RHE from reference [5]; $^{\nabla}$ pH ≈ 6.8; $^{\perp}$ pH ≈ 8.2; † pH ≈ 6.7; $^{\diamond}$ pH ≈ 7.2; $^{\angle}$ pH ≈ 3; ‡ pH ≈ 7.6; $^{\top}$ pH ≈ 4.2; $^{+}$ at E = -1.7 V vs. SCE (pH not reported)

2.2 Initial activation of CO_2

The first step in any electrocatalytic reduction reaction of CO_2 is the initial activation of the CO_2 molecule. It is often claimed that activation and reduction of CO_2 is difficult, because the first electron transfer to form the $CO_2^{\bullet -}$ radical intermediate has a very negative redox potential (-1.9 V vs. NHE), or because CO_2 is a very stable molecule.[4,22] Neither statement is accurate. The electrocatalyst stabilizes the $CO_2^{\bullet -}$ radical or reaction intermediate by the formation of a chemical bond, leading to a less negative redox potential. With the right electrocatalyst, it is possible to reduce CO_2 to CO or HCOOH at very low overpotential, which is related to the mechanism of a two-electron process, typically consisting of only one intermediate, which is relatively easily optimized.[7,9] Enzymes such as formate dehydrogenase and carbon monoxide dehydrogenase are indeed effective reversible catalysts for the electrocatalytic conversion of CO_2 to formate and carbon monoxide (and vice versa), respectively, exhibiting negligible overpotentials.[23]

We consider four redox reactions related to the activation of CO_2 (eq. 2.1-2.4):

$$CO_2 + H^+ + e^- \rightarrow {}^*COOH \tag{2.1}$$

$$CO_2 + H^+ + e^- \rightarrow {}^*OCHO \tag{2.2}$$

$$CO_2 + e^- \rightarrow {}^*COO^- \tag{2.3}$$

$$H^+ + 2e^- \rightarrow {}^*H^- \tag{2.4}$$

Eq. 2.1 and 2.2 are proton-coupled electron transfer (PCET) reactions and have been considered in a recent computational study by Studt et al. for deriving trends in selectivity among (post-)transition metal surfaces.[24] They argued that *COOH is the more likely first intermediate for CO formation, and *OCHO the more likely intermediate for the formation of formic acid (an assertion that is generally agreed upon in the literature). Using calculated binding energies, they generally find good agreement between their predictions and experiment: post-transition metals such Pb and Sn prefer to bind via the oxygen and are selective towards formic acid, whereas transition metal electrodes prefer to bind via the carbon. Interestingly, in two instances their calculations deviate from the experimental observations in Table 2.1: silver is predicted to be an excellent catalyst for the formation of formic acid, whereas palladium is predicted to have the lowest onset potential for the formation of CO. They ascribe these differences to kinetic effects not included in their calculations. Interestingly, in the molecular electrocatalysis community the views on the initial activation of CO_2 appear to be subtly different. The initial binding of CO_2 to the catalyst does not involve a CPET step such as Eq. 2.1 and 2.2, both rather an electron-transfer mediated CO_2 binding step, as indicated by eq. 2.3. The CO_2^- anion adduct is generally bound to the metal center of the catalyst.

For instance, for a cobalt-(proto)porphyrin catalyst, CO_2 binding takes place if the cobalt center changes oxidation state from Co(II) to Co(I), with the electronic density flowing onto the $^*CO_2$ ligand, formally written as in Eq. 2.5 and 2.6:

$$Co(II) + e^- \rightarrow Co(I) \tag{2.5}$$

$$Co(I) + CO_2 \rightarrow Co(II) - [CO_2^-] \tag{2.6}$$

Subsequent protonation or CPET steps then generate the $^*COOH$ or $^*COOH^-$ intermediates. If this step is rate-determining, the pH dependence of CO_2 activation may differ from the pH dependence of the competing HER, which is confirmed by DFT calculations.[25] Shen et al. used this different pH dependence of the CO_2RR and HER pathways to explain the strong pH dependence of the overall product selectivity on graphite-immobilized Co-protoporphyrin, with H_2 being the primary product at pH = 1 but CO being the primary product at pH = 3.[26] Theoretical work showed that CO_2RR proceeds through different metal coordinated CO_2^- intermediates leading to either CO or HCOOH, similar to different binding modes of $CO_2^{\bullet -}$ on metal electrodes.[27] A very similar mechanistic model was proposed by Wuttig et al. for the gold-catalyzed CO_2RR, suggesting that also on gold the $^*CO_2^-$ intermediate, and not $^*COOH$, is the relevant activated form of CO_2.[28] Recent computational work by Chen et al. has confirmed that on Ag(111), adsorbed CO_2 is highly sensitive to the presence of an electric field, as e.g. modeled by the presence of a cation.[29] Although Chen et al. do not write the formation of $^*CO_2$ as an electron-transfer step, the resulting $^*CO_2$ is highly polarizable, and therefore sensitive to pH and cation effects (see section on Reaction- and Process Conditions).

A somewhat similar situation exists for the formation of formate/formic acid on molecular catalysts. Among the metal porphyrins, we recently showed that Rh, Sn and In protoporphyrins have a high selectivity towards formic acid in aqueous electrolyte.[30] DFT calculations suggest that the key intermediate is an anionic hydride, formed through Eq. 2.4, as has been previously suggested in the molecular catalysis literature.[31,32] The anionic hydride performs a nucleophilic attack of the carbon of the CO_2, yielding $HCOO^-$. Again, the reaction is triggered by a potential-induced change in oxidation state of the catalyst, either of the metal center (in the case of Rh) or on the ligand (in the case of In and Sn). The stability of the resulting species is crucial to the subsequent elementary step and the formation of either CO or $HCOOH/HCOO^-$. Interestingly, such a (lattice-)hydride mechanism was recently proposed for nanostructured copper-hydride catalysts with a much enhanced selectivity for formic acid ("normal" copper yields primarily CO as a two-electron product).[33]

2.3 Carbon-carbon bond formation

One of the most interesting observations in the electrocatalytic reduction of CO_2 is the formation of species with one or more carbon-carbon bonds, which till date mostly has been reported for copper-based electrodes. Elucidation of the pathway(s) from CO_2 or CO to C_2 products has been the subject of several experimental[14,34–38] and theoretical studies.[39–43] Previous work from our group demonstrated the presence of two separate pathways for the formation of ethylene, each of which has a different intermediate: a surface insensitive pathway through a shared intermediate with the methane pathway, and a reaction path that takes place on Cu(100) at low overpotential through an adsorbed CO dimer intermediate.[36] This CO dimer intermediate has been proposed in several experimental[34,37] and theoretical studies.[39–41] DFT calculations have shown that the C-C coupling is only observed when a decoupled proton-electron transfer is assumed for the rate-determining steps,[39] and not when CPET is assumed for every step in the mechanism.[43,44] Moreover, the CO dimer configuration was found to be energetically feasible only when a charged water layer is taken into account,[40] and the activation energy for its formation is more favorable on Cu(100) compared to Cu(111),[40,42] in agreement with experimental observations. Although Wuttig et al.[38] could not find spectroscopic signature of adsorbed OCCO and CHO species, they could not conclusively rule out the possibility of these or other surface species to be formed from COads, due to obscurity of OCCO by (bi)carbonate desorption and possible lower C-O oscillator strengths in case of CHO species. Recently, Pérez-Gallent et al.[45] have provided evidence for a hydrogenated CO dimer intermediate (OCCOH) at low overpotentials in LiOH electrolyte during CO reduction using FTIR spectroscopy supported with density functional theory (DFT) calculations. The vibrational bands of 1191 and 1584 cm^{-1} observed during the reduction of CO, were assigned to the C-O-H and C=O stretching modes of this hydrogenated dimer intermediate, which was found to be structure sensitive, since its formation was only observed on Cu(100) and not on Cu(111), in agreement with previous studies.[35,42]

Besides ethylene, other valuable C_2 products are acetaldehyde and ethanol. These three C_2 species are formed through common intermediates on Cu(100) up to a selectivity-determining intermediate, the hydrogenation of which is inclined towards ethylene.[39] However, ethanol formation is more favorable on undercoordinated copper sites,[46] unlike ethylene formation, which prefers pristine (100) terraces.[37,42]

Although the formation of higher order (C_{3+}) hydrocarbons is rarely observed, some studies have reported the formation of these products to occur via C-C coupling as well. C-C coupling between CO and C_2H_4 precursors has been reported to form n-propanol on agglomerates of oxide-derived copper nanocrystals.[47] For this mechanism, the defect sites are proposed to be the catalytic active sites. Moreover, polymerization of adsorbed -CH_2 species has been proposed as mechanism for the formation of higher order hydrocarbons on bimetallic PdAu electrodes.[48]

2.4 Reaction- and Process conditions

The influence of electrolyte composition, process- and reaction conditions has been acknowledged since the early experiments on CO_2RR.[16,49–51] The nature of the electrolyte (aqueous or non-aqueous), pH, the identity of ionic species, or a combination of these factors, all influence the activity or selectivity of CO_2RR. However, the interpretation of these effects has remained poorly understood, and only recently systematic work has been performed to understand these effects.[52–54] Moreover, other phenomena have been highlighted recently, such as the influence of local pH, buffering strength and mass transport[55–58] as well as the existence and influence of homogeneously catalyzed chemical reactions during the CO_2RR.[59,60]

Previously the influence of the electrolyte was investigated in terms of different (bulk) pH or ionic species.[50,51] The interpretation of the effects of the aqueous electrolyte, ionic species and pH is complicated by a complex interplay of several of these factors, which makes it hard to ascribe a certain effect to a single parameter. Firstly, there has been controversy about the real active intermediate during CO_2 reduction. Most authors acknowledge that dissolved CO_2 is the active species, whereas some cases of bicarbonate as active species especially towards formate have been reported.[61–63] The settlement of the H_2CO_3/HCO_3^- equilibrium in water complicates conclusive statements about the role of bicarbonate on formate formation, which would ideally require in situ measurement of local concentrations of bicarbonate and formate during voltammetry. Secondly, the (bulk) pH, electrolyte composition and buffer capacity influence the concentrations of the carbonaceous species in solution[64] and selectivity of CO_2RR.[52,65] Recently, enhanced CO_2RR activity in bicarbonate electrolyte compared to other electrolytes under similar conditions, was proposed to be associated with the formation of a bicarbonate-CO_2 complex leading to an increase in effective CO_2 concentration in vicinity of the electrode.[66] The authors claim that bicarbonate is the primary source of carbon in the formation of CO on gold, and generalize this role of bicarbonate to all CO-producing electrocatalysts. On the other hand, Wuttig et al. conclude that bicarbonate is not explicitly involved in the rate-limiting step of CO formation on gold.[67] Instead, bicarbonate acts as a proton donor past the rate-limiting step, and as a sluggish buffer solution maintaining the bulk pH.

Additionally, the influence of the electrolyte can be associated with the presence of cationic or anionic species as was discovered by Hori and coworkers.[49,50] Several research groups have reported cation effects on CO_2RR, where larger cations usually favor CO_2RR and the C_2/C_1 ratio. Till date there are in principle two explanations to rationalize this cation effect. On one hand, the degree of cation hydration is proposed to play a role.[50,68,69] The cations differ in outer Helmholtz plane (OHP) potential, which leads to different local proton and CO_2 concentrations and subsequently different product selectivity for CO_2RR. On the other hand, the stabilization of the negatively charged intermediate by the cation has been proposed.[29,70] The onset potential for ethylene depends on the cation nature,

while for methane no correlation has been found with cation size. This trend is in agreement with the observation of a hydrogenated dimer intermediate (OCCOH) only with smaller cations. This hydrogenated dimer is the key intermediate for the C-C coupling as discussed in the previous section.[45]

The effect of anions on the CO_2RR has been investigated in the literature, although less extensively compared to cations, and the studies generally consist of halide effects on copper electrodes.[16,51,53] These effects are generally explained in terms of halide adsorption on the catalyst surface, altering the electronic structure and subsequently the CO_2RR activity and selectivity, which are also dependent on the halide size and concentration.[53] Moreover, specifically adsorbed halide anions can suppress proton adsorption, favoring CO_2RR with respect to HER.[51]

Apart from bulk pH effects, the importance of the pH gradients and local pH has been the subject of several studies recently.[55,56] It is generally known that during CO_2RR, an alkaline pH is manifested in the vicinity of the electrode, as result of proton consumption and hydroxide formation under cathodic conditions. This local pH change is proportional to the current density.[71] The concentration of the electrolyte, in particular, the buffer capacity plays an important role on the local pH near the electrode. Moreover, the electrode morphology may also induce variations in the local pH, which can alter the product selectivity, as mentioned in a previous section. On Cu electrocatalysts, the selectivity toward ethylene can be favored by lowering the buffer capacity or by changing the electrode structure to obtain high current densities and thereby a high local pH.[56] Additionally, the selectivity can be steered toward ethylene by increasing the CO_2 pressure, leading to enhanced local CO concentration and CO coverage. Although a different product spectrum was observed under similar conditions, Varela et al.[55] reported similar conclusions regarding the effect of buffer capacity and local pH on the product selectivity of CO_2RR on Cu electrodes. The difference in product spectrum was presumed to be a result of different electrode morphology. In addition to properties indirectly affecting the mass transport of protons or CO_2 (electrode morphology, buffer capacity, etc.), forced or controlled mass transport also have been shown to influence the product selectivity of CO_2RR.[57,58] Improved mass transport is generally associated with local pH approximating the bulk pH and enhanced local CO_2 concentration. However, improved mass transport does not necessarily lead to increased activity or selectivity of CO_2RR, since it may affect the competing HER as well. Rotating disc or cylinder experiments on Cu have shown that CO_2RR activity decreases with higher rotation rate, while HER activity increases together with a change in selectivity from CH_4 to CO.[58] Recently, it was found that direct water reduction is the HER pathway in competition with CO_2RR instead of proton reduction, which is diffusion-limited at an acidic pH of 2.5.[57] The suppression of water reduction is the result of adsorbed CO on the copper electrode and is more pronounced at low rotation rates (< 500 rpm). CO_2RR was found to be less sensitive to transport limitations compared to HER.[72]

Another consequence of a local alkaline pH as result of the concomitant HER during CO_2RR, is the occurrence of chemical reactions, which may be homoge-

neously catalyzed.[59,60] We recently found that Cannizzaro-type reactions can take place during CO_2RR, where aldehydes disproportionate into their corresponding carboxylic acid and primary alcohol.[60] This phenomenon is catalyzed by the local alkaline pH near the electrode, and is therefore important in poorly buffered and unbuffered electrolytes. The obtained products (acids and alcohols) should be distinguished from direct CO_2 reduction products. This work will be discussed in chapter 3.

2.5 Electrode morphology and (sub)surface atoms

Besides the chemical nature of the electrocatalyst, the electrode morphology has been widely studied with the aim to understand and enhance CO_2RR activity and selectivity. Examples include different single crystals which have been the subject of previous research.[14] More recently nano-[73–77] and mesostructured[72,78–81] catalysts and oxide-derived electrodes[82–87] have shown interesting properties influencing the CO_2RR activity and selectivity such as coordination number of active sites, particle size, readsorption of intermediates, interparticle distance and transport phenomena.

Rough or high surface-area surfaces such as copper nanoparticles have been shown to exhibit improved hydrocarbon selectivity compared with smooth surfaces, due to increased population of undercoordinated sites.[73] Cubic shaped copper nanocrystals are able to steer the selectivity towards ethylene with respect to methane.[74] The surface structure consists mainly of (100) facets, which is presumed to be key for the high C_2/C_1 ratio. Similar results were obtained by Loiudice et al.,[75] who reported an optimal cube size due to a balance between edge- and plane sites. Another type of roughened electrodes, copper nanofoams, turned out to increase faradaic efficiency towards formic acid at the expense of CH_4 and C_2H_4, and to form propylene.[76]

In addition to specific sites of nanoparticles, a particle size effect of Cu nanoparticles has been reported,[77] in which the authors showed that the activity for H_2 and CO is increased with decreasing particle size (< 5 nm), while the selectivity towards hydrocarbons is decreased. This observation was attributed to higher amount of undercoordinated sites (CN < 8), which promote HER and CO formation due to stronger chemisorption of the CO intermediate. Since different synthesis methods of Cu nanoparticles and experimental conditions for CO_2 reduction were used, it is hard to generalize the results of these studies in terms of morphology effects of Cu nanoparticles.

Apart from the nanostructure, more recently the mesostructure of copper electrodes also has been shown to play an important role in the product selectivity of C_1 vs. C_2 products. The local pH and retention time of key intermediates inside the pores of mesoporous Cu electrodes can be altered, steering the selectivity towards ethane and ethylene.[78] Chen et al.[79] reported robust Cu mesocrystals, prepared by in situ reduction of CuCl thin films during CO_2RR, which exhibit high activity and stability toward ethylene ($C_2H_4/CH_4 \approx 18$) at -0.99 V vs. RHE. These mesocrystals

exhibit Cu(100) facets and steps, contrary to regular Cu nanoparticles or Cu foils, and CO adsorption is preferred on these sites, leading to high faradaic efficiency towards C_2H_4 on the Cu mesocrystals. Investigation of mesoscale phenomena have demonstrated the effects of particle size and distance on the product selectivity for well-defined Cu catalysts.[80] Readsorption of the CO intermediates, followed by their further reduction is found to be associated with small interparticle distance and larger nanoparticle sizes, whereas small nanoparticles suffer from poisoning of active sites by CO. Control of these mesoscale parameters could be used to tune the selectivity of CO_2RR. The role of the mesostructure on the selectivity has also been shown on gold electrodes.[72] Hydrogen evolution was shown to be suppressed by increasing the porosity of the electrode, while CO_2RR is more resistant to transport limitations caused by porous electrodes. On a similar note, it was found that efficient CO_2 transport on porous Cu hollow fibre electrodes, which exhibit many defect sites, increases CO selectivity.[81]

In 2012, research conducted by Kanan and coworkers revealed the increased energetic efficiency and stability of CO_2RR on oxide-derived (OD) electrocatalysts, which were obtained by reducing metal-oxide films. Improved CO_2RR activity has been reported for e.g. OD gold, OD copper and OD lead.[11,82,83] To date there are various other papers published regarding CO_2/CO reduction on OD copper electrodes,[84–87] but the key factor responsible for the improved selectivity and activity of oxide-derived electrocatalysts is still unclear. In this respect, increased stabilization of the CO_2 anion radical ($CO_2^{\bullet-}$) by grain boundaries and (sub)surface oxygen or oxidized species have been reported to play a role, although no consensus has been reached to date.[88–90]

On OD Au, high selectivity to CO at low overpotential was found, which was ascribed to improved stabilization of $CO_2^{\bullet-}$ on the OD Au compared to polycrystalline Au.[11] Similar conclusion has been drawn for OD Cu for the formation of CO.[85] Additionally, on copper the enhanced activity and stability compared to polycrystalline Cu depend on the initial thickness of the Cu_2O layers and is not significant for thin films (< 3 μm).[82,86] Later, remarkable improvement of the selectivity toward ethanol, acetate and n-propanol for CO reduction on similar electrodes, was reported.[87] The authors exclude the influence of nanocrystallite size or morphology on the enhanced CO activity, and associate the improved selectivity with grain boundaries instead, facilitating strong CO binding sites.[88,89]

Eilert et al.[90] demonstrated the role of subsurface oxygen in the oxide-derived copper electrocatalysts by in situ ambient pressure XPS and quasi in situ EELS in a transmission electron microscope. They proposed that subsurface oxygen modifies the electrocatalyst's electronic structure by reducing σ-repulsion, leading to increased CO binding energies, and consequently higher CO coverage, which promotes C_2 selectivity. The authors assumed that influence of grain boundaries in the oxide-derived Cu, as discussed before, originated from residual oxygen present in the subsurface. Key in this mechanism was the presence of near-surface sites, which inhibited diffusion of subsurface oxygen to the surface and thereby protonation to form water. DFT calculations have shown that interstitial oxygen species are stable

at Cu(111) subsurface, contrary to Cu(211), and are capable of improving CO_2 binding to the surface.[91]

When Cu_xO is used directly for CO_2RR, methanol,[17,92] ethanol,[19,20] and ethylene[19] were observed as major products. It is often assumed that during CO_2RR, the Cu_xO electrocatalyst should be completely converted to metallic Cu. However, Lee and coworkers[93] showed that a residual oxide layer remains present on the surface during CO_2RR and they proposed the surface oxide and OD-metallic layer as key reaction sites for catalysis. They also reported the formation of C_3-C_4 products due to a synergistic effect between Cu_2O and Cl adsorption, which resulted in a higher population of Cu^+ species.[94] Similar results were obtained by Mistry et al.,[15] who showed that Cu^+ species are resistant to reduction and considered the active species for improved selectivity toward ethylene. The role of Cu^+ was contradicted by Xiao et al.,[95] who demonstrate a synergistic effect of surface Cu^+ and Cu^0, which improves the CO_2 activation and CO dimerization. Individual Cu^+ species affect the CO_2RR efficiency and selectivity negatively. The presence of both, surface Cu^+ and Cu^0, can be caused by subsurface oxygen,[96] which is in agreement with the importance of subsurface oxygen discussed in the previous paragraph.

2.6 In situ spectroscopic investigation of CO_2 reduction

In situ spectroscopy techniques can provide very useful information about electrocatalytic reactions such as reaction intermediates adsorbed on the electrode surface, and dissolved species involved in the reaction. The technique most often used is FTIR spectroscopy. A general review on in situ FTIR spectroelectrochemistry was given by Ye et al.[97] Major bottlenecks related to external reflection FTIR are the high ohmic resistance in the thin layer solution, hindered mass transport conditions, and interference due to infrared absorption from bulk water. Another often used spectroelectrochemical technique is Surface enhanced Raman spectroscopy (SERS), which provides very sensitive characterization of adsorbed species at the electrode surface. A drawback of SERS is the local enhancement of spectroscopic signals which leads to a relatively biased representation of the electrode surface as you only see the "hotspots". Osawa et al.[98] showed that surface enhanced absorption spectroscopy (SEIRAS) in an attenuated total reflection (ATR) configuration may solve the aforementioned limitations of FTIR and SERS. More recently, some studies have utilized in situ x-ray absorption spectroscopy (XAS) to characterize the surface during CO_2RR aimed at pinpointing the active catalytic species. Here we briefly discuss recent in situ spectroscopic studies that have revealed novel insight on the electrochemical CO_2 reduction.

During CO_2RR, gaseous products such as CO, and H_2 from the concomitant hydrogen evolution in aqueous media negatively affect the spectroscopic measurement due to bubble formation. For this reason, most of the early studies concerning

FTIR of CO_2 electrochemical reduction were performed in non-aqueous solutions, avoiding hydrogen evolution. Recently, Figueiredo et al.[99] showed the high sensitivity of CO_2 reduction to the presence of residual water in acetonitrile using in situ FTIR and SERS. They showed that in non-dry conditions adsorbed CO is the major product at low overpotentials, and that (bi)carbonates are formed at Cu, Pt, Au, Pd and Ag electrodes from the chemical conversion of CO_2 by a significantly high concentration of OH- species formed from water reduction. As a consequence, (bi)carbonate formation was found to be propotional to the water content. The formation of oxalate was only observed for Pb electrodes at extremely high overpotentials.

The formation of the higher order hydrocarbons on Cu electrodes proceeds via an adsorbed CO species, although the rate-limiting step is not agreed upon by experimental[4,5,13,34,37] and theoretical[39–41,43,100] studies. Wuttig and coworkers[38] utilized SEIRAS to reveal that adsorbed CO species are bound to the electrode surface at potentials < -0.60 V vs. RHE, independent of pH, but weakly dependent on the potential. Spectroscopic studies shed light on the concerted or sequential nature of proton- and electron transfer pathways related to CO_2RR on various electrodes.[28,101] In situ ATR-SEIRAS revealed the fundamentally different proton coupling behavior between CO_2 reduction and hydrogen evolution reaction (HER), which plays an important role in the selectivity toward CO vs. H_2 on gold.[28] The authors in this work reported a rate-limiting single electron transfer (ET) to CO_2, which was decoupled from proton transfer (PT) from hydronium, bicarbonate or carbonic acid. In contrast, PT from these species was rate limiting for the HER, leading to H_{ads}. The vibrational band between $\approx$ 1900 - 2050 cm^{-1}, ascribed to CO adsorbed on Au bridge sites, was argued by Dunwell et al.[66] to be the result of Pt deposition of the counter electrode on the Au working electrode.

Another aspect often studied with in situ spectroscopy is the (change in) surface structure during CO_2RR. Pander et al.[102] investigated the role of metastable surface oxides for CO_2 reduction on tin, indium, lead and bismuth electrodes, by means of ATR-IR. The results indicate the competition between CO_2 and H^+ for reaction sites (oxidized or metallic sites), depending on the nature of the electrode. Very recently, ATR-IR and SERS have also been utilized to indirectly monitor (reconstruction of) the surface during CO_2RR.[103] Moreover, the oxide derived catalysts (as discussed in the previous section) have been probed by XAS[15,93,104] and ambient pressure XPS[90] in order to gain insight in the chemical state of the active (Cu) species.

As discussed, spectroscopic studies of electrochemical CO_2 reduction provide information of high importance for the better understanding of the reaction intermediates and products. Yet, the number of studies, especially concerning in situ XAS and XPS, is still limited, and the opportunities for following studies and technical development is very wide.

2.7 Computational approaches for CO_2 reduction

Over the last decades, computational electrochemistry has increased in importance to predict, explain or support the outcome of experiments. Density Functional Theory (DFT) calculations applied to the electrode/electrolyte interface is a far from simple endeavor, but much progress has been made in improving models. A review of the achievements and challenges within first-principles computational electrochemistry is given by Calle-Vallejo et al.,[105] and a more comprehensive review on multiscale simulations from the atomic to the system scale can be found elsewhere.[106] In this section, we will limit ourselves to recent advances and key scientific challenges of computational approaches with respect to the electrocatalytic reduction of CO_2 and CO.

Since its introduction by Nørskov et al.,[107] the computational hydrogen electrode (CHE) has been widely employed for computations in electrocatalysis, in particular for CO_2 and CO electroreduction. Using this model together with DFT to calculate the adsorption energies of the intermediates, one can gain mechanistic insight in the possible reaction pathways, and can estimate the potentials at which the redox reactions take place.[39,100,108] However, models based on the CHE typically assume concerted proton-coupled electron transfer steps (CPET), and are therefore not fully applicable for reaction pathways where decoupled proton- and electron transfer steps are involved. Sequential proton-electron transfer (SPET) steps have been observed on molecular and oxide electrocatalysts, as well as on metallic electrocatalysts, making them pH sensitive.[5,109,110] Recently, a simple methodology was introduced that allows to predict the transition between coupled and decoupled proton-electron transfer pathways[25] based on the accurate calculation of acid-base equilibrium constants.[111] Using this methodology, the experimental pH dependence of CO_2 reduction on immobilized cobalt protoporphyrin IX has been rationalized.[26]

The presence of linear correlations between adsorption energies of similar adsorbates, known as scaling relations,[112] is advantageous for reducing the complexity of DFT-based catalytic models and facilitate the simultaneous analysis of numerous materials. However, these scaling relations pose extra constraints for finding optimal electrocatalysts with low overpotentials, and are therefore extensively studied.[113–115] There have been various recent efforts undertaken to break or circumvent scaling relations, especially between the intermediates of the electrocatalytic OER, ORR and CO_2RR.[42,116,117] The strategy is clear, although in practice difficult to implement experimentally: one of the intermediates needs to be significantly stabilized with respect to the other. For instance, the preference of Cu(100) for the production of ethylene and ethanol over methane has been explained on the basis of the breaking of scaling relations between adsorbed CO and CO dimers on that facet due to strong ensemble effects upon CO dimerization.[42] Another example is the nearly reversible reduction of CO_2 to CO on CODH enzymes, the active site of which does not obey the scaling relationship between adsorbed CO and COOH.[118] Furthermore, Li and Sun[119] and Peterson and Nørskov[108] discussed

several strategies in this respect for CO_2RR: tuning of metal surfaces such as to obtain low-coordination sites and introduction of p-block dopants or oxophilic sites. Other ways to depart from scaling relations are the modification of the electrolyte composition,[116] anchoring active ligands on the surface or at the active sites,[120] the search for transition-metal-free electrocatalysts and the decoupling of PT and ET transfers.

As mentioned before, much work has been devoted to copper electrodes, because of their ability to produce hydrocarbons and alcohols in significant quantities. DFT studies have been mainly carried out to propose reaction pathways and to explain the selectivity on different electrocatalysts or surface sites. Durand et al.[121] showed that the stability of the key intermediates increases in the order Cu(111) < Cu(100) < Cu(211), which implies that the preferred sites for hydrocarbon formation on copper are low-coordination sites such as steps and kinks.[121,122] Note that CHE-based models do not generally incorporate reaction barriers, which is another important topic under study in CO_2 and CO electroreduction.[123,124] Nie et al.[43] showed the importance of elementary step kinetics on the mechanism of CO_2 reduction to C_1 products. Formation of either a CHO or COH adsorbed intermediate from CO hydrogenation determines the selectivity on Cu(111). CH_x species are formed via the more kinetically favorable COH intermediate, which eventually leads to methane and ethylene. However, when only reaction free energies are taken into account, the lowest-energy pathway to methane/methanol would be through a CHO intermediate, as reported by Peterson et al.[100]

Recently, Xiao et al.[125] argued that adsorbate solvation is not (sufficiently) taken into account in the previous studies by Nie et al.[43] and Montoya et al.,[40] and proposed a mechanism on Cu(111) where surface water is claimed to influence the selectivity towards hydrocarbons compared to alcohol products. The modeling of solvation is crucial when attempts are made to break scaling relations and is often overlooked or taken into account as a constant correction to the adsorption energies calculated in vacuum.[39,100,107,108] However, it was recently found that solvation restores the scalability broken under vacuum.[116]

In summary, significant progress has been made in the past few years towards a comprehensive understanding of CO_2/CO electroreduction. Numerous challenges still lie ahead, which currently prevent the development of accurate materials screening routines for the design of new CO_2/CO reduction materials.[126] To date, there are no reports of in silico designed catalysts for CO_2/CO reduction that have been successfully implemented experimentally. We hope that future advances in pH- and potential-dependent reaction barriers, solvation and scaling relations will enable such developments.

2.8 Future directions and perspectives

Electrocatalytic CO_2 reduction is considered a potential means to alleviate CO_2 accumulation in the atmosphere, and store intermittent renewable energy in elec-

trofuels. In order to verily contribute to a sustainable carbon cycle, large-scale implementation of this process is eventually needed. In the last few decades significant progress has been made mainly regarding the design of highly active or selective electrocatalysts, and their mechanism for CO_2RR. However, it is of crucial importance to realize the importance of other related aspects discussed in this review, electrode morphology, (sub)surface structure, reaction- and process conditions, not only from a mechanistic point of view, but from an engineering perspective as well. Particularly, not only the electrode/electrolyte interface should be studied, but transport phenomena, catalyst stability and electrolyte/solvent effects should be optimized as well. In this endeavor it is desired and even necessary to combine computational and in situ spectroelectrochemical techniques. Ideally one would like to combine all the different parameters in a (computational) model instead of a theoretical model that provides only (mechanistic) information for a specific case limited by various boundary conditions. We believe that future CO_2RR research should deviate from solely finding or improving highly active/selective electrocatalysts, and rather should focus on the joint action of all relevant aspects in order to become a viable option for the production of electrofuels.

2.9 References

[1] D. T. Whipple, P. J. A. Kenis, *J. Phys. Chem. Lett.* **2010**, *1*, 3451–3458.

[2] J. Durst, A. Rudnev, A. Dutta, Y. Fu, J. Herranz, V. Kaliginedi, A. Kuzume, A. A. Permyakova, Y. Paratcha, P. Broekmann, T. J. Schmidt, *Chimia* **2015**, *69*, 769–776.

[3] J.-P. Jones, G. K. S. Prakash, G. A. Olah, *Isr. J. Chem.* **2014**, *54*, 1451–1466.

[4] Y. Hori, *In Modern Aspects of Electrochemistry Vol. 42*, Springer, New York, **2008**.

[5] R. Kortlever, J. Shen, K. J. P. Schouten, F. Calle-Vallejo, M. T. M. Koper, *J. Phys. Chem. Lett.* **2015**, *6*, 4073–4082.

[6] Z. W. Seh, J. Kibsgaard, C. F. Dickens, I. Chorkendorff, J. K. Nørskov, T. F. Jaramillo, *Science* **2017**, *355*, eaad4998.

[7] Y. Hori, H. Wakebe, T. Tsukamoto, O. Koga, *Electrochim. Acta* **1994**, *39*, 1833–1839.

[8] X. Min, M. W. Kanan, *J. Am. Chem. Soc.* **2015**, *137*, 4701–4708.

[9] R. Kortlever, I. Peters, S. Koper, M. T. M. Koper, *ACS. Catal.* **2015**, *5*, 3916–3923.

[10] E. R. Cave, J. H. Montoya, K. P. Kuhl, D. N. Abram, T. Hatsukade, C. Shi, C. Hahn, J. K. Nørskov, T. F. Jaramillo, *Phys. Chem. Chem. Phys.* **2017**, *19*, 15856–15863.

[11] Y. Chen, C. W. Li, M. W. Kanan, *J. Am. Chem. Soc.* **2012**, *134*, 19969–19972.

[12] T. Hatsukade, K. P. Kuhl, E. R. Cave, D. N. Abram, T. F. Jaramillo, *Phys. Chem. Chem. Phys.* **2014**, *16*, 13814–13819.

[13] K. P. Kuhl, E. R. Cave, D. N. Abram, T. F. Jaramillo, *Energy Environ. Sci.* **2012**, *5*, 7050–7059.

[14] Y. Hori, I. Takahashi, O. Koga, N. Hoshi, *J. Mol. Catal. A: Chem.* **2003**, *199*, 39–47.

[15] H. Mistry, A. S. Varela, C. S. Bonifacio, I. Zegkinoglou, I. Sinev, Y.-W. Choi, K. Kisslinger, E. A. Stach, J. C. Yang, P. Strasser, B. R. Cuenya, *Nat. Commun.* **2016**, *7*, 12123.

[16] H. Yano, T. Tanaka, M. Nakayama, K. Ogura, *J. Electroanal. Chem.* **2004**, *565*, 287–293.

[17] M. Le, M. Ren, Z. Zhang, P. T. Sprunger, R. L. Kurtz, J. C. Flake, *J. Electrochem. Soc.* **2011**, *158*, E45–E49.

[18] K. W. Frese Jr., S. C. Leach, D. P. Summers, *US4609441A* **1986**.

[19] D. Ren, Y. Deng, A. D. Handoko, C. S. Chen, S. Malkhandi, B. S. Yeo, *ACS Catal.* **2015**, *5*, 2814–2821.

[20] D. Chi, H. Yang, Y. Du, T. Lv, G. Sui, H. Wang, J. Lu, *RCS Adv.* **2014**, *4*, 37329–37332.

[21] Y. Song, R. Peng, D. K. Hensley, P. V. Bonnesen, L. Liang, Z. Wu, H. M. M. III, M. Chi, C. Ma, B. G. Sumpter, A. J. Rondinone, *ChemistrySelect* **2016**, *1*, 6055–6061.

[22] E. E. Benson, C. P. Kubiak, A. J. Sathrum, J. M. Smieja, *Chem. Soc. Rev.* **2009**, *38*, 89–99.

[23] F. A. Armstrong, J. Hirst, *Proc. Natl. Acad. Sci.* **2011**, *108*, 14049–14054.

[24] J. S. Yoo, R. Christensen, T. Vegge, J. K. Nørskov, F. Studt, *ChemSusChem* **2016**, *9*, 358–363.

[25] A. J. Göttle, M. T. M. Koper, *Chem. Sci.* **2017**, *8*, 458–465.

[26] J. Shen, R. Kortlever, R. Kas, Y. Y. Birdja, O. Diaz-Morales, Y. Kwon, I. Ledezma-Yanez, K. J. P. Schouten, G. Mul, M. T. M. Koper, *Nat. Commun.* **2015**, *6*, 8177.

[27] J. Shen, M. J. Kolb, A. J. Göttle, M. T. M. Koper, *J. Phys. Chem. C* **2016**, *120*, 15714–15721.

[28] A. Wuttig, M. Yaguchi, K. Motobayashi, M. Osawa, Y. Surendranath, *Proc. Natl. Acad. Sci.* **2016**, *113*, E4585–E4593.

[29] L. D. Chen, M. Urushihara, K. Chan, J. K. Nørskov, *ACS Catal.* **2016**, *6*, 7133–7139.

[30] Y. Y. Birdja, J. Shen, M. T. M. Koper, *Catal. Today* **2017**, *288*, 37–47.

[31] B. H. Solis, A. G. Maher, D. K. Dogutan, D. G. Nocera, S. Hammes-Schiffer, *Proc. Natl. Acad. Sci.* **2016**, *113*, 485–492.

[32] A. J. Göttle, M. T. M. Koper, *J. Am. Chem. Soc.* **under revision**.

[33] Q. Tang, Y. Lee, D.-Y. Li, W. Choi, C. W. Liu, D. Lee, D. en Jiang, *J. Am. Chem. Soc.* **2017**, *139*, 9728–9736.

[34] K. J. P. Schouten, Y. Kwon, C. J. M. van der Ham, Z. Qin, M. T. M. Koper, *Chem. Sci.* **2011**, *2*, 1902–1909.

[35] K. J. P. Schouten, E. P. Gallent, M. T. M. Koper, *ACS Catal.* **2013**, *3*, 1292–1295.

[36] K. J. P. Schouten, Z. Qin, E. P. Gallent, M. T. M. Koper, *J. Am. Chem. Soc.* **2012**, *134*, 9864–9867.

[37] M. Gattrell, N. Gupta, A. Co, *J. Electroanal. Chem.* **2006**, *594*, 1–19.

[38] A. Wuttig, C. Liu, Q. Peng, M. Yaguchi, C. H. Hendon, K. Motobayashi, S. Ye, M. Osawa, Y. Surendranath, *ACS Cent. Sci.* **2016**, *2*, 522–528.

[39] F. Calle-Vallejo, M. T. M. Koper, *Angew. Chem. Int. Ed.* **2013**, *52*, 7282–7285.

[40] J. H. Montoya, C. Shi, K. Chan, J. K. Nørskov, *J. Phys. Chem. Lett.* **2015**, *6*, 2032–2037.

[41] J. D. Goodpaster, A. T. Bell, M. Head-Gordon, *J. Phys. Chem. Lett.* **2016**, *7*, 1471–1477.

[42] H. Li, Y. Li, M. T. M. Koper, F. Calle-Vallejo, *J. Am. Chem. Soc.* **2014**, *136*, 15694–15701.

[43] X. Nie, M. R. Esopi, M. J. Janik, A. Asthagiri, *Angew. Chem. Int. Ed.* **2013**, *52*, 2459–2462.

[44] J. H. Montoya, A. A. Peterson, J. K. Nørskov, *ChemCatChem* **2013**, *5*, 737–742.

[45] E. Pérez-Gallent, M. C. Figueiredo, F. Calle-Vallejo, M. T. M. Koper, *Angew. Chem. Int. Ed.* **2017**, *56*, 3621–3624.

[46] I. Ledezma-Yanez, E. P. Gallent, M. T. M. Koper, F. Calle-Vallejo, *Catal. Today* **2016**, *262*, 90–94.

[47] D. Ren, N. T. Wong, A. D. Handoko, Y. Huang, B. S. Yeo, *J. Phys. Chem. Lett.* **2016**, *7*, 20–24.

[48] R. Kortlever, I. Peters, C. Balemans, R. Kas, Y. Kwon, G. Mul, M. T. M. Koper, *Chem. Commun.* **2016**, *52*, 10229–10232.

[49] Y. Hori, A. Murata, R. Takahashi, S. Suzuki, *J. Chem. Soc. Chem. Commun.* **1988**, *0*, 17–19.

[50] A. Murata, Y. Hori, *Bull. Chem. Soc. Jpn.* **1991**, *64*, 123–127.

[51] K. Ogura, J. R. Ferrell III, A. V. Cugini, E. S. Smotkin, M. D. Salazar-Villalpando, *Electrochim. Acta* **2010**, *56*, 381–386.

[52] M. R. Singh, E. L. Clark, A. T. Bell, *Phys. Chem. Chem. Phys.* **2015**, *17*, 18924–18936.

[53] A. S. Varela, W. Ju, T. Reier, P. Strasser, *ACS Catal.* **2016**, *6*, 2136–2144.

[54] A. Schizodimou, G. Kyriacou, *Electrochim. Acta* **2012**, *78*, 171–176.

[55] A. S. Varela, M. Kroschel, T. Reier, P. Strasser, *Catal. Today* **2016**, *260*, 8–13.

[56] R. Kas, R. Kortlever, H. Yilmaz, M. T. M. Koper, G. Mul, *ChemElectroChem* **2015**, *2*, 354–358.

[57] H. Ooka, M. C. Figueiredo, M. T. M. Koper, *Langmuir* **2017**, *33*, 9307–9313.

[58] C. F. C. Lim, D. A. Harrington, A. T. Marshall, *Electrochim. Acta* **2017**, *238*, 56–63.

[59] O. R. Luca, A. Q. Fenwick, *J. Photochem. Photobiol. B* **2015**, *152*, 26–42.

[60] Y. Y. Birdja, M. T. M. Koper, *J. Am. Chem. Soc.* **2017**, *139*, 2030–2034.

[61] Y. Hori, S. Suzuki, *J. Electrochem. Soc.* **1983**, *130*, 2387–2390.

[62] B. Innocent, D. Pasquier, F. Ropital, F. Hahn, J.-M. Leger, K. Kokoh, *Appl. Catal. B: Environ.* **2010**, *94*, 219–224.

[63] R. Kortlever, K. H. Tan, Y. Kwon, M. T. M. Koper, *J. Solid State Electrochem.* **2013**, *17*, 1843–1849.

[64] H. Zhong, K. Fujii, Y. Nakano, F. Jin, *J. Phys. Chem. C* **2015**, *119*, 55–61.

[65] N. Yoshihara, M. Arita, M. Noda, *Chem. Lett.* **2017**, *46*, 125–127.

[66] M. Dunwell, Q. Lu, J. M. Heyes, J. Rosen, J. G. Chen, Y. Yan, F. Jiao, B. Xu, *J. Am. Chem. Soc.* **2017**, *139*, 3774–3783.

[67] A. Wuttig, Y. Yoon, J. Ryu, Y. Surendranath, *J. Am. Chem. Soc.* **2017**, *139*, 17109–17113.

[68] M. R. Singh, Y. Kwon, Y. Lum, I. Joel W. Ager, A. T. Bell, *J. Am. Chem. Soc.* **2016**, *138*, 13006–13012.

[69] M. R. Thorson, K. I. Siil, P. J. A. Kenis, *J. Electrochem. Soc.* **2013**, *160*, F69–F74.

[70] E. Pérez-Gallent, G. Marcandalli, M. C. Figueiredo, F. Calle-Vallejo, M. T. M. Koper, *J. Am. Chem. Soc.* **2017**, *139*, 16412–16419.

[71] N. Gupta, M. Gattrell, B. Macdougall, *J. Appl. Electrochem.* **2006**, *36*, 161–172.

[72] A. S. Hall, Y. Yoon, A. Wuttig, Y. Surendranath, *J. Am. Chem. Soc.* **2015**, *137*, 14834–14837.

[73] W. Tang, A. A. Peterson, A. S. Varela, Z. P. Jovanov, L. Bech, W. J. Durand, S. Dahl, J. K. Nørskov, I. Chorkendorff, *Phys. Chem. Chem. Phys.* **2012**, *14*, 76–81.

[74] F. S. Roberts, K. P. Kuhl, A. Nilsson, *Angew. Chem. Int. Ed.* **2015**, *54*, 5179–5182.

[75] A. Loiudice, P. Lobaccaro, E. A. Kamali, T. Thao, B. H. Huang, J. W. Ager, R. Buonsanti, *Angew. Chem. Int. Ed.* **2016**, *55*, 5789–5792.

[76] S. Sen, D. Liu, G. T. R. Palmore, *ACS Catal.* **2014**, *4*, 3091–3095.

[77] R. Reske, H. Mistry, F. Behafarid, B. R. Cuenya, P. Strasser, *J. Am. Chem. Soc.* **2014**, *136*, 6978–6986.

[78] K. D. Yang, W. R. Ko, J. H. Lee, S. J. Kim, H. Lee, M. H. Lee, K. T. Nam, *Angew. Chem. Int. Ed.* **2017**, *56*, 796–800.

[79] C. S. Chen, A. D. Handoko, J. H. Wan, L. Ma, D. Ren, B. S. Yeo, *Catal. Sci. Technol.* **2015**, *5*, 161–168.

[80] H. Mistry, F. Behafarid, R. Reske, A. S. Varela, P. Strasser, B. R. Cuenya, *ACS Catal.* **2016**, *6*, 1075–1080.

[81] R. Kas, K. K. Hummadi, R. Kortlever, P. de Wit, A. Milbrat, M. W. Luiten-Olieman, N. E. Benes, M. T. Koper, G. Mul, *Nat. Commun.* **2016**, *7*, 10748.

[82] C. W. Li, M. W. Kanan, *J. Am. Chem. Soc.* **2012**, *134*, 7231–7234.

[83] C. H. Lee, M. W. Kanan, *ACS Catal.* **2015**, *5*, 465–469.

[84] A. Dutta, M. Rahaman, N. C. Luedi, M. Mohos, P. Broekmann, *ACS Catal.* **2016**, *6*, 3804–3814.

[85] M. Ma, K. Djanashvili, W. A. Smith, *Phys. Chem. Chem. Phys.* **2015**, *17*, 20861–20867.

[86] R. Kas, R. Kortlever, A. Milbrat, M. T. M. Koper, G. Mul, J. Baltrusaitis, *Phys. Chem. Chem. Phys.* **2014**, *16*, 12194–12201.

[87] C. W. Li, J. Ciston, M. W. Kanan, *Nature* **2014**, *508*, 504–507.

[88] X. Feng, K. Jiang, S. Fan, M. W. Kanan, *ACS Cent. Sci.* **2016**, *2*, 169–174.

[89] A. Verdaguer-Casadevall, C. W. Li, T. P. Johansson, S. B. Scott, J. T. McKeown, M. Kumar, I. E. L. Stephens, M. W. Kanan, I. Chorkendorff, *J. Am. Chem. Soc.* **2015**, *137*, 9808–9811.

[90] A. Eilert, F. Cavalca, F. S. Roberts, J. Osterwalder, C. Liu, M. Favaro, E. J. Crumlin, H. Ogasawara, D. Friebel, L. G. M. Pettersson, A. Nilsson, *J. Phys. Chem. Lett.* **2017**, *8*, 285–290.

[91] J. Xiao, A. Kuc, T. Frauenheim, T. Heine, *J. Mater. Chem. A* **2014**, *2*, 4885–4889.

[92] K. W. Frese, Jr., *J. Electrochem. Soc.* **1991**, *138*, 3338–3344.

[93] D. Kim, S. Lee, J. D. Ocon, B. Jeong, J. K. Lee, J. Lee, *Phys. Chem. Chem. Phys.* **2015**, *17*, 824–830.

[94] S. Lee, D. Kim, J. Lee, *Angew. Chem. Int. Ed.* **2015**, *54*, 14701–14705.

[95] H. Xiao, W. A. Goddard III, T. Cheng, Y. Liu, *Proc. Natl. Acad. Sci.* **2017**, *114*, 6685–6688.

[96] M. Favaro, H. Xiao, T. Cheng, W. A. Goddard, J. Yano, E. J. Crumlin, *Proc. Natl. Acad. Sci.* **2017**, *114*, 6706–6711.

[97] J.-Y. Ye, Y.-X. Jiang, T. Sheng, S.-G. Sun, *Nano Energy* **2016**, *29*, 414–427.

[98] M. Osawa in *Diffraction and Spectroscopic Methods in Electrochemistry (Advances in Electrochemical Science and Engineering)*, *Vol. 9*, (Eds.: R. C. Alkire, D. M. Kolb, J. Lipkowski, P. N. Ross), Wiley-VCH, New York, NY, USA, **2006**, pp. 269–314.

[99] M. C. Figueiredo, I. Ledezma-Yanez, M. T. M. Koper, *ACS Catal.* **2016**, *6*, 2382–2392.

[100] A. A. Peterson, F. Abild-Pedersen, F. Studt, J. Rossmeisl, J. K. Nørskov, *Energy Environ. Sci.* **2010**, *3*, 1311–1315.

[101] N. J. Firet, W. A. Smith, *ACS Catal.* **2017**, *7*, 606–612.

[102] J. E. Pander, III, M. F. Baruch, A. B. Bocarsly, *ACS Catal.* **2016**, *6*, 7824–7833.

[103] C. M. Gunathunge, X. Li, J. Li, R. P. Hicks, V. J. Ovalle, M. M. Waegele, *J. Phys. Chem. C* **2017**, *121*, 12337–12344.

[104] A. Eilert, F. S. Roberts, D. Friebel, A. Nilsson, *J. Phys. Chem. Lett.* **2016**, *7*, 1466–1470.

[105] F. Calle-Vallejo, M. T. M. Koper, *Electrochim. Acta* **2012**, *84*, 3–11.

[106] T. Jahnke, G. Futter, A. Latz, T. Malkow, G. Papakonstantinou, G. Tsotridis, P. Schott, M. Gérard, M. Quinaud, M. Quiroga, A. Franco, K. Malek, F. Calle-Vallejo, R. F. de Morais, T. Kerber, P. Sautet, D. Loffreda, S. Strahl, M. Serra, P. Polverino, C. Pianese, M. Mayur, W. Bessler, C. Kompis, *J. Power Sources* **2016**, *304*, 207–233.

[107] J. K. Nørskov, J. Rossmeisl, A. Logadottir, L. Lindqvist, J. R. Kitchin, T. Bligaard, H. J'onsson, *J. Phys. Chem. B* **2004**, *108*, 17886–17892.

[108] A. A. Peterson, J. K. Nørskov, *J. Phys. Chem. Lett.* **2012**, *3*, 251–258.

[109] M. T. M. Koper, *Phys. Chem. Chem. Phys.* **2013**, *15*, 1399–1407.

[110] M. T. M. Koper, *J. Solid State Electrochem.* **2016**, *20*, 895–899.

[111] R. Casasnovas, J. Ortega-Castro, J. Frau, J. Donoso, F. Muñoz, *Int. J. Quantum Chem.* **2014**, *114*, 1350–1363.

[112] F. Abild-Pedersen, J. Greeley, F. Studt, J. Rossmeisl, T. R. Munter, P. Moses, E. Skúlason, T. Bligaard, J. K. Nørskov, *Phys. Rev. Lett.* **2007**, *99*, 016105.

[113] F. Calle-Vallejo, J. I. Martínez, J. M. García-Lastra, J. Rossmeisl, M. T. M. Koper, *Phys. Rev. Lett.* **2012**, *108*, 116103.

[114] M. M. Montemore, J. W. Medlin, *Catal. Sci. Technol.* **2014**, *4*, 3748–3761.

[115] F. Calle-Vallejo, D. Loffreda, M. T. M. Koper, P. Sautet, *Nat. Chem.* **2015**, *7*, 403–410.

[116] F. Calle-Vallejo, A. Krabbe, J. M. García-Lastra, *Chem. Sci.* **2017**, *8*, 124–130.

[117] H. Shin, Y. Ha, H. Kim, *J. Phys. Chem. Lett.* **2016**, *7*, 4124–4129.

[118] H. A. Hansen, J. B. Varley, A. A. Peterson, J. K. Nørskov, *J. Phys. Chem. Lett.* **2013**, *4*, 388–392.

[119] Y. Li, Q. Sun, *Adv. Energy Mater.* **2016**, *6*, 1600463.

[120] M.-J. Cheng, Y. Kwon, M. Head-Gordon, A. T. Bell, *J. Phys. Chem. C* **2015**, *119*, 21345–21352.

[121] W. J. Durand, A. A. Peterson, F. Studt, F. Abild-Pedersen, J. K. Nørskov, *Surf. Sci.* **2011**, *605*, 1354–1359.

[122] Z. Zhao, Z. Chen, X. Zhang, G. Lu, *J. Phys. Chem. C* **2016**, *120*, 28125–28130.

[123] C. Shi, K. Chan, J. S. Yoo, J. K. Nørskov, *Org. Process Res. Dev.* **2016**, *20*, 1424–1430.

[124] J. Hussain, H. Jónsson, E. Skúlason, *Faraday Discuss.* **2016**, *195*, 619–636.

[125] H. Xiao, T. Cheng, W. A. Goddard III, *J. Am. Chem. Soc.* **2017**, *139*, 130–136.

[126] Z. P. Jovanov, H. A. Hansen, A. S. Varela, P. Malacrida, A. A. Peterson, J. K. Nørskov, I. E. L. Stephens, I. Chorkendorff, *J. Catal.* **2016**, *343*, 215–231.

CHAPTER 3

The Importance of Cannizzaro-Type Reactions during Electrocatalytic Reduction of Carbon Dioxide

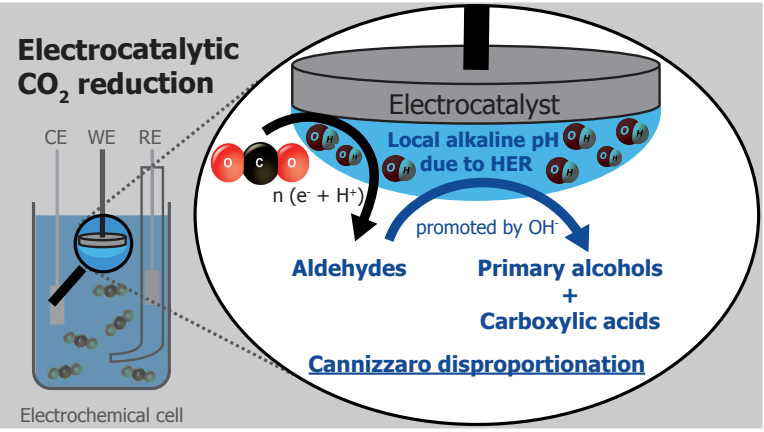

This chapter is based on the article:
Yuvraj Y. Birdja and Marc T. M. Koper, J. Am. Chem. Soc., 2017, 139, 2030-2034

Abstract

A seemingly catalytically inactive electrode, boron-doped diamond (BDD), is found to be active for CO_2 and CO reduction to formaldehyde and even methane. At very cathodic potentials, formic acid and methanol are formed as well. However, these products are the result of base-catalyzed Cannizzaro-type disproportionation reactions. A local alkaline environment near the electrode surface, caused by the hydrogen evolution reaction, initiates aldehyde disproportionation promoted by hydroxide ions, which leads to the formation of the corresponding carboxylic acid and alcohol. This phenomenon is strongly influenced by the electrolyte pH and buffer capacity and not limited to BDD or formaldehyde, but can be generalized to different electrode materials and to C_2 and C_3 aldehydes as well. The importance of these reactions is emphasized as the formation of acids and alcohols is often ascribed to direct CO_2 reduction products. The results obtained here may explain the concomitant formation of acids and alcohols often observed during CO_2 reduction.

3.1 Introduction

The production of fuels or fine chemicals from water, CO_2, and sunlight is a promising way to store solar energy and alleviate CO_2 accumulation in the atmosphere, one of the main causes of global warming since the industrial revolution. Research activities on (photo)electrocatalytic reduction of CO_2 have therefore increased exponentially, especially in the past few years. Different reaction products have been observed depending on, e.g., the nature of the electrocatalyst, the electrolyte, the pH, etc.[1–5] Unfortunately, the existing electrocatalysts for the CO_2 reduction still suffer from the competing hydrogen evolution reaction (HER), high overpotentials, and poor selectivity toward a desired product.

Boron-doped diamond (BDD) is a popular electrode material in electrochemistry, because of its interesting properties such as a wide potential window, high stability, robustness under extreme conditions (potential, temperature, pressure), and low background capacitive currents. BDD finds its use in electrochemistry mainly as a substrate for electrodeposition or nanoparticles and for electroanalytical purposes.[6,7] In the field of electrocatalytic CO_2 reduction, BDD has been used as a substrate for catalysts as diverse as RuO_2 layers,[8] Cu nanoparticles,[9] and metal complexes.[10] BDD has not been investigated as an electrocatalyst for CO_2 reduction until recently, when Nakata et al. reported high faradaic efficiency toward formaldehyde (HCHO) as well as a small amount of formic acid (HCOOH).[11] The standard equilibrium potentials for HCOOH, HCHO, and CO are obtained from formation energies in aqueous media at atmospheric pressure and 25 °C[12] and given in Table 3.1. Note that E^0_{eq} for HCOOH is pH-dependent for pH > 4, due to the dissociation of HCOOH into $HCOO^-$ and H^+.

Table 3.1 Standard Equilibrium Potentials for Reactions:
p CO_2 + **q** (e^- + H^+) → **Product** + **r** H_2O

p	**q**	**product**	**r**	$\mathbf{E^0_{eq}(V_{RHE})}$	
1	2	HCOOH	0	-0.20	$(pH \leq 4)$
				-0.20 + 0.059 · (pH - 4)	$(pH > 4)$
1	4	HCHO	1	-0.08	
1	2	CO	1	-0.11	

It is well-known that the local pH at the electrode-electrolyte interface plays a crucial role for numerous electrochemical reactions.[13–19] In aqueous media, cathodic potentials lead to a local alkaline environment caused by the consumption of protons and/or production of hydroxide ions (Equations 3.1 and 3.2).

$$2H^+ + 2e^- \rightarrow H_2 \tag{3.1}$$

$$2H_2O + 2e^- \rightarrow H_2 + 2OH^- \tag{3.2}$$

The influence of the local pH variations is often neglected, although it is very important, as the local pH change may lead not only to a shift in the effective overpotential but also to the formation of other species by base-catalyzed chemical or disproportionation reactions. It is evident that the effect of the local pH should be known for a correct interpretation of the data, especially for mechanistic studies. Possible organic transformations related to the reduction of CO_2 have recently been discussed from a general point of view.[20] In this context, aldehydes are the most important intermediates/products, because of their diverse reactivity. The Cannizzaro reaction is a base-catalyzed disproportionation reaction of an aldehyde, devoid of α-H atoms, into the corresponding carboxylic acid and alcohol.[21–23] Aldehydes with α-H atoms do not undergo the Cannizzaro disproportionation, as the aldol reaction is much faster. In the aldol reaction, C-C bond formation occurs by addition of the α-carbon of one aldehyde/ketone molecule to the carbonyl-carbon of another molecule under the influence of a base.[24,25]

In this work we elaborate on the utilization of BDD as electrocatalyst for the electrochemical CO_2 reduction under ambient conditions in acidic media. We will discuss the importance of disproportionation and chemical reactions on product distributions often encountered with CO_2 electroreduction also on other electrode materials. We will show that a supposedly inactive material such as BDD is active for the reduction of CO_2 to methane and the concomitant formation of methanol and formic acid, as a result of base-catalyzed Cannizzaro reactions.

3.2 Experimental Section

The electrochemical experiments were carried out in a conventional three-electrode cell where the working electrode and counter electrode compartments were separated by a nafion membrane (Nafion 115). BDD discs of 3 mm or 10 mm diameter (Windsor Scientific Ltd., UK) were embedded in Teflon and used as working electrodes. The counter and reference electrodes were a platinum gauze and a reversible hydrogen electrode (RHE), respectively. For correct measurements versus the RHE scale, the luggin capillary and the RHE compartment were filled with CO_2-saturated electrolyte before CO_2 reduction. Electrolyte solutions were prepared with high-purity perchloric acid (Merck Suprapur), sodium perchlorate (Sigma-Aldrich, ACS reagent), and ultrapure water (Millipore Milli-Q gradient A10 system, 18.2 MΩ·cm). The reported current density is IR corrected and normalized by the geometric surface area of the BDD disc. During voltammetry, online electrochemical mass spectrometry (OLEMS) was utilized for the detection of volatile reaction products and online high performance liquid chromatography (online HPLC) for the analysis of nonvolatile reaction products as described before.[26,27] The reported concentrations of liquid products are an average of two or three independent measurements. Additionally, the data points of each specific experiment are recorded

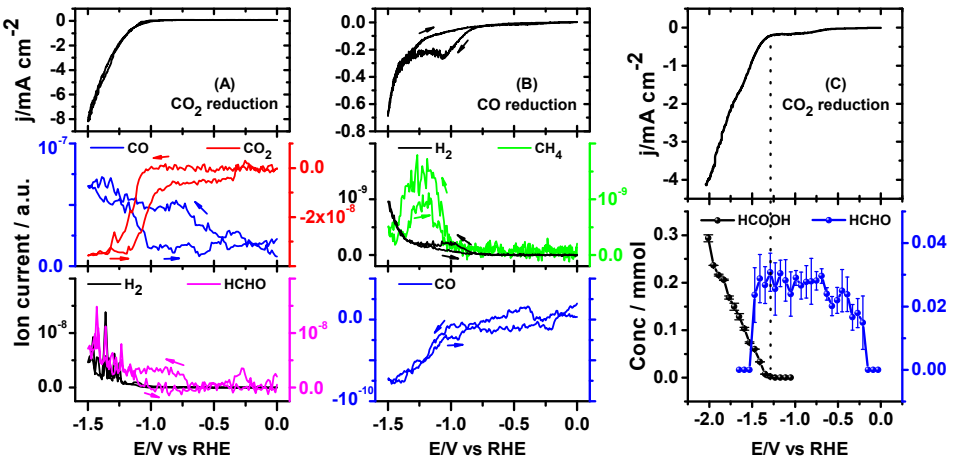

Figure 3.1 Volatile products detected during reduction of (A) CO_2 and (B) CO, and liquid products detected during (C) CO_2 reduction on BDD in 0.001 M $HClO_4$ + 0.099 M $NaClO_4$ electrolyte. Scan rate: 1 mV s^{-1}

.

as the average of two injections of one sample in HPLC, since a slightly different chromatogram also adds an uncertainty to the calculated concentration. The latter source of error is more important for low concentrations (< 0.05 mM), while the deviation in concentration resulting from repeated experiments is dominant for high concentrations.

3.3 Results and Discussion

Prior to each experiment, the BDD electrode was cleaned by ultrasonication in concentrated HNO_3 and water. A Raman spectrum of the BDD electrode is given in Appendix A (Figure A.1). After ultrasonication, blank cyclic voltammograms were recorded in 0.001 M $HClO_4$ + 0.099 M $NaClO_4$ at a scan rate of 500 mV s^{-1} until a stable voltammogram was obtained (typically around 50 cycles) to ensure a clean surface, as shown in Figure A.2a. Experiments on BDD in a CO_2-saturated electrolyte show higher current densities compared to those in an Ar-saturated electrolyte, implying that BDD is active for CO_2 reduction (Figure A.2b). Figure 3.1 shows the formation of volatile species during (A) CO_2 reduction and (B) CO reduction, and (C) the formation of nonvolatile species during CO_2 reduction. Besides H_2, CO_2, and CO, the mass fragment of HCHO is observed, which is in agreement with the literature[11] and our HPLC data (Figure 3.1C), except for lower faradaic efficiencies for HCHO and HCOOH, as shown in Figure A.3. The lower faradaic efficiencies are the result of an electrolyte with higher proton concentration, leading to the formation of a significant amount of H_2 compared to the work by

Nakata et al.[11] Remarkably, Figure 3.1B shows the formation of CH_4 during CO reduction on BDD. The current measured during CO_2 reduction is much higher compared to the current measured during CO reduction, probably due to suppression of the HER by CO. The reason why no CH_4 is detected during CO_2 reduction is assumed to be related to the small amount of CO produced, needed for further reduction to CH_4. The production of CH_4 during CO reduction is not limited to pH 3, but is also observed in electrolytes with a pH between 1 and 7. Our previous experiments and DFT calculations suggest that CH_3OH is an intermediate in the further reduction toward CH_4 on cobalt protoporphyrins immobilized on pyrolytic graphite.[28,29] However, a similar pathway is not likely for CO_2 or CO reduction on BDD, since CH_4 is not detected with OLEMS during methanol reduction on BDD. Even though the amount of CH_4 is not expected to be high, this finding is very intriguing as BDD activity for CO_2 reduction beyond formaldehyde has not been reported before. Very recently it was shown that metal impurities in catalysts and electrolytes can have significant effects on the catalytic activity for CO_2 reduction.[30,31] Since our experiments are conducted on high surface area BDD electrodes and on relatively small time scales, the catalyst poisoning by metal ion impurities in the electrolyte as discussed by Wuttig et al. are assumed to be negligible. Moreover, the promotion of CO_2 reduction by impurities in carbon materials, especially trace levels of copper leading to CH_4, is assumed not to affect our experiments on BDD, since a cleaning procedure is followed similar to one suggested by Lum et al. needed for removal of these metallic impurities and the voltammogram recorded afterward does not show additional redox peaks (Figure A.2a inset). For these reasons we believe that the formation of CH_4 on BDD is not the result of metallic impurities promoting the CO_2 reduction toward CH_4, but can be ascribed to the electrochemical activity of BDD for CO_2 reduction. As pristine pyrolytic graphite is not active for CO_2 reduction[28] and does not produce HCHO, HCOOH, CH_3OH, or CH_4, the activity of BDD is likely associated with its sp^3-hybridized carbon atoms.

In addition to the formation of HCHO, Figure 3.1C shows the formation of HCOOH at more cathodic potentials ($<$ -1.3 V_{RHE}). This could be due to the fact that BDD has some activity for CO_2 reduction to HCOOH,[11] but the same trend for HCOOH is observed during direct reduction of HCHO, as shown in Figure 3.2A. Importantly, the onset potential of HCOOH production is the same as the onset of the HER. The formation of HCOOH, an oxidation product of HCHO, under reducing conditions is believed to be the result of a disproportionation reaction such as the Cannizzaro reaction. The H_2 evolution at less negative potentials (approximately between -0.5 and -1.3 V_{RHE}) is the result of proton reduction, and at more negative potentials ($<$ -1.3 V_{RHE}) caused by direct water reduction similar to results obtained previously on pyrolytic graphite in perchloric acid of pH 3.[28] The direct water reduction produces OH^- ions in the vicinity of the electrode surface (Equation 3.2), which promote the disproportionation reaction. The Cannizzaro reaction is expected to form CH_3OH as well which is not detected with HPLC due

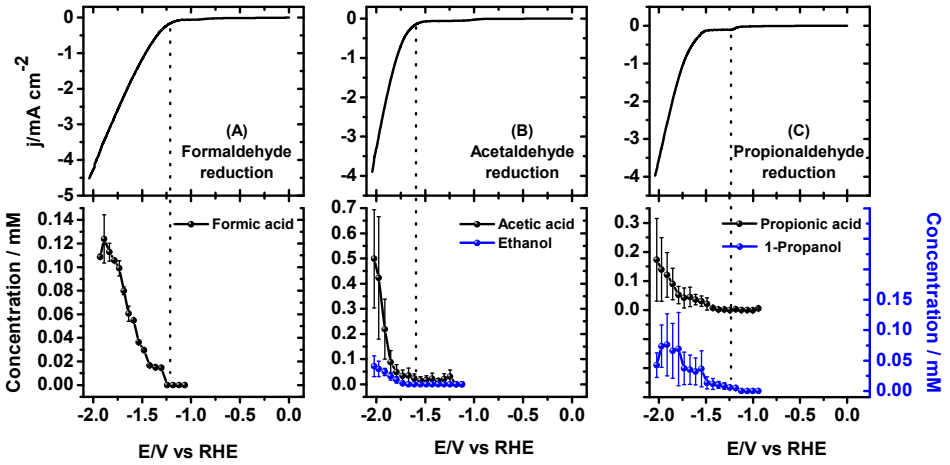

Figure 3.2 Liquid products detected during reduction of (A) 100 mM formaldehyde, (B) 100 mM acetaldehyde and (C) 100 mM propionaldehyde on BDD in 0.001 M $HClO_4$ + 0.099 M $NaClO_4$ electrolyte. Scan rate: 1 mV s^{-1}

.

to sensitivity limitations. However, as shown in Figure A.4, CH_3OH is detected with OLEMS and with HPLC when the HCHO concentration is increased.

We also investigated the formation of liquid products from the C_2 and C_3 aldehydes, acetaldehyde and propionaldehyde, under reducing conditions as shown in Figure 3.2B,C. Both, the primary alcohols and carboxylic acids, are observed commencing together with the HER akin to HCHO reduction. This observation justifies and generalizes the involvement of a disproportionation reaction at negative potentials. The product distributions suggest a Cannizzaro type disproportionation reaction, although the classical Cannizzaro reaction does not take place with aldehydes having α-H atoms. However, Cannizzaro products from aldehydes with α-H atoms have been observed before.[32] When the C_1-C_3 aldehydes are treated with different concentrations of NaOH, the carboxylic acids and alcohols are formed, as displayed in Figure A.5. It can be seen that the amount of alcohol and carboxylic acid formed depends on the concentration of NaOH analogous to a higher local concentration of OH^- at more negative potentials. If self-disproportionation is the dominant mechanism, the expected yields of alcohol and carboxylic acid should be around 50:50%, which is not obtained in our aldehyde reduction experiments. A factor 10 higher yield is observed for propionic acid compared to 1-propanol during propionaldehyde reduction (Figure 3.2C), which suggests the involvement of at least one other reaction pathway or a mechanism not corresponding to the classical Cannizzaro mechanism.

The formation of C_2-C_3 alcohols and carboxylic acids is probably associated with a catalytic or kinetic effect, where near the BDD surface the aldol reaction is

suppressed or the Cannizzaro reaction is preferred over the aldol reaction. Ethanol and acetic acid as products of disproportionation reactions of acetaldehyde have been reported before. Cook et al. have reported a homogeneously catalyzed disproportionation of acetaldehyde into acetic acid and ethanol.[33] Nagai et al. found several products including acetic acid and ethanol formed by a noncatalytic reaction pathway of acetaldehyde under hydrothermal conditions.[34] A catalytic effect of BDD for the disproportionation reactions is unlikely as the reduction of the C_1-C_3 aldehydes on a pyrolytic graphite electrode in the same electrolyte also leads to the formation of carboxylic acids and alcohols as shown in Figure A.6. Additionally, the Cannizzaro products for formaldehyde disproportionation, HCOOH and CH_3OH, are also observed on gold and copper electrodes as depicted in Figure A.7. The fact that no aldol reaction products are detected suggests that the presence of the electrode surface plays a role. Even though the classical Cannizzaro and aldol reactions were originally reported for homogeneous alkaline solutions, a variety of heterogeneous and catalytic systems for these reactions have been investigated for formaldehyde[35–38] and acetaldehyde[39–42] as well. Several groups have reported that surface OH^- can initiate Cannizzaro disproportionation of surface adsorbed HCHO leading to formate ions and methoxy groups.[35–37] A mechanism including a nucleophilic-addition transformation of HCHO to dioxymethylene (CH_2O_2) which subsequently reacts with a HCHO molecule to form formate and methoxy groups has been proposed.[43]

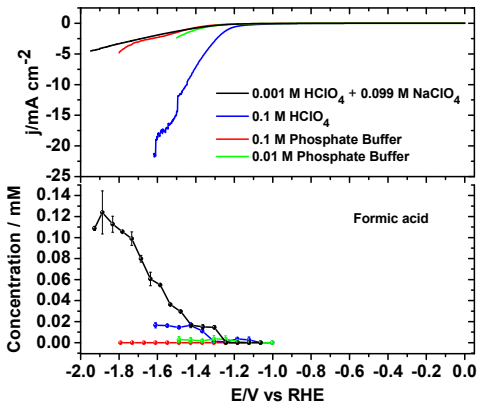

Figure 3.3 Formic acid formation during reduction of formaldehyde in perchloric acid (pH 1 and pH 3), 0.1 M phosphate buffer pH 6.8, and 0.01 M phosphate buffer pH 6.8. Scan rate: 1 mV s^{-1}

.

The importance of the local pH (gradient) near the electrode is demonstrated by the reduction of formaldehyde in different electrolytes as shown in Figure 3.3. A small amount HCOOH is observed in a 0.1 M $HClO_4$ electrolyte while trace amounts or no HCOOH are observed in phosphate buffers of pH 6.8, depending on

the buffer capacity. The higher the buffer capacity, the less sensitive the local pH is to changes, the smaller the possibility of disproportionation reactions to occur. In case of the 0.1 M $HClO_4$ electrolyte, the local environment is very acidic and the local concentration of hydroxide ions near the electrode surface is lower compared to perchloric acid of pH 3, which results in the formation of less HCOOH.

In the recent literature there are several studies where formaldehyde, methanol, formic acid or acetaldehyde, ethanol, acetic acid or propionaldehyde, propionic acid and 1-propanol have been observed during CO_2 electroreduction in different electrolytes on different electrodes.[44–49] Our results show that one should be careful not to misinterpret the observation of carboxylic acids and alcohols to be a result of direct CO_2 reduction. Especially in the quest for novel catalytic materials for CO_2 electroreduction toward liquid products, the involvement of disproportionation reactions should be evaluated. Specifically, ethanol formation always seems to go hand-in-hand with acetate formation, suggesting that they may be (partially) formed from acetaldehyde disproportionation. Moreover, the use of buffer solutions is recommended in order to avoid disproportionation reactions and control experiments are recommended when using alkaline electrolytes to evaluate the stability of products and intermediates.

3.4 Conclusions

In conclusion, this work has illustrated the existence and the importance of disproportionation reactions during electroreduction of CO_2. These reactions lead to product distributions which should be distinguished from direct CO_2 reduction products. The formation of carboxylic acids and alcohols is shown to be the result of disproportionation of aldehydes, which is promoted by the local alkaline environment in the vicinity of the electrode surface, caused by the HER. This phenomenon is strongly affected by the pH and buffer capacity of the electrolyte and can be generalized to other electrode materials and to C_2 and C_3 aldehydes as well. Moreover, it is revealed that BDD has the ability to further reduce CO to methane. The BDD activity should therefore be taken into account when BDD is used as a substrate for catalysts for CO_2 and CO reduction. The involvement of the disproportionation reactions results in a pathway leading to desirable products such as formic acid, acetic acid, methanol, and ethanol during CO_2 electroreduction, different from the direct CO_2 reduction pathway toward these liquid products.

3.5 References

[1] Y. Hori, *In Modern Aspects of Electrochemistry Vol. 42*, Springer, New York, **2008**.

[2] Y. Hori, A. Murata, R. Takahashi, *J. Chem. Soc. Faraday Trans. 1* **1989**, *85*, 2309–2326.

[3] A. Murata, Y. Hori, *Bull. Chem. Soc. Jpn.* **1991**, *64*, 123–127.

[4] M. R. Thorson, K. I. Siil, P. J. A. Kenis, *J. Electrochem. Soc.* **2013**, *160*, F69–F74.

[5] R. Kortlever, J. Shen, K. J. P. Schouten, F. Calle-Vallejo, M. T. M. Koper, *J. Phys. Chem. Lett.* **2015**, *6*, 4073–4082.

[6] R. G. Compton, J. S. Foord, F. Marken, *Electroanalysis* **2003**, *15*, 1349–1363.

[7] L. Hutton, M. E. Newton, P. R. Unwin, J. V. Macpherson, *Anal. Chem.* **2009**, *81*, 1023–1032.

[8] N. Spataru, K. Tokuhiro, C. Terashima, T. N. Rao, A. Fujishima, *J. Appl. Electrochem.* **2003**, *33*, 1205–1210.

[9] N. Yang, F. Gao, C. E. Nebel, *Anal. Chem.* **2013**, *85*, 5764–5769.

[10] S. A. Yao, R. E. Ruther, L. Zhang, R. A. Franking, R. J. Hamers, J. F. Berry, *J. Am. Chem. Soc.* **2012**, *134*, 15632–15635.

[11] K. Nakata, T. Ozaki, C. Terashima, A. Fujishima, Y. Einaga, *Angew. Chem. Int. Ed.* **2014**, *53*, 871–874.

[12] A. J. Bard, R. Parsons, J. Jordan, *Standard Potentials in Aqueous Solution*, Marcel Dekker, New York, **1985**.

[13] A. T. Kuhn, C. Y. Chan, *J. Appl. Electrochem.* **1983**, *13*, 189–207.

[14] I. Katsounaros, J. C. Meier, S. O. Klemm, A. A. Topalov, P. U. Biedermann, M. Auinger, K. J. Mayrhofer, *Electrochem. Commun.* **2011**, *13*, 634–637.

[15] S. Strbac, *Electrochim. Acta* **2011**, *56*, 1597–1604.

[16] M. Nobial, O. Devos, O. R. Mattos, B. Tribollet, *J. Electroanal. Chem.* **2007**, *600*, 87–94.

[17] N. Gupta, M. Gattrell, B. Macdougall, *J. Appl. Electrochem.* **2006**, *36*, 161–172.

[18] R. Kas, R. Kortlever, H. Yilmaz, M. T. M. Koper, G. Mul, *ChemElectroChem* **2015**, *2*, 354–358.

[19] A. S. Varela, M. Kroschel, T. Reier, P. Strasser, *Catal. Today* **2016**, *260*, 8–13.

[20] O. R. Luca, A. Q. Fenwick, *J. Photochem. Photobiol. B* **2015**, *152*, 26–42.

[21] S. Cannizzaro, *Justus Liebigs Ann. Chem.* **1853**, *88*, 129–130.

[22] C. G. Swain, A. L. Powell, W. A. Sheppard, C. R. Morgan, *J. Am. Chem. Soc.* **1979**, *101*, 3576–3583.

[23] D. Basavaiah, D. S. Sharada, A. Veerendhar, *Tetrahedron Lett.* **2006**, *47*, 5771–5774.

[24] J. March, *Advanced Organic Chemistry: Reactions, Mechanisms and Structure*, John Wiley & Sons, New York, 4th, **1992**.

[25] J. Clayden, N. Greeves, S. Warren, P. Wothers, *Organic Chemistry*, Oxford University Press, **2001**.

[26] A. H. Wonders, T. H. M. Housmans, V. Rosca, M. T. M. Koper, *J. Appl. Electrochem.* **2006**, *36*, 1215–1221.

[27] Y. Kwon, M. T. M. Koper, *Anal. Chem.* **2010**, *82*, 5420–5424.

[28] J. Shen, R. Kortlever, R. Kas, Y. Y. Birdja, O. Diaz-Morales, Y. Kwon, I. Ledezma-Yanez, K. J. P. Schouten, G. Mul, M. T. M. Koper, *Nat. Commun.* **2015**, *6*, 8177.

[29] J. Shen, M. J. Kolb, A. J. Göttle, M. T. M. Koper, *J. Phys. Chem. C* **2016**, *120*, 15714–15721.

[30] A. Wuttig, Y. Surendranath, *ACS Catal.* **2015**, *5*, 4479–4484.

[31] Y. Lum, Y. Kwon, P. Lobaccaro, L. Chen, E. L. Clark, A. T. Bell, J. W. Ager, *ACS. Catal.* **2016**, *6*, 202–209.

[32] F. P. B. van der Maeden, H. Steinberg, T. J. de Boer, *Recl. Trav. Chim. Pays-Bas* **1972**, *91*, 221–228.

[33] J. Cook, J. E. Hamlin, A. Nutton, P. M. Maitlis, *J. Chem. Soc. Chem. Commun.* **1980**, 144–145.

[34] Y. Nagai, S. Morooka, N. Matubayasi, M. Nakahara, *J. Phys. Chem. A* **2004**, *108*, 11635–11643.

[35] J. Yu, X. Li, Z. Xu, W. Xiao, *Environ. Sci. Technol.* **2013**, *47*, 9928–9933.

[36] G. Busca, J. Lamotte, J.-C. Lavalley, V. Lorenzelli, *J. Am. Chem. Soc.* **1987**, *109*, 5197–5202.

[37] M.-T. Chen, Y.-S. Lin, Y.-F. Lin, H.-P. Lin, J.-L. Lin, *J. Catal.* **2004**, *228*, 259–263.

[38] J.-C. Lavalley, J. Lamotte, G. Busca, V. Lorenzelli, *J. Chem. Soc. Chem. Commun.* **1985**, 1006–1007.

[39] Z. Sun, L. Kong, X. Ding, C. Du, X. Zhao, J. Chen, H. Fu, X. Yang, T. Cheng, *Phys. Chem. Chem. Phys.* **2016**, *18*, 9367–9376.

[40] B. Wen, Y. H. Yeom, E. Weitz, W. M. Sachtler, *Appl. Catal. B* **2004**, *48*, 125–131.

[41] S. Luo, J. L. Falconer, *J. Catal.* **1999**, *185*, 393–407.

[42] M. A. Natal-Santiago, J. M. Hill, J. A. Dumesic, *J. Mol. Catal. A: Chem.* **1999**, *140*, 199–214.

[43] J. R. B. Gomes, J. A. N. F. Gomes, *Surf. Sci.* **2000**, *446*, 283–293.

[44] Y. Hori in *Handbook of Fuel Cells: Fundamentals, Technology and Application*, *Vol. 2: Electrocatalysis*, (Eds.: W. Vielstich, H. A. Gasteiger, A. Lamm), John Wiley & Sons Ltd., Chichester, UK, **2003**, Chapter 48, pp. 720–733.

[45] K. P. Kuhl, E. R. Cave, D. N. Abram, T. F. Jaramillo, *Energy Environ. Sci.* **2012**, *5*, 7050–7059.

[46] C. W. Li, J. Ciston, M. W. Kanan, *Nature* **2014**, *508*, 504–507.

[47] E. Bertheussen, A. Verdaguer-Casadevall, D. Ravasio, J. H. Montoya, D. B. Trimarco, C. Roy, S. Meier, J. Wendland, J. K. Norskov, I. E. L. Stephens, I. Chorkendorff, *Angew. Chem.* **2016**, *128*, 1472–1476.

[48] A. Verdaguer-Casadevall, C. W. Li, T. P. Johansson, S. B. Scott, J. T. McKeown, M. Kumar, I. E. L. Stephens, M. W. Kanan, I. Chorkendorff, *J. Am. Chem. Soc.* **2015**, *137*, 9808–9811.

[49] E. B. Cole, P. S. Lakkaraju, D. M. Rampulla, A. J. Morris, E. Abelev, A. B. Bocarsly, *J. Am. Chem. Soc.* **2010**, *132*, 11539–11551.

CHAPTER 4

Molecular catalysis of CO_2 reduction

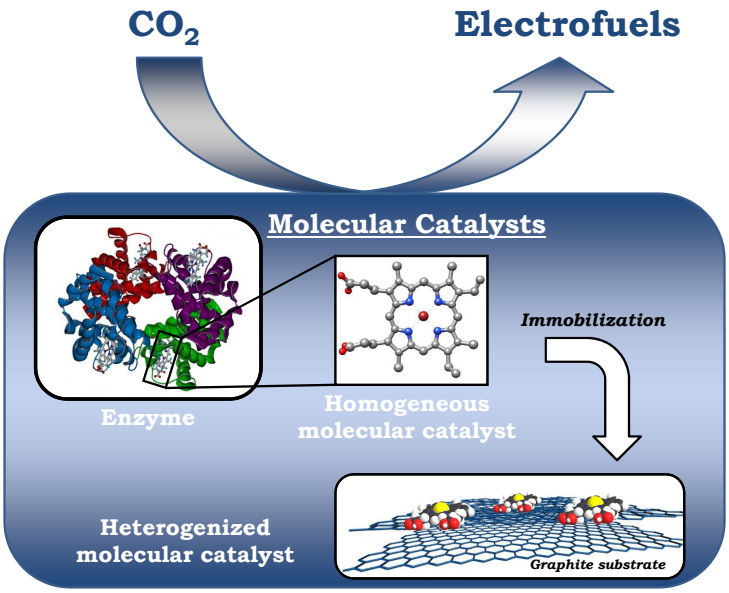

4.1 Introduction

Molecular catalysis of electrochemical reactions is carried out by electrochemically generated species, which are able to oxidize or reduce the reactant molecule, using multiple (proton-coupled) electron transfer steps. The catalytic cycle is closed by regeneration of the initial molecular catalyst. Activation of small molecules such as H_2, O_2 and CO_2 by molecular catalysts has been widely studied, especially in an attempt to address the challenges described in chapter 1.[1,2]

In the case of carbon dioxide, seminal work performed by Vol'pin et al. showed that the CO_2 molecule can be activated by coordination to a transition metal center.[3,4] Fundamental knowledge on the coordination chemistry of CO_2, and on the relevance for catalysis has been acquired throughout the years.[5–7] Molecular catalysis of CO_2 reduction is mostly carried out by (transition-)metal complexes. The molecular approaches are interesting, since they generally allow for high selectivity, high activity and fine-tuning of the catalyst e.g. to mimic efficient enzymes. Consequently, they are able to provide important mechanistic insight.[8,9] Moreover, from a practical perspective, it is straightforward and relatively simple to employ the molecular catalyst by dissolving it in the supporting electrolyte solution. Unfortunately, molecular catalysts are usually less durable than heterogeneous electrocatalysts, and the formation of species beyond 2-electron transfer products (carbon monoxide, formate, oxalate) is scarce.[10,11] Additionally, one may run into solubility issues, especially when working in aqueous media.

4.2 Overview of molecular catalysts for CO_2 electroreduction

Depending on the type of ligands, the homogeneous molecular catalysts for CO_2 reduction can be roughly categorized in:[12]

1. Macrocyclic metal complexes e.g. porphyrins, phthalocyanines, corroles and cyclams.

2. Polypyridyl metal complexes containing e.g. 2,2'-bipyridine (bpy), 1,10-phenanthroline (phen) or 2,2'; 6',2"-terpyridine (tpy) ligands.

3. Phosphine metal complexes containing e.g. 1,2-bis(diphenylphosphino)ethane (dppe) and triphenylphosphine (PPh3) ligands.

Examples of the backbone of macrocyclic complexes often used as molecular CO_2 reduction catalysts are shown in Figure 4.1a-d. Examples of ligands related to polypyridyl- and phosphine complexes are shown in respectively Figure 4.1e-f and Figure 4.1h,i. For a more complete list of different ligands and metal complexes, the reader is referred to excellent reviews in the field.[1,10,12,13]

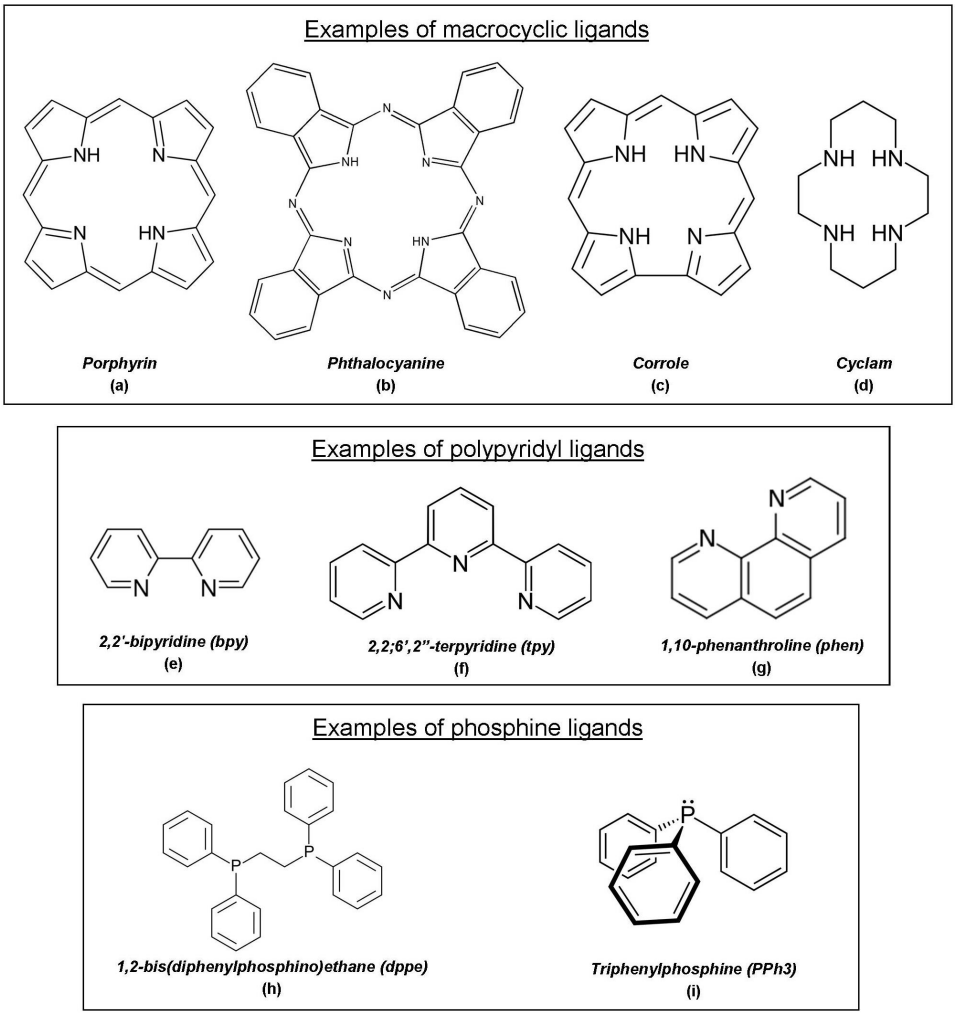

Figure 4.1 Examples of unsubstituted ligands often observed in metal complexes for CO_2 electroreduction: (a-d) macrocyclic ligands, (e-g) polypyridyl ligands and (h,i) phosphine ligands.

In the remainder of this thesis, we will focus on metalloporphyrins. This planar macrocyle has a versatile chemistry and broad range of applications, due to its stability, and variety of possible properties, which can be obtained by modification of peripheral substituents and metal centers. Examples of important metalloporphyrins in nature are heme in the red blood cells (iron porphyrin), and chlorophyll in plants (porphyrin with Mg center). Due to the planarity of the macrocycle, interaction

with the metal center is possible from both sides of the plane. Extensive work on porphyrin (electro)chemistry in general has been summarized in the literature.[14–16]

With respect to the electrocatalytic CO_2 reduction by metalloporphyrins, Fe and Co metal centers have received considerable attention. Savéant and coworkers investigated iron porphyrins to gain insight in the mechanism of CO_2 reduction toward CO.[17] They found that addition of Lewis- and Brønsted acids significantly improves the selectivity toward CO, and the stability of the catalyst.[18–21] Furthermore, modification of the metal center was shown to change the dominant product from CO to HCOOH.[22] Additionally, they report on substituent effects of the catalyst.[23–25] The investigation of CO_2 reduction on these porphyrins started mainly under homogeneous conditions in non-aqueous electrolytes, but more recently shifted toward aqueous electrolytes.[26,27]

4.3 Heterogenization of molecular catalysts

Heterogenization of molecular catalysts can be considered as the bridge between homogeneous- and heterogeneous catalysis, where the catalyst is immobilized on a preferably inert surface. Heterogenization of molecular catalysts is attractive, since much less catalyst is required compared to homogeneous conditions, and the catalyst can be used even when it is not soluble in the supporting electrolyte. Moreover, there are more attractive prospects for industrial scale-up purposes such as generally better robustness and durability of the heterogenized catalyst, and the ability to circumvent product-catalyst separation.[13]

After adsorption, the porphyrin is usually oriented with the macrocycle parallel to the surface.[16] There are several ways of immobilizing the (molecular) catalyst on a surface, *viz.* covalent- or non-covalent adsorption, electropolymerization on the surface, and dispersion in polymer films.[28–30] Studies have been performed on several molecular catalysts, immobilized on different substrates, and by various methods.[13]

Although interesting systems, showing high selectivity and activity for CO_2 reduction, have been reported for heterogenized molecular catalysts, we still lack detailed fundamental insight in order to efficiently produce electrofuels, with high stability. Therefore, it is very important to perform systematic studies to obtain insight beyond the empirical level, especially because of the many variables which may influence the system, as will be discussed in more detail in the subsequent chapters.

4.4 References

[1] J.-M. Savéant, *Chem. Rev.* **2008**, *108*, 2348–2378.

[2] C. Costentin, M. Robert, J.-M. Savéant, *Current Opinion in Electrochem.* **2017**, *1*, 26–31.

[3] M. E. Vol'pin, I. S. Kolomnikov, T. S. Lobeeva, *Izvest. Akad. Nauk SSSR Ser. Khim.* **1969**, *2084*.

[4] M. E. Vol'pin, I. S. Kolomnikov, *Pure Appl. Chem.* **1973**, *33*, 567–582.

[5] W. Leitner, *Coord. Chem. Rev.* **1996**, *153*, 257–284.

[6] D. H. Gibson, *Chem. Rev.* **1996**, *96*, 2063–2095.

[7] X. Yin, J. R. Moss, *Coord. Chem. Rev.* **1999**, *181*, 27–59.

[8] J. Bonin, A. Maurin, M. Robert, *Coord. Chem. Rev.* **2017**, *334*, 184–198.

[9] H. Takeda, C. Cometto, O. Ishitani, M. Robert, *ACS Catal.* **2017**, *7*, 70–88.

[10] J. P. Collin, J. P Sauvage, *Coord. Chem. Rev.* **1989**, *93*, 245–268.

[11] C. Costentin, M. Robert, J.-M. Savéant, *Chem. Soc. Rev.* **2013**, *42*, 2423–2436.

[12] E. E. Benson, C. P. Kubiak, A. J. Sathrum, J. M. Smieja, *Chem. Soc. Rev.* **2009**, *38*, 89–99.

[13] J. L. Inglis, M. T. MacLean, B. J. Pryce, J. G. Vos, *Coord. Chem. Rev.* **2012**, *256*, 2571–2600.

[14] *The Porphyrin Handbook*, *Vol. 1-10*, (Eds.: K. M. Kadish, K. M. Smith, R. Guilard), Academic Press, San Diego, **2000**.

[15] W. Auwärter, D. Écija, F. Klappenberger, J. V. Barth, *Nature Chem.* **2015**, *7*, 105–120.

[16] J. M. Gottfried, *Surf. Sci. Reports* **2015**, *70*, 259–379.

[17] M. Hammouche, D. Lexa, J. M. Savéant, *J. Electroanal. Chem.* **1988**, 347–351.

[18] I. Bhugun, D. Lexa, J.-M. Savéant, *J. Am. Chem. Soc.* **1994**, 5015–5016.

[19] I. Bhugun, D. Lexa, J.-M. Savéant, *J. Am. Chem. Soc.* **1996**, 1769–1776.

[20] I. Bhugun, D. Lexa, J.-M. Savéant, *J. Phys. Chem.* **1996**, *100*, 19981–19985.

[21] M. Hammouche, D. Lexa, M. Momenteau, J.-M. Savéant, *J. Am. Chem. Soc.* **1991**, 8455–8466.

[22] L. Chen, Z. Guo, X.-G. Wei, C. Gallenkamp, J. Bonin, E. Anxolabéhère-Mallart, K.-C. Lau, T.-C. Lau, M. Robert, *J. Am. Chem. Soc.* **2015**, *137*, 10918–10921.

[23] C. Costentin, S. Drouet, M. Robert, J.-M. Savéant, *Science* **2012**, *338*, 90–94.

[24] C. Costentin, M. Robert, J.-M. Savéant, *Acc. Chem. Res.* **2015**, *48*, 2996–3006.

[25] I. Azcarate, C. Costentin, M. Robert, J.-M. Savéant, *J. Am. Chem. Soc.* **2016**, *138*, 16639–16644.

[26] A. Maurin, M. Robert, *J. Am. Chem. Soc.* **2016**, *138*, 2492–2495.

[27] J.-M. Savéant, *ChemElectroChem* **2016**, *3*, 1967–1977.

[28] R. W. Murray, *Acc. Chem. Res.* **1980**, *13*, 135–141.

[29] R. W. Murray, A. G. Ewing, R. A. Durst, *Anal. Chem.* **1987**, *59*, 379A–390A.

[30] C. Sun, R. Gobetto, C. Nervi, *New J. Chem.* **2016**, *40*, 5656–5661.

CHAPTER 5

Influence of the Metal center of Metalloprotoporphyrins on the Electrocatalytic CO_2 reduction to Formic acid

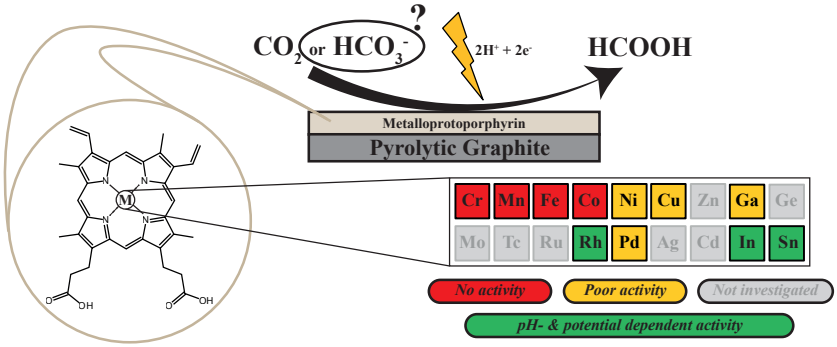

This chapter is based on the article:
Yuvraj Y. Birdja, Jing Shen and Marc T. M. Koper, Catal. Today, 2017, 288, 37-47

Abstract

Electrocatalytic conversion of carbon dioxide has gained much interest for the synthesis of value-added chemicals and solar fuels. Important issues such as high overpotentials and competition of hydrogen evolution still need to be overcome for deeper insight into the reaction mechanism in order to steer the selectivity towards specific products. Herein we report on several metalloprotoporphyrins immobilized on a pyrolytic graphite electrode for the selective reduction of carbon dioxide to formic acid. No formic acid is detected on Cr-, Mn-, Co- and Fe-protoporphyrins in perchloric acid of pH 3, while Ni-, Pd-, Cu- and Ga-protoporphyrins show only a little formic acid. Rh, In and Sn metal centers produce significant amounts of formic acid. However, the faradaic efficiency varies from 1 to 70 % depending on the metal center, the pH of the electrolyte and the applied potential. The differentiation of the faradaic efficiency for formic acid on these metalloprotoporphyrins is strongly related to the activity of the porphyrin for the hydrogen evolution reaction. CO_2 reduction on Rh-protoporphyrin is shown to be coupled strongly to the hydrogen evolution reaction, whilst on Sn- and In-protoporphyrin such strong coupling between the two reactions is absent. The activity for the hydrogen evolution increases in the order In < Sn < Rh metal centers, leading to faradaic efficiency for formic acid increasing in the order Rh < Sn < In metal centers. In-protoporphyrin is the most stable and shows a high faradaic efficiency of ca. 70 %, at a pH of 9.6 and a potential of -1.9 V vs RHE. Experiments in bicarbonate electrolyte were performed in an attempt to qualitatively study the role of bicarbonate in formic acid formation.

5.1 Introduction

In the past few decades the consequences of anthropogenic carbon dioxide accumulation in the atmosphere have been addressed repeatedly. It is nowadays generally accepted that the increasing carbon dioxide levels in the atmosphere pose serious problems if no action is taken.[1] The emission of CO_2 has increased since the industrial revolution, leading to an increased amount of CO_2 in the atmosphere.[2] Accumulation of atmospheric CO_2 leads to the greenhouse effect which contributes to global warming and climate change. Another important sustainability issue is the depletion of fossil fuel sources which is caused by an increasing world population and a changing lifestyle, resulting in an increasing energy demand. Mankind is still strongly dependent on fossil fuels for its energy consumption. A drawback of the use of fossil fuels is the production of CO_2 after combustion which is often simply released in the atmosphere. In the past couple of years much research has been done to mitigate CO_2 accumulation[3–6] and search for renewable energy sources.[7–9] A promising way to utilize CO_2 is by electrochemical CO_2 conversion. Compared to other methods the advantage of electrochemical conversion, when operational on an industrial scale, is two-fold: it reduces the CO_2 emissions in the atmosphere on one hand, and it produces renewable fuels and commodity chemicals on the other. Moreover, additional advantages are the fact that the process can be carried out at ambient conditions, water can be used as hydrogen source and, if the electricity used is produced from renewable sources, one can contribute to a completely sustainable carbon cycle. However, there are still significant hurdles which should be overcome or circumvented, such as the competition of the hydrogen evolution reaction, high overpotentials for CO_2 reduction, poor solubility of CO_2 in aqueous media and the poor selectivity for specific fuels. For implementation in the current infrastructure, liquid fuels are more convenient than gaseous fuels. Therefore much work has been focused on the selective production of methanol, ethanol and formic acid. These fuels can be employed directly in fuel cells to produce electricity (e.g. Direct Methanol Fuel Cell and Direct Formic Acid Fuel Cell). Electroreduction of CO_2 to formic acid is less complex and therefore easier to optimize compared to alcohols, as only two electrons need to be transferred.

Molecular catalysts have been gaining more attention lately as they are relatively inexpensive and more abundantly available compared to (noble) metal catalysts. They usually show high activities and good selectivities for various reactions which can be tuned by modifying the catalyst with additional ligands, using electron-donating or electron-withdrawing groups.[10–13] In homogeneous electrocatalysis, these catalysts are often dissolved in non-aqueous solvents, as they are poorly soluble in aqueous electrolytes. Furthermore, large amounts of catalyst are needed to dissolve in the electrolyte. CO_2 can bind to a metal center which results in its activation[14] by a weakened C-O interaction due to transfer of electron density. After coordination to a metal center, reactions can take place which were initially not possible for free CO_2. Many different molecular catalysts have been reported

for CO_2 reduction such as porphyrins, phthalocyanines, cyclams, phosphines and polypyridines.[15,16]

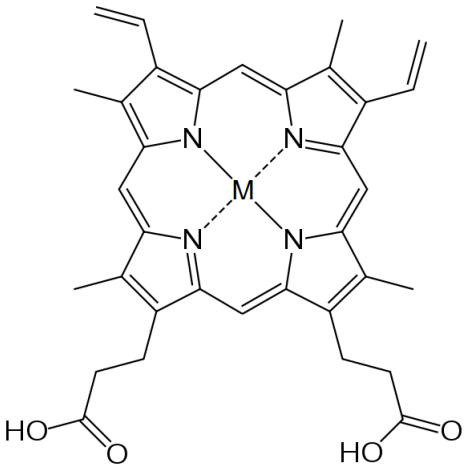

Figure 5.1 Chemical structure metalloprotoporphyrins

Immobilization of molecular catalysts should in principle combine the best of both worlds: molecular catalysis on heterogeneous surfaces.[17,18] A system with high efficiency and selectivity can be created whereby the catalyst structure can be modified by addition of specific ligands e.g. to change the catalyst electronic properties which is very useful for mechanistic studies or controlling the selectivity. Furthermore, only a small amount of the catalyst is required and even catalysts insoluble in certain solvents can still be used when immobilized on a surface. Deactivation processes often encountered in homogeneous systems, such as dimerization and aggregation of the catalyst, can be circumvented. In the literature many different systems based on immobilized catalysts have been described: covalent attachment of the catalyst by using e.g. aryl diazonium salts, 4-aminopyridine,[19–21] non-covalent attachment of the catalyst (drop-casting)[22,23] and dispersion of the catalyst in polymer films.[24–27]

In this work we will focus on one type of molecular catalysts, namely metalloprotoporphyrins (MPPs) which are a subgroup of the more general metalloporphyrins. Metalloporphyrins are complexes that consist of a metal center within a heterocyclic macrocycle composed of four pyrole groups attached to each other with methine bridges. Protoporphyrins have two vinyl, two propionic acid and four methyl groups attached to the porphyrin ring as shown in Figure 5.1. Metalloprotoporphyrins are an important precursor for essential molecules in biology such as the heme-group in our red bloodcells and chlorophylls in plants (protoporphyrins with respectively an Fe^{2+} and Mg^{2+} metal centers). Furthermore it has been shown that (immobilized) metallo(proto)porphyrins are good catalysts for e.g. the oxygen reduction

reaction, hydrogen evolution reaction, carbon dioxide reduction and nitrate reduction.[10,16,28,29] Savéant and Robert and coworkers have conducted extensive research on molecular catalysts for CO_2 reduction and how to influence the selectivity.[30,31] They recently showed that CO or HCOOH is produced by changing the metal center of the complex.[32] The selectivity issue is important from a fundamental point of view and therefore also the subject of theoretical studies,[33,34] in which it has been shown that a different binding mode of CO_2 to the metal center leads to either CO or HCOOH.

In this paper, the selectivity towards formic acid is investigated experimentally where the role of the metal center is scrutinized by studying the pH effect, the concomitant hydrogen evolution and the nature of the electroactive species (i.e. CO_2 or HCO_3^-) on different metalloprotoporphyrins immobilized on pyrolytic graphite.

5.2 Experimental

The electrochemical experiments were performed in a one-compartment three-electrode cell at room temperature and ambient pressure. All glassware was first cleaned by boiling in a 1:1 mixture of concentrated sulfuric and nitric acid. Before each experiment the glassware was boiled three times in ultrapure water (Millipore MilliQ gradient A10 system, 18.2 MΩ·cm). The long-term electrolysis experiments were carried out in a two-compartment three-electrode cell (H-type cell), where the working electrode (WE) and counter electrode (CE) compartments were separated by a nafion membrane (Nafion 115).

The WE was a pyrolytic graphite (PG) disc with a diameter of 5 mm or 10 mm used in a hanging meniscus configuration. The large PG electrodes were used for HPLC measurements to generate larger amounts of products. The reported current density is normalized by the geometric surface area of the WE. A platinum gauze and a reversible hydrogen electrode (RHE) in the same electrolyte were used as CE and reference electrode (RE) respectively. Unless mentioned otherwise, the potentials in this paper are referred to this reference electrode. Prior to each experiment, the WE was polished with sandpaper (first P600 and then P1000) and ultrasonicated for approximately 2-3 minutes in water. Blank cyclic voltammograms were recorded at a scan rate of 500 mV s^{-1} until a stable voltammogram was obtained (typically around 50 cycles) to ensure a clean PG surface. After immobilization of porphyrins a blank cyclic voltammogram was recorded again in order to qualitatively verify the immobilization of the porphyrin (as shown in Figure B.1 in Appendix B). Metalloprotoporphyrins (MPPs) were immobilized on PG by drop casting from a 0.01 M borate solution of pH 10 in which the porphyrin was dissolved to a concentration of 0.5 mM.[35]

Electrolyte solutions were prepared with ultrapure water. Pyrolytic graphite working electrodes were cut in-house from a high purity pyrolytic graphite plate (PY001009, Graphite Store, USA). High purity chemicals were used: perchloric acid and phosphoric acid (Merck Suprapur), potassium phosphate mono- and dibasic

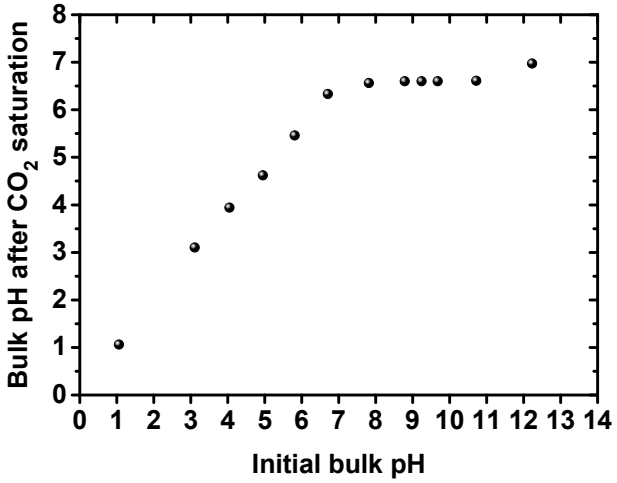

Figure 5.2 Bulk pH of the used electrolytes before and after CO_2 saturation

(Sigma Aldrich, TraceSelect), potassium phosphate tribasic (Sigma Aldrich, Reagent grade), sodium perchlorate (Sigma Aldrich, ACS reagent) and potassium bicarbonate (Sigma Aldrich, trace metals basis). All the porphyrins were purchased from Frontier Scientific and used without further purification. Before each experiment the cell was deaerated with argon (Linde, Argon 6.0 Scientific). For CO_2 reduction, the cell was saturated with CO_2 by purging the cell with CO_2 (Linde, Carbon dioxide 4.5) for at least 20 minutes. Hydrogen 6.0 Scientific (Linde) was used for the RHE reference electrode. A μ-Autolab Type III (Metrohm Autolab B.V.) was used for voltammetric experiments with sample collection and an IviumStat or CompactStat (Ivium Technologies) was used to perform chronoamperometry and electrochemical impedance spectroscopy. Experiments were carried out in unbuffered perchloric acid of pH 1 and 3 and in a variety of different phosphate buffer solutions in the pH range of 3 to 12 (see table B.1 in the Appendix B). Although the actual pH will be lower when the electrolyte is saturated with CO_2, the different electrolytes will be referred to by their pH as measured prior to CO_2 saturation. Figure 5.2 shows the relation between the pH before and after CO_2 saturation indicating that the pH after CO_2 saturation is approximately the same (≈ 6.6) for almost all neutral and alkaline phosphate buffers. As we will see later, there are differences between these initially neutral and alkaline electrolytes in terms of faradaic efficiencies and product distribution. Therefore for a better discrimination between the different electrolytes we refer to them by the initial bulk pH. For correct measurements versus the RHE scale, the Luggin capillary and the RHE compartment were also filled with CO_2 saturated electrolyte. Furthermore, under reduction conditions, especially when H_2 is evolved, the pH near the electrode ("local pH") may differ from the pH in the bulk. This may affect the onset potential for product formation as well as product

selectivity. As quite high currents were obtained, especially at the ⌀ 10 mm PG electrode, ohmic drop could not be neglected. Hence, the solution resistance was determined by potentiostatic electrochemical impedance spectroscopy. The obtained value was used to correct the voltammograms after the electrochemical data was collected. For chronoamperometry (electrolysis experiments) the potentiostat's IR compensation function was used to compensate for ohmic drop during measurement. Details can be found in Appendix B, section B.2.

OnLine Electrochemical Mass Spectrometry (OLEMS) was utilized for the detection of volatile reaction products. A tip, which is placed close ($\approx$ 10 μm) to the electrode surface, continuously collects volatile reaction products from the electrode interface. The tip has a diameter of 0.5 mm and consists of a porous teflon cylinder (average pore size 10-14 μm) in a Kel-F holder and is connected to an EvoLution mass spectrometer (European Spectrometry Systems Ltd.) by a PEEK capillary.[36] A Quadrupole Mass Spectrometer Prisma QMS200 (Pfeiffer) is brought to vacuum with a TMH-071P turbo molecular pump(60 l s^{-1}, Pfeiffer) and a Duo 2.5 rotary vane pump (2.5m^3 h^{-1}, Pfeiffer). Prior to experiments, the tip was cleaned in 0.2 M $K_2Cr_2O_7$ in 2 M H_2SO_4 and rinsed with ultrapure water. A SEM voltage between 1200 V and 2400 V was used for the different mass fragments. All mass fragments showed a decay during measurement which is the result of slow equilibration of the pressure in the system. This was corrected for by subtracting a double exponential fit to datapoints where no change in activity is observed from the whole dataset. The mass fragments shown in this paper are all background corrected in this manner.

Online High Performance Liquid Chromatography (online HPLC) is the technique employed to analyze non-volatile reaction products. A similar tip to the one for OLEMS, however, without a porous teflon cylinder, is placed near the electrode surface.[37] Samples with a volume of 60 μl were collected with a fraction collector (FRC-10A, Shimadzu) at a rate of 60 μl min^{-1} (LC-20AT pump, Shimadzu). Since the scan rate of the potential sweep during sample collection was 1 mV s^{-1}, each sample held the averaged concentration of a 60 mV potential difference. The samples were analyzed after voltammetry with HPLC (Prominence HPLC, Shimadzu). The samples were placed in an auto-sampler (SIL-20A) which injects 20 μl of the sample into the column. An Aminex HPX 87-H (Bio-Rad) column with a Micro-Guard Cation H Cartridge (Bio-Rad) in front were used. The eluent was 5 mM H_2SO_4 and the eluent flow rate 0.6 ml min^{-1}. The column and the refractive index detector (RID-10A) were maintained at a temperature of 35 °C.

The reported results were all reproduced at least twice and all electrochemical measurements (CV, OLEMS, online HPLC and Chronoamperometry) showed qualitatively the same results (HCOOH trend, current densities, onset potentials, etc.). From a quantitative point of view, the results sometimes could be slightly different, which is ascribed to a different PG surface each time after polishing the PG electrode as can be observed from the blank voltammograms recorded prior to the experiments. This is also the reason that for the standard error analysis in the HPLC results, only the concentration analysis of liquid phase is taken into account

(concentrations are often low and the baseline noisy, which leads to different peak areas for different experiments).

5.3 Results & Discussion

5.3.1 Activity of Metalloprotoporphyrins in perchloric acid pH 3

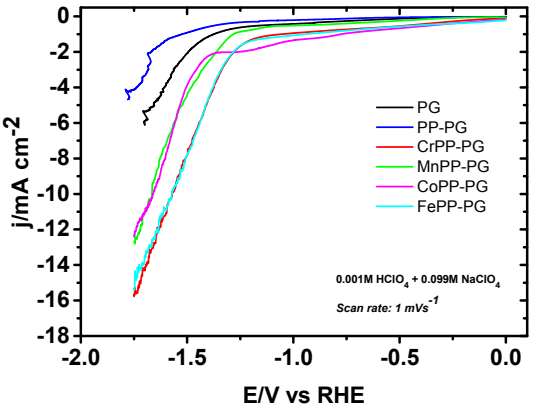

Figure 5.3 Linear Sweep Voltammetry in CO_2 saturated 0.001 M $HClO_4$ + 0.099 M $NaClO_4$. Scan rate: 1 mV s^{-1}.

For a proper attribution of the effect of the metal center on the activity or selectivity for the electrocatalytic CO_2 reduction, the influence of the bare substrate (PG) and the porphyrin macrocycle should first be known. Therefore, CO_2 reduction on pristine PG and on metal-less or free base PP immobilized on PG (denoted as PP-PG) was investigated. With online HPLC during voltammetry it was confirmed that no formic acid or other liquid products are produced at any potential on pristine PG nor on PP-PG. On-Line Electrochemical Mass Spectrometry showed that the only product from CO_2 reduction on PG and PP-PG is H_2 (see Figure B.2 in Appendix B and also reference.[38])

Some of the investigated protoporphyrins with certain metal centers produce no formic acid or amounts lower than the detection limit. These protoporphyrins have a Cr, Mn, Co or Fe center. With OLEMS, no gaseous products other than H_2 are observed on MnPP, InPP, CrPP, SnPP and GaPP (Figure B.4). On FePP, RhPP and CuPP small amounts of CH_4 are detected and on NiPP small amounts of CO and CH_4 are detected as shown in Figure B.5. CoPP was recently shown to produce CO at pH 3 with high faradaic efficiency but no formic acid which is in agreement with our results. Moreover, a lower amount of CO was formed at pH 1 together with methane and a small amount of formic acid.[38] Comparing the curves in Figure

5.3, it can be seen that PP-PG has a lower current compared to the pristine PG. The other MPPs show higher currents, indicating that the metalloprotoporphyrins are active for the hydrogen evolution reaction (HER) or CO_2 reduction, while PP presumably blocks active sites for HER and CO_2 reduction on PG. This confirms that the metal center is of importance for catalysis. The fluctuations in the CV at very negative potentials are the result of H_2 bubble formation and their detachment from the electrode surface. The current spikes appear skewed in some of the later voltammograms because of the post-measurement Ohmic drop correction.

In addition to the MPPs which are not active for formic acid production from CO_2, there is a set of MPPs which produce trace amounts of formic acid, as shown in Figure 5.4a. These are the MPPs with Ni, Ga, Pd or Cu metal centers. The results have been reproduced and the standard errors in the concentration are shown in the graphs as well. OLEMS results again do not show significant amounts of other CO_2 reduction products besides H_2.

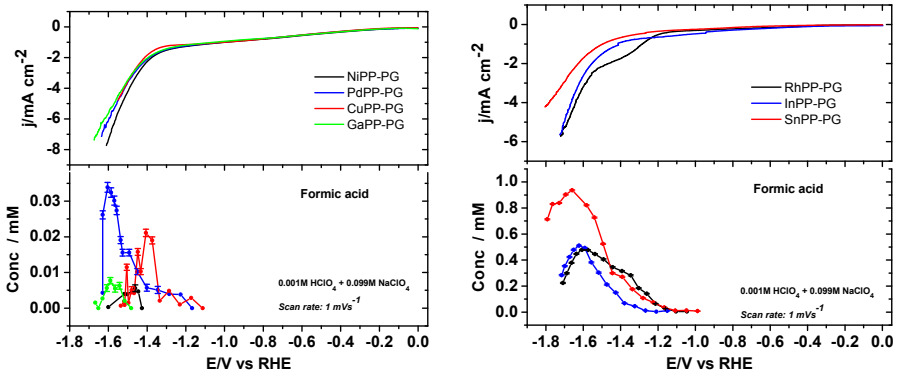

(a) Poorly active MPPs **(b)** Active MPPs

Figure 5.4 Formic acid production on Metalloprotoporphyrins in 0.001 M $HClO_4$ + 0.099 M $NaClO_4$. Scan rate: 1 mV s^{-1}.

The most interesting MPPs for this study are SnPP, InPP and RhPP as these are able to produce significant amounts of formic acid from CO_2 as seen in Figure 5.4b. As with the other MPPs there are no significant amounts of reaction products other than H_2 observed with OLEMS. All of these protoporphyrins show the same trend in formic acid concentration during Linear Sweep Voltammetry, with SnPP and RhPP having a slightly less negative onset potential for HCOOH formation than InPP. In and Sn metal centers were also identified to be active for CO_2 reduction to formic acid on phthalocyanines which are similar molecular catalysts to porphyrins.[39] More interesting is the fact that RhPP produces significant amounts of formic acid from CO_2. It has been reported that In and Sn metal electrodes mainly produce HCOOH, while Rh metal mostly forms H_2.[40] Rh metal only shows activity for CO_2 reduction at elevated pressures.[41] Rh complexes have been shown to be active

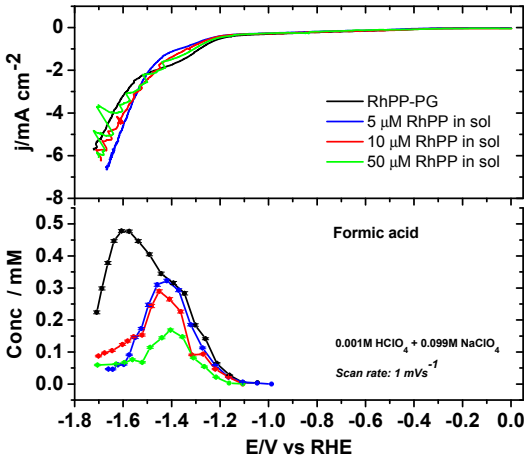

Figure 5.5 CO_2 reduction on PG in RhPP containing electrolytes and immobilized RhPP on PG. Electrolyte solution 0.001 M $HClO_4$ + 0.099 M $NaClO_4$. Scan rate: 1 mV s^{-1}.

for hydrogenation of CO_2 to formic acid, albeit that they often do not operate in aqueous media without specific ligands.[42–44] Much research has been done on CO_2 hydrogenation to formic acid, but electrocatalytic reduction of CO_2 to formic acid on Rh porphyrins or similar Rh molecular catalysts has not been investigated in depth. Older work exists on Rh complexes dissolved in non-aqueous media[45,46] for which formic acid production was also observed.

In Figure 5.5, a comparison is made between immobilized RhPP on PG and different amounts of RhPP in the electrolyte with a pristine PG electrode. The current densities and the trends in HCOOH concentration are similar. However, at a certain potential the formic acid concentration reaches a maximum and starts to decrease for RhPP in solution, while the RhPP-PG electrode continues to produce formic acid. The maximum for RhPP-PG is higher and at more negative potentials compared to RhPP in solution. Another observation is that a larger concentration of RhPP in solution leads to a lower amount of formic acid produced. This can be explained by inhibition of active sites with more RhPP molecules present in solution. These results show the superiority of immobilized metalloprotoporphyrins with respect to metalloprotoporphyrins dissolved in the aqueous electrolyte.

5.3.2 Activity of Metalloprotoporphyrins in other electrolytes

The formic acid producing MPPs from the previous paragraph were studied for their pH dependence is investigated in order to obtain more mechanistic insight. The aim is to deduce the origin of the activity of RhPP for CO_2 reduction to formic

acid and identify possible differences between the MPPs as well as to identify the optimal conditions for formic acid formation.

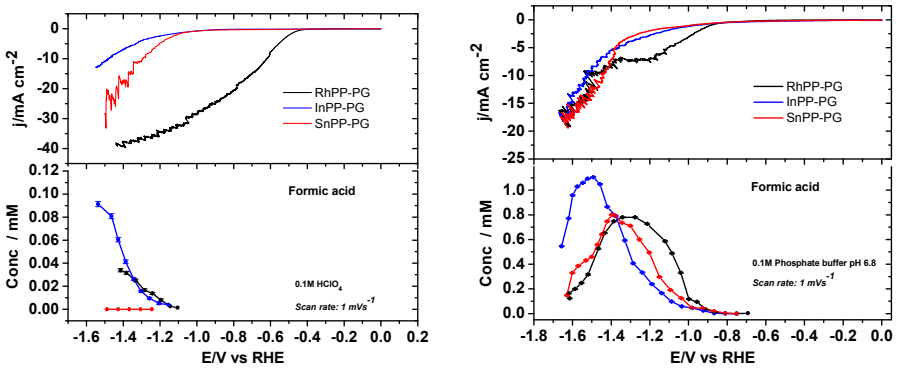

(a) pH = 1 **(b)** pH = 6.8

Figure 5.6 CO_2 reduction on formic acid producing MPPs in (a) 0.1 M $HClO_4$ and (b) phosphate buffer of pH 6.8. Scan rate: 1 mV s^{-1}.

In the 0.1 M $HClO_4$ electrolyte, all of these MPPs produce significantly less formic acid than in pH = 3 $HClO_4$ electrolyte as shown in Figure 5.6a. Interestingly, a difference between the three formic acid producing MPPs is observed. In pH 1 InPP and RhPP still produce some HCOOH while SnPP only shows negligible amounts of HCOOH. The current generated by the InPP is much smaller compared to that of the other porphyrins. This is ascribed to a lower activity for hydrogen evolution, which also influences the faradaic efficiencies as will be discussed in a following section. Moreover, the onset potentials of the current profiles of the MPPs are quite different, in that RhPP has the least negative onset potential and InPP the most negative onset potential. This is probably associated with a difference in activity for the HER on these MPPs. In pH 6.8 (0.1 M phosphate buffer) comparable amounts of formic acid are formed as in pH 3, as illustrated in Figure 5.6b.

Different phosphate buffer solutions were used for the study in electrolytes with a pH range from 3 till 12. Even though the bulk pH will be lower when the electrolyte is saturated with CO_2, the different electrolytes will be referred to by their pH as measured prior to CO_2 saturation. The formic acid production during the negative potential sweep on the three HCOOH-producing MPPs in the different electrolytes is shown in Figure 5.7a -5.9a. The current profiles of RhPP show a plateau between -0.9 V and -1.5 V (see inset) while InPP and SnPP show no such plateau current (this is also visible in Figures 5.4b and 5.6b). On RhPP the formic acid concentration profile shows a maximum which appears to be at potentials within this plateau region. Moreover, the HCOOH concentration profiles for RhPP are slightly shifted towards positive potentials for higher pH whereas those for InPP and SnPP do not show such a potential shift. This is better visible when the concentration profiles are normalized by their maximum concentration (as

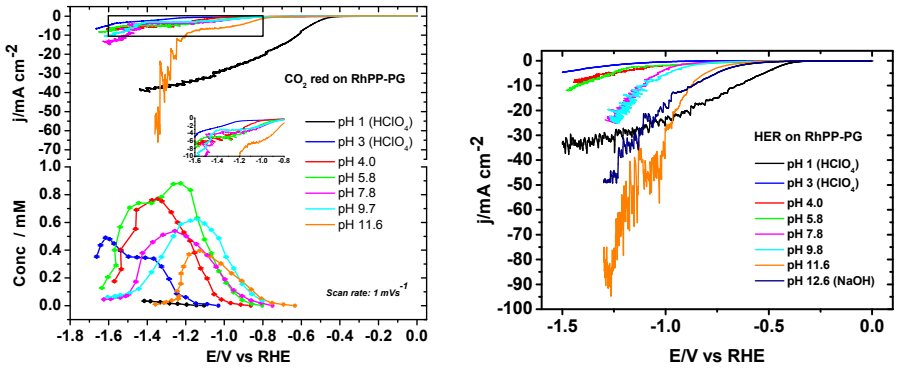

(a) (b)

Figure 5.7 CO_2 reduction (a) and hydrogen evolution (b) on RhPP in electrolytes with different pHs

shown in Figure B.6 in Appendix B). In the same figures 5.7b - 5.9b the hydrogen evolution current on the three MPPs is shown in the same electrolytes. In these voltammograms no current plateau region is observed as for CO_2 reduction on RhPP, implying that this plateau feature is specifically related to CO_2 reduction. Moreover, there is a clear distinction between the current profiles in the different phosphate buffer electrolytes for all MPPs. The onset of hydrogen evolution seems strongly related to the pH of the phosphate buffers. At high pH (11.6) there is less negative onset of H_2 evolution and very high currents, while low pH (4 and 5.8) shows a more negative onset potential for HER and the currents are low. In general, the currents are much higher for RhPP compared to InPP and SnPP, indicating the better activity of RhPP for the HER. Comparing the current profiles for CO_2 reduction and HER on all three MPPs, the HER is somewhat inhibited by CO_2 reduction as the reduction onset is delayed to more negative potential and the currents are much lower. For RhPP the onset of the HER is close to/within the plateau region. The maximum HCOOH production also lies within this potential range and shifts to positive potentials with higher pH. As the maximum of HCOOH production can be interpreted to be the result of the competition between hydrogen evolution and CO_2 reduction, it seems plausible to associate the current plateau with this competition. The fact that the current plateau is not observed for InPP and SnPP could be due to the decoupling or weak coupling between CO_2 reduction and HER on these materials. The onset potential of the HER is more negative for SnPP and InPP compared to RhPP. The competition of CO_2 reduction and HER is important for high faradaic efficiencies towards HCOOH as will be discussed in a later section.

To investigate the pH effect more quantitatively, we define the onset potential for HCOOH and H_2. The onset potential is determined based on the HCOOH concentration profile and the current profiles. The onset potential based on the

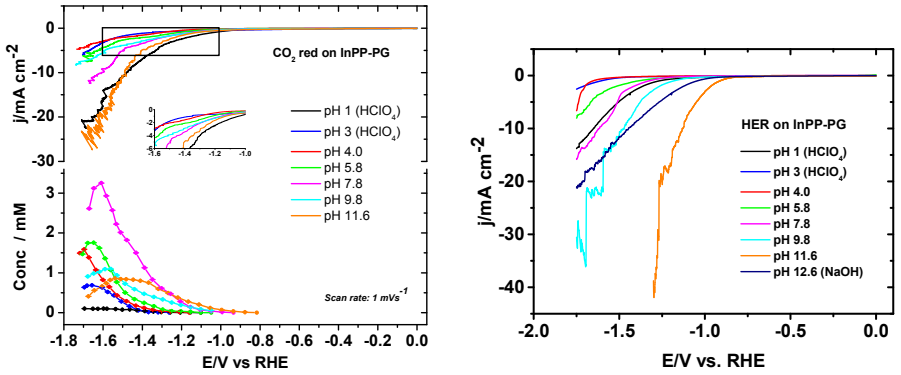

(a) (b)

Figure 5.8 CO_2 reduction (a) and hydrogen evolution (b) on InPP in electrolytes with different pHs

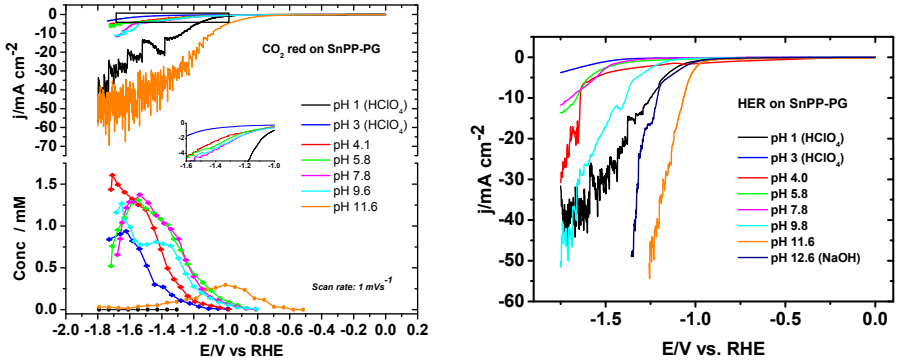

(a) (b)

Figure 5.9 CO_2 reduction (a) and hydrogen evolution (b) on SnPP in electrolytes with different pHs

concentration is defined as the average potential of the potentials where the concentration of HCOOH reaches 0.01 mM, 0.03 mM and 0.05 mM. The potentials corresponding to these different concentrations lead to a similar trend. This is shown in Figure B.7 in Appendix B. Similarly, the onset potential based on the current density is defined as the average of the potentials corresponding to different current densities within the range of 0.25 - 1 mA cm^{-2}. The onset potentials are converted to the NHE scale, and the trends for the 3 MPPs are shown in Figure 5.10. The data within the shaded area correspond to the phosphate buffer electrolytes. Note that the analysis of the onset potentials is only performed for a better comparison between the different MPPs and not to derive underlying mechanistic information.

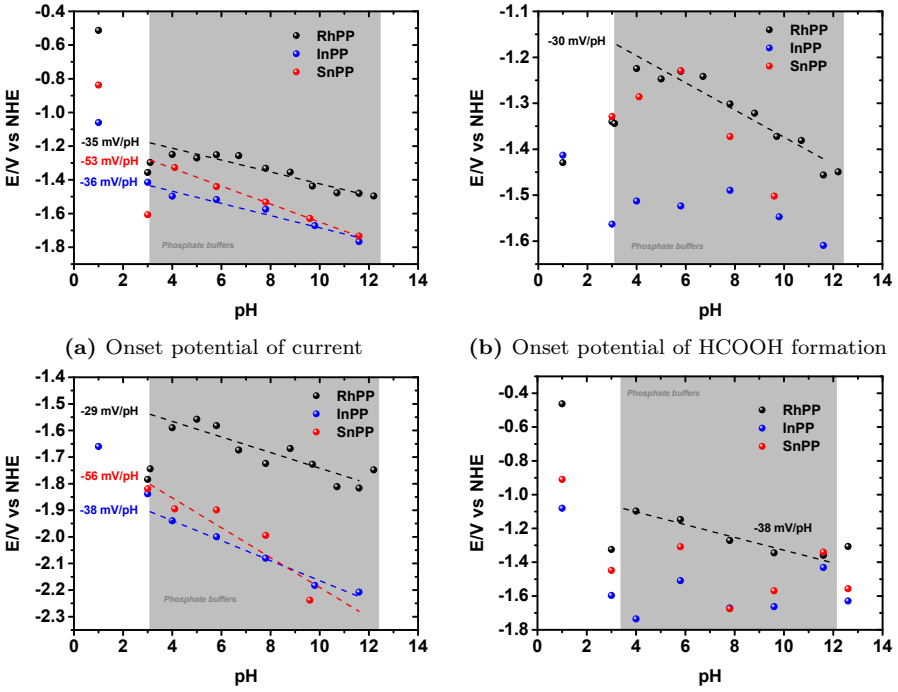

(a) Onset potential of current

(b) Onset potential of HCOOH formation

(c) Potential of maximum HCOOH formation

(d) Onset potentials HER

Figure 5.10 Onset potentials based on (a) the current for CO_2-saturated solution, (b)the HCOOH concentration profile, (c) the maximum concentration of HCOOH and (d) the current of the HER

The difference in pH before and after CO_2 saturation as mentioned in the experimental section, will not affect these results, since all the MPPs are measured in the same electrolyte. The buffer capacity of the electrolyte may play an important role on the selectivity for CO_2 reduction.[47,48] As shown in Figure B.10, a higher buffer capacity leads to higher currents and affects the catalytic activity of the porphyrin towards formic acid. Therefore, the electrolyte pH is not the only factor influencing the catalytic activity of the immobilized porphyrins The onset potentials at pH 1 are quite different, because the influence of proton reduction is dominant here. As can be seen in Figure 5.10a, the onset potential shows a linear dependence on pH for all MPPs. The pH dependence (slope) is not the same for the three MPPs. The onset potential of SnPP shifts with 53 $\pm$ 2 mV pH^{-1} while for InPP and RhPP they shift with 36 $\pm$ 5 and 35 $\pm$ 4 mV pH^{-1}. A slope of 59 mV pH^{-1} on the NHE potential scale would indicate a concerted proton-electron transfer mechanism.[49] It is difficult to say if SnPP follows a concerted proton-electron transfer mechanism solely based on the analysis of the onset potentials. However, the results indicate

that there is probably a difference in mechanism between SnPP on one hand and RhPP and InPP on the other hand. Another distinction between SnPP and RhPP or InPP is the fact that at pH 11.6 only small amounts of HCOOH are formed on SnPP, while reasonable amounts of HCOOH are produced on InPP and RhPP. For RhPP similar pH dependences are observed for the onset of HCOOH and for H_2 formation (Figures 5.10a and 5.10d), indicating that the CO_2 reduction to HCOOH on RhPP is coupled to the concomitant HER, as already suggested before. InPP and SnPP do not exhibit a clear linear pH dependence for HER (see Figure 5.10d), which suggests that the trend observed in Figure 5.10a is related to the CO_2 reduction rather than to the HER. On InPP and SnPP, CO_2 reduction and HER are not strongly coupled, as concluded before. On RhPP the potentials of maximum HCOOH production (Figure 5.10c) show a similar slope to that of the onset potentials of HCOOH (Figure 5.10b) confirming the earlier observation of a potential shift of the concentration profiles with pH, in contrast to InPP and SnPP where a similar slope is only observed for the HCOOH maxima and onset potential of the current (Figures 5.10a and 5.10c). Furthermore, the onset potentials of RhPP are always at more positive potentials compared to those of InPP and SnPP. This difference in onset potentials confirms that RhPP is more active for the HER.

5.3.3 Faradaic Efficiencies

For a further comparison of the activity between the MPPs, the faradaic efficiencies were determined during 2 hour electrolysis in a two-compartment cell. The faradaic efficiencies for formic acid in $HClO_4$, pH 3 for all the three MPPs at different potentials are shown as a function of time in Figure 5.11. For RhPP and SnPP the faradaic efficiencies always decay with time to values of $\approx$ 1-2%. Interestingly InPP seems to reach a steady state value of $\approx$ 10-15 %. This indicates that the immobilized porphyrins on PG are not very stable or deactivate rather quickly, especially RhPP-PG and SnPP-PG. Improving the performance of the immobilized porphyrins is beyond the scope of this paper. However, we believe that the deactivation is related to the catalyst instead of deposition of poisoning species on the surface or blockage of the active sites by intermediates. As shown in Figure B.9 the blank voltammogram of the immobilized porphyrin on PG is compared with the blank voltammogram after CO_2 reduction or HER. It can be seen that the porphyrin-specific redox peaks have disappeared and the background current has changed. Therefore we believe that the decrease in activity is associated with deactivation of the porphyrin structure or detachment of the porphyrin from PG. It is assumed that the very negative potentials ultimately are destructive for the immobilized porphyrins. RhPP shows lower faradaic efficiencies compared to SnPP which in turn is lower compared to InPP. The faradaic efficiencies determined after 10 minutes in $HClO_4$ pH = 3 are plotted against the applied potentials in Figure 5.12a. The potential where the highest faradaic efficiencies are obtained in pH 3 is around E = -1.3 V for RhPP, around E = -1.9 V for InPP, and approximately E = -1.5 V for SnPP. This

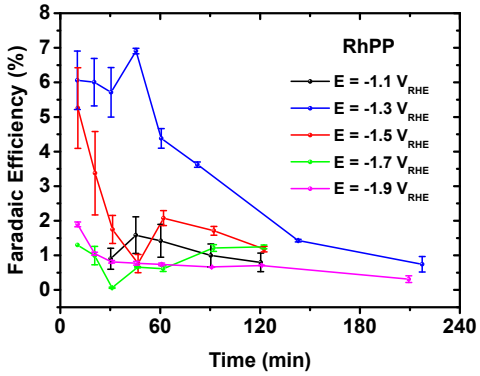

(a) RhPP

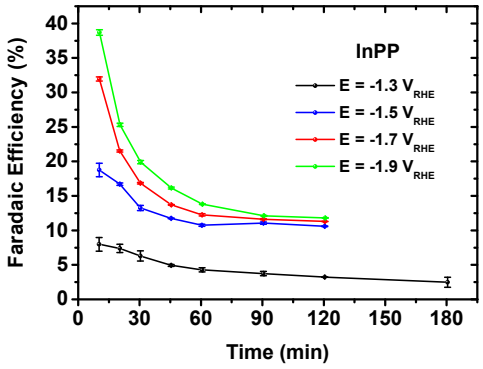

(b) InPP

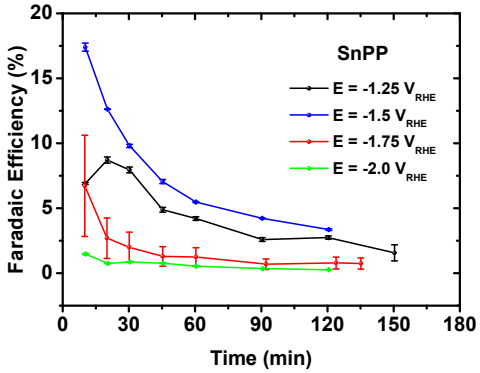

(c) SnPP

Figure 5.11 Faradaic efficiencies in 0.001 M $HClO_4$ + 0.099 M $NaClO_4$ on different MPPs as a function of time

trend depends on the electrolyte, as can be seen in Figure 5.12b, where the same is depicted for a phosphate buffer of pH 5.8. When only experiments at an applied potential of E = -1.5 V are considered, the influence of the pH can be revealed as seen in Figure B.8 in Appendix B. The initial faradaic efficiency of the different MPPs as a function of pH is shown in Figure 5.13. The faradaic efficiency of InPP at pH 9.6 seems to be optimal and reaches a value close to 70 %.

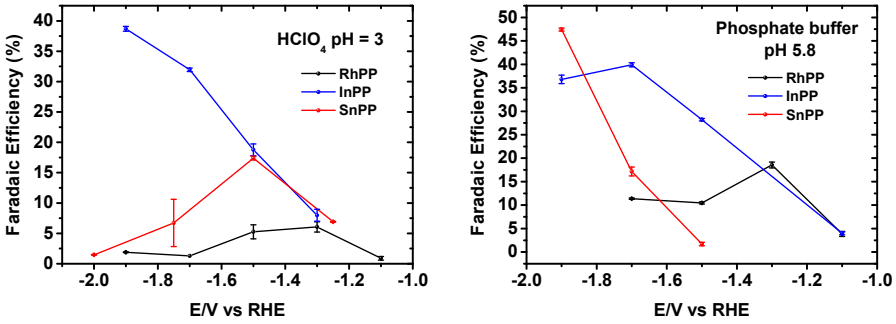

Figure 5.12 Faradaic efficiencies determined at t = 10 min, as a function of potential in (a) 0.001 M $HClO_4$ + 0.099 M $NaClO_4$ and (b) phosphate buffer of pH 5.8

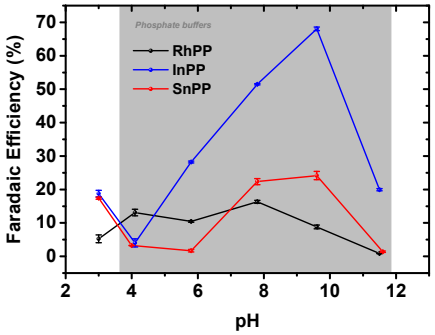

Figure 5.13 Faradaic efficiencies determined at t = 10 min, at E = -1.5 V as a function of pH

5.3.4 Electroactive species

The fact that even in quite alkaline electrolytes HCOOH is produced, could indicate that not (only) CO_2 is the electroactive species but for instance bicarbonate is involved in the formation of formate. In the literature on electrocatalytic CO_2 reduction there has been controversy about the real electroactive species during

CO_2 reduction at different pH and at different catalysts. Often dissolved CO_2 has been identified as the electroactive species,[50,51] but there are also systems where bicarbonate has been suggested to be the key reactant specifically for the formation of formic acid/formate.[52–56]

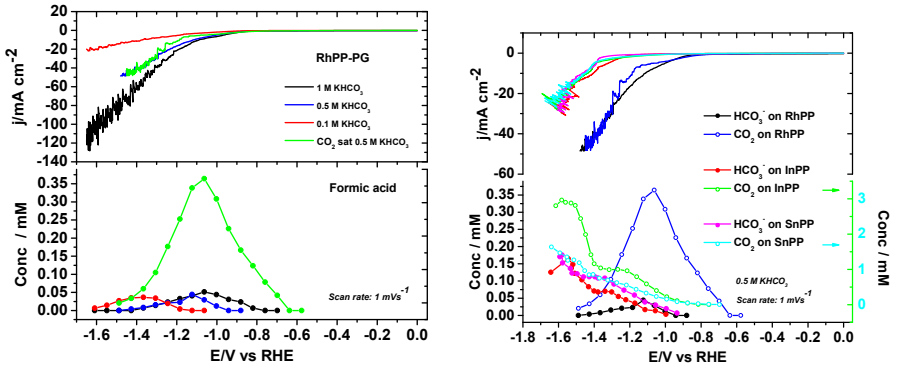

(a) CO_2/HCO_3^- reduction on RhPP **(b)** Effect of CO_2 on HCOOH concentration

Figure 5.14 CO_2/HCO_3^- reduction in $KHCO_3$ on the different MPPs. Scan rate: 1 mV s^{-1}.

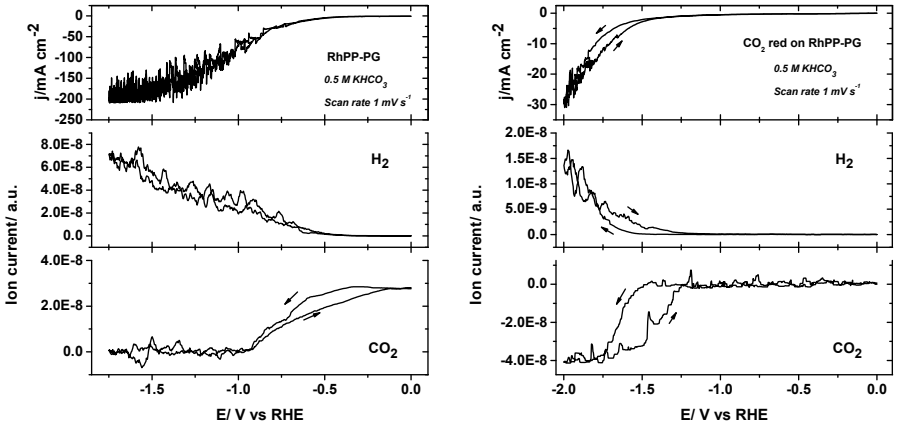

(a) Without CO_2 bubbling **(b)** With CO_2 bubbling

Figure 5.15 H_2 and CO_2 signals during CO_2/HCO_3 reduction in 0.5 M $KHCO_3$. Scan rate: 1 mV s^{-1}.

To probe the role of HCO_3^-, we studied different concentrations of $KHCO_3$ as electrolyte with and without CO_2 saturation. In Figure 5.14a it is shown that a higher concentration of $KHCO_3$ leads to a larger amount of HCOOH formed on

RhPP when no CO_2 is sparged through the solution. If the electrolyte is saturated with CO_2 an even larger amount of HCOOH is produced. This is observed for InPP and SnPP as well, as shown in Figure 5.14b. The HCOOH concentration on InPP and SnPP is increased by a factor of more than 10 when CO_2 is purged through the solution. These results give a first impression that CO_2 should be the dominant electroactive species, however, it is still not conclusive enough to rule out HCO_3^- as reactive species. OLEMS experiments in $KHCO_3$ with and without CO_2 bubbling shown in Figure 5.15, indicate that CO_2 does have an influence as the H_2 evolution and CO_2 consumption are delayed. Even without CO_2 saturation, the CO_2 mass signal decreases during the negative potential sweep implying that the origin of the formed HCOOH is the $KHCO_3$ electrolyte itself. However, during the negative potential sweep the pH in the vicinity of the working electrode increases as a result of the reactions shown in equations (5.1) and (5.2). This higher local pH could lead to a local conversion of CO_2 to HCO_3^- (equation (5.3)), which may influence the direct bicarbonate reduction mechanism to formate. In previous studies, direct bicarbonate reduction has been suggested on palladium, lead and copper electrodes.[53–56] The experiments performed in this study only provide qualitative information about the influence of CO_2 and HCO_3^-. The simultaneous measurement of the local concentrations of formate, CO_2 and bicarbonate during voltammetry is crucial in order to shed more light on this debate.

$$2H^+ + 2e^- \rightarrow H_2 \tag{5.1}$$

$$2H_2O + 2e^- \rightarrow H_2 + 2OH^- \tag{5.2}$$

$$CO_2 + OH^- \rightarrow HCO_3^- \tag{5.3}$$

5.4 Conclusions

In this study we investigated the influence of the metal center of metalloprotoporphyrins for the electrocatalytic reduction of CO_2 towards formic acid. We found that Sn, In and Rh metal centers are able to produce significant amounts of HCOOH while Ni, Ga, Pd and Cu metal centers only show trace amounts of HCOOH. Metalloprotoporphyrins with Cr, Mn, Co or Fe centers do not produce measurable amounts of HCOOH. Moreover, immobilizing the MPPs on PG shows increased activity and stability compared to homogeneous catalysis with the complex in solution.

The hydrogen evolution reaction plays an important role in the difference in activity towards HCOOH formation on RhPP, InPP and SnPP. RhPP is the most active for HER and InPP the least active. Consequently, InPP shows high faradaic efficiency towards HCOOH formation from CO_2 and RhPP low faradaic efficiency. SnPP lies in between with moderate activity for HER and faradaic efficiency towards

HCOOH. All catalysts deactivate with time, however, the deactivation of InPP seems to be less compared to RhPP and SnPP.

All three HCOOH-producing MPPs show a pH dependence for CO_2 reduction as well as for HER. At very low pH, the proton reduction is dominant which results in little or no HCOOH formed. At very alkaline pHs, the HER also seems to be dominant, leading to poor selectivity towards HCOOH. The optimal pH is around 9.6 for InPP and between 7-10 for SnPP. The ideal situation (highest faradaic efficiencies) is different for the three MPPs in terms of electrolyte solution and applied potential. The best performance observed in this study is for InPP in pH 9.6 electrolyte where faradaic efficiencies of ≈ 70 % were obtained.

This work highlights some important properties of metalloprotoporphyrins for electrocatalytic CO_2 reduction to formic acid. However, there is no concensus yet about the electroactive species for the formation of formic acid. Quantitative measurement of HCO_3^-, CO_2 and HCOOH concentrations during voltammetry would be necessary in this respect. For a detailed investigation of the mechanism, the support of theoretical calculations such as in ref.[34] is also desirable.

5.5 References

[1] I. Dincer, *Energy Policy* **1999**, *27*, 845–854.

[2] IPCC in *Climate Change 2014: Synthesis Report. Contribution of Working Groups I, II and III to the Fifth Assessment Report of the Intergovernmental Panel on Climate Change*, (Eds.: Core Writing Team, R. K. Pachauri, L. A. Meyer), IPCC, Geneva, Switzerland, **2014**, 151 pp.

[3] S. Bachu, *Prog. Energ. and Combust Sci* **2008**, *34*, 254–273.

[4] S. I. Plasynski, J. T. Litynski, H. G. McIlvried, R. D. Srivastava, *Crit. Rev. Plant Sci.* **2009**, *28*, 123–138.

[5] M. Aresta, A. Dibenedetto, *Catal. Today* **2004**, *98*, 455–462.

[6] N. S. Spinner, J. A. Vega, W. E. Mustain, *Catal. Sci. Technol.* **2012**, *2*, 19–28.

[7] N. Panwar, S. Kaushik, S. Kothari, *Renew. Sustain. Energy Rev.* **2011**, *15*, 1513–1524.

[8] H. Lund, *Energy* **2007**, *32*, 912–919.

[9] R. Baños, F. Manzano-Agugliaro, F. Montoya, A. A. C. Gil, J. Gómez, *Renewable and Sustainable Energy Reviews* **2011**, *15*, 1753–1766.

[10] A. Lü, Y. Fang, M. Zhu, S. Huang, Z. Ou, K. M. Kadish, *J. Porphyrins Phthalocyanines* **2012**, *16*, 310–315.

[11] C. Costentin, S. Drouet, M. Robert, J.-M. Savéant, *Science* **2012**, *338*, 90–94.

[12] S. Yamazaki, Y. Yamada, S. Takeda, M. Goto, T. Ioroi, Z. Siromaa, K. Yasuda, *Phys. Chem. Chem. Phys.* **2010**, *12*, 8968–8976.

[13] A. Ghosh, *J. of Mol. Struct. (Theochem)* **1996**, *388*, 359–363.

[14] M. E. Vol'pin, I. S. Kolomnikov, *Pure Appl. Chem.* **1973**, *33*, 567–582.

[15] E. E. Benson, C. P. Kubiak, A. J. Sathrum, J. M. Smieja, *Chem. Soc. Rev.* **2009**, *38*, 89–99.

[16] J. L. Inglis, M. T. MacLean, B. J. Pryce, J. G. Vos, *Coord. Chem. Rev.* **2012**, *256*, 2571–2600.

[17] R. W. Murray, *Acc. Chem. Res.* **1980**, *13*, 135–141.

[18] W. A. Herrmann, C. W. Kohlpaintner, *Angew. Chem. Int. Ed. Engl.* **1993**, *32*, 1524–1544.

[19] A. Yeşildağ, D. Ekinci, *Electrochim. Acta* **2010**, *55*, 7000–7009.

[20] T. Atoguchi, A. Aramata, A. Kazusaka, M. Enyo, *J. Chem. Soc. Chem. Commun.* **1991**, 156–157.

[21] T. Atoguchi, A. Aramata, A. Kazusaka, M. Enyo, *J. Electroanal. Chem.* **1991**, *318*, 309–320.

[22] T. Yoshida, K. Kamato, M. Tsukamoto, T. Iida, D. Schlettwein, D. W. M. Kaneko, *J. Electroanal. Chem.* **1995**, *385*, 209–225.

[23] T. de Groot, PhD thesis, Eindhoven University of Technology, **2007**.

[24] A. Deronzier, J.-C. Moute, *Acc. Chem. Res.* **1989**, *22*, 249–255.

[25] J. Roncali, *J. Mater. Chem.* **1999**, *9*, 1875–1893.

[26] A. Bettelheim, B. A. White, S. A. Raybuck, R. W. Murray, *Inorg. Chem.* **1987**, *26*, 1009–1017.

[27] A. Giraudeau, D. Schaming, J. Hao, R. Farha, M. Goldmann, L. Ruhlmann, *J. Electroanal. Chem.* **2010**, *638*, 70–75.

[28] R. Boulatov in *Fuel Cell Catalysis. A surface science approach*, (Ed.: M. T. M. Koper), John Wiley & Sons , Inc., New York, **2009**, Chapter 18, pp. 637–693.

[29] J. Shen, Y. Y. Birdja, M. T. M. Koper, *Langmuir* **2015**, *31*, 8495–8501.

[30] C. Costentin, M. Robert, J.-M. Savéant, *Acc. Chem. Res.* **2015**, *48*, 2996–3006.

[31] A. Maurin, M. Robert, *J. Am. Chem. Soc.* **2016**, *138*, 2492–2495.

[32] L. Chen, Z. Guo, X.-G. Wei, C. Gallenkamp, J. Bonin, E. Anxolabéhère-Mallart, K.-C. Lau, T.-C. Lau, M. Robert, *J. Am. Chem. Soc.* **2015**, *137*, 10918–10921.

[33] J. Shen, M. J. Kolb, A. J. Göttle, M. T. M. Koper, *J. Phys. Chem. C* **2016**, *120*, 15714–15721.

[34] J. S. Yoo, R. Christensen, T. Vegge, J. K. Nørskov, F. Studt, *ChemSusChem* **2016**, *9*, 358–363.

[35] M. T. de Groot, M. T. M. Koper, *Phys. Chem. Chem. Phys.* **2008**, *10*, 1023–1031.

[36] A. H. Wonders, T. H. M. Housmans, V. Rosca, M. T. M. Koper, *J. Appl. Electrochem.* **2006**, *36*, 1215–1221.

[37] Y. Kwon, M. T. M. Koper, *Anal. Chem.* **2010**, *82*, 5420–5424.

[38] J. Shen, R. Kortlever, R. Kas, Y. Y. Birdja, O. Diaz-Morales, Y. Kwon, I. Ledezma-Yanez, K. J. P. Schouten, G. Mul, M. T. M. Koper, *Nat. Commun.* **2015**, *6*, 8177.

[39] N. Furuya, K. Matsui, *J. Electroanal. Chem.* **1989**, *271*, 181–191.

[40] M. Azuma, K. Hashimoto, M. Hiramoto, M. Watanabe, T. Sakata, *J. Electrochem. Soc.* **1990**, *137*, 1772–1778.

[41] Y. Hori, *In Modern Aspects of Electrochemistry Vol. 42*, Springer, New York, **2008**.

[42] F. Gassner, W. Leitner, *J. Chem. Soc. Chem. Commun.* **1993**, *19*, 1465.

[43] J.-C. Tsai, K. M. Nicholas, *J. Am. Chem. Soc.* **1992**, *114*, 5117–5124.

[44] F. Hutschka, A. Dedieu, M. Eichberger, R. Fornika, W. Leitner, *J. Am. Chem. Soc.* **1997**, *119*, 4432–4443.

[45] S. Slater, J. H. Wagenknecht, *J. Am. Chem. Soc.* **1984**, *106*, 5368–5370.

[46] C. M. Bolinger, N. Story, B. P. Sullivan, T. J. Meyer, *Inorg. Chem.* **1988**, *27*, 4582–4587.

[47] R. Kas, R. Kortlever, H. Yilmaz, M. T. M. Koper, G. Mul, *ChemElectroChem* **2015**, *2*, 354–358.

[48] A. S. Varela, M. Kroschel, T. Reier, P. Strasser, *Catal. Today* **2016**, *260*, 8–13.

[49] M. T. M. Koper, *Chem. Sci.* **2013**, *4*, 2710–2723.

[50] P. van Rysselberghe, J. M. M. George J. Alkire and, *J. Am. Chem. Soc.* **1946**, *68*, 2050–2055.

[51] T. E. Teeter, P. V. Rysselberghe, *J. Chem. Phys.* **1954**, *22*, 759–760.

[52] M. Spichiger-Ulmann, J. Augustynski, *Helvetica Chimica Acta* **1986**, *69*, 632–634.

[53] M. Spichiger-Ulmann, J. Augustynski, *J. Chem. Soc. Faraday Trans.* **1985**, *81*, 713–716.

[54] B. Podlovchenko, E. Kolyadko, S. Lu, *J. Electroanal. Chem.* **1994**, *373*, 185–187.

[55] B. Innocent, D. Pasquier, F. Ropital, F. Hahn, J.-M. Leger, K. Kokoh, *Appl. Catal. B: Environ.* **2010**, *94*, 219–224.

[56] R. Kortlever, K. H. Tan, Y. Kwon, M. T. M. Koper, *J. Solid State Electrochem.* **2013**, *17*, 1843–1849.

CHAPTER 6

Effects of Substrate and Polymer encapsulation on CO_2 Electroreduction by Immobilized Indium(III) protoporphyrin

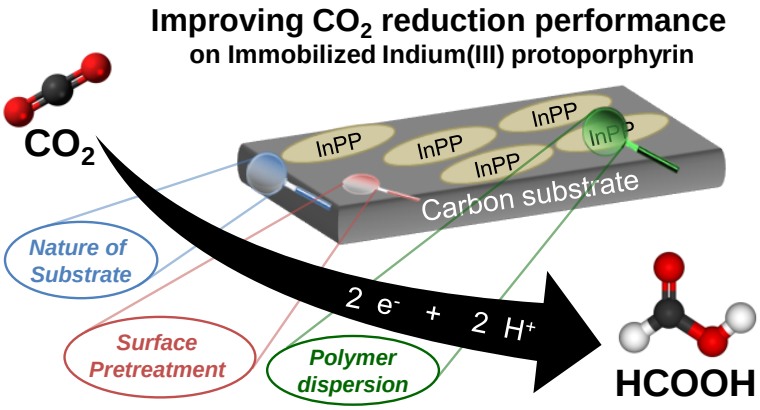

This chapter is based on the article:
Yuvraj Y. Birdja, Rafaël E. Vos, Tim A. Wezendonk, Lin Jiang, Freek Kapteijn and Marc T. M. Koper, ACS Catal., under revision

Abstract

Heterogenization of molecular catalysts for CO_2 electroreduction has attracted significant research activity, due to the combined advantages of homogeneous and heterogeneous catalysts. In this work, we demonstrate the strong influence of the nature of the substrate on the selectivity and reactivity of electrocatalytic CO_2 reduction, as well as on the stability of the studied immobilized indium(III) protoporphyrin IX, for electrosynthesis of formic acid. Additionally, we investigate strategies to improve the CO_2 reduction by tuning chemical functionality of the substrate surface by means of electrochemical and plasma treatment, and by catalyst encapsulation in polymer membranes. We point out several underlying factors that affect the performance of electrocatalytic CO_2 reduction. The insights gained here, allow one to optimize heterogenized molecular systems for enhanced CO_2 electroreduction without modification of the catalyst itself.

6.1 Introduction

The electrocatalytic reduction of carbon dioxide (CO_2RR) is a potentially efficacious strategy to tackle the global energy concerns, particularly, to close the carbon cycle, and store renewable electrical energy in chemicals or fuels.[1] The latter is highly desired due to the intermittent character of renewable energy production. The last decades have experienced the discovery and development of various electrocatalysts, which all lead to a diversity of products with different selectivity and activity.[2–4] Besides heterogeneous CO_2 electrocatalysis using metal, metal alloy, or metal-derived, nanostructured electrocatalysts, molecular catalysis of CO_2 has shown interesting properties, and have undergone a striking development over the years..[5–8] Molecular catalysts are generally considered to yield high selectivity and activity, and can be designed in such a way to mimick enzymes used in nature to efficiently catalyze specific electrochemical reactions such as hydrogen evolution, water oxidation, carbon dioxide reduction, and oxygen reduction.[6,9] Although their stability and solubility in aqueous electrolytes and their poor robustness are often drawbacks, molecular catalysts are widely used to decipher mechanistic insight due to their well-known molecular structure and their efficiency. Hence, many studies have been performed on intrinsic catalyst properties such as the influence of the metal center[10–12] and ligands.[13–17] The focus herein will be on metalloporphyrins, a subgroup of molecular catalysts extensively used for CO_2RR research.[18,19] In previous work, we reported that cobalt(II) and indium(III) protoporphyrin IX (InPP) immobilized on pyrolytic graphite exhibit high selectivity toward carbon monoxide and formic acid, respectively.[12,20]

The usually poor solubility of molecular catalysts in aqueous media, and need for large amounts of catalyst related to homogeneous molecular catalysts, can be overcome by heterogenization. The molecular catalyst is immobilized on a conductive electrode, which we will refer to as "the substrate" in the remainder of this article. An additional advantage of immobilization of the catalyst is the more facile product separation, if utilized in a large-scale industrial process. Carbon materials are often employed as substrate owing to their relatively low cost, robustness and inert nature toward many (electro)chemical reactions. Examples are pyrolytic graphite, glassy carbon and more recently boron doped diamond, carbon nanotubes, and graphene.[21–23] Carbon materials exhibit a rich surface chemistry, and their surface functionalization has been proved to play an important role in their electrochemistry.[24] Studies by Morozan et al. and Rigsby et al. demonstrate the important influence of the carbon support of porphyrins on the selectivity of the oxygen reduction reaction.[22,25] Magdesieva et al. reported on activated carbon supports with different pore sizes for CO_2RR on various porphyrin and phthalocyanine complexes, leading to different selectivity.[26] However, little systematic or comparative work has been performed hitherto, to elucidate the intrinsic influence of the substrate or surface functionalization. The choice of a specific substrate is

often solely based on empirical considerations, which not necessarily is the optimal system.

Modification of electrodes started in the early '80s with several methods such as chemisorption or covalent attachment of species on the electrode surface, encapsulation of species in polymer films, or electropolymerization of monomers directly on the electrode..[27,28] More recently, Yaghi and coworkers developed a covalent organic framework of porphyrin building blocks, which showed promising results for CO_2RR.[29] An overview of various catalyst-modified electrodes for CO_2RR has been given by Sun et al.[30] From heterogeneous electrocatalysis of CO_2RR, it is known that the electrode morphology and (sub)surface structure significantly influence the activity and selectivity.[31–33] Moreover, the use of polymers has been shown to enhance CO_2RR efficiency on cobalt phthalocyanines.[34–36] In the field of heterogenized molecular catalysis of CO_2RR, the effects of such substrate modifications are still unexplored. The importance of chemical functionality on the adsorption and reactivity, as extensively discussed by McCreery,[24] is the inspiration of the idea that substrate modification may impact the reactivity, selectivity, and stability of CO_2RR. In a recent review, the importance of so-called secondary phenomena in molecular electrocatalysis have been highlighted.[37] It would be very attractive to be able to tailor the surface chemistry in such way, to enhance CO_2RR performance.

In this study we focus on extrinsic properties of the molecular catalyst, particularly related to the immobilization of the molecular catalyst. This work is a step toward a systematic investigation of chemical functionality of carbon substrates, and chemical environment for heterogenized molecular catalysts. Herein, we study InPP immobilized on different carbon materials, basal-plane pyrolytic graphite (PG), glassy carbon (GC) and boron doped diamond (BDD), and evince the important role of the substrate, its pretreatment and the use of polymer membranes for immobilization, on the CO_2RR performance. The current work demonstrates the improvement of CO_2RR performance on heterogenized indium(III) protoporphyrin IX by modifying the substrate, its chemical functionality, and chemical environment of the catalyst. The findings can function as a first step in trying to improve other heterogenized molecular systems as well.

6.2 Experimental

The electrochemical experiments were carried out with a potentiostat (IviumStat or CompactStat, Ivium Technologies), in a conventional three-electrode cell, where the working electrode (WE) and counter electrode (CE) compartments were separated by a nafion membrane (Nafion 115). Basal-plane pyrolytic graphite, glassy carbon, and boron doped diamond discs (5, 5, 10 mm diameter respectively) were used as WE. The counter and reference electrode (RE) were a platinum wire and a reversible hydrogen electrode respectively. For correct measurements versus the RHE scale, the luggin capillary and the RHE compartment were filled with CO_2 saturated electrolyte before CO_2 reduction. The electrolyte is 0.1 M phosphate buffer of pH

9.6 ± 0.1, prepared with K_2HPO_4, K_3PO_4 and ultrapure water (Millipore MilliQ gradient A10 system, 18.2 MΩ·cm). The choice for this pH was based on the enhanced HCOOH selectivity observed previously.[12] The reported current densities were always normalized by the geometric surface area of the WE, and in some cases additional normalization by the amount of active species was performed for correct comparison of the activity. The potentials were corrected for ohmic drop by the potentiostat during measurement. Generally, potentiostatic bulk electrolysis was performed at E = -1.5 V vs. RHE for 90 minutes, with manual collection of 100 μl samples at certain times, and analyzed by High Performance Liquid Chromatography. The reported concentrations of liquid products, or subsequently calculated faradaic efficiency (FE) are an average of 3 - 5 independent experiments with freshly prepared electrodes. Additionally, the data points for each experiment were obtained by the average of three injections of the same sample. The dominant contribution of the uncertainty in concentration/FE resulted from the different experiments. Additional experimental details can be found in Appendix C.

6.3 Results and Discussion

6.3.1 Substrate effect

We compare the selectivity and activity for CO_2RR on InPP immobilized on PG, GC and BDD substrates. The immobilization procedure and amount of InPP dropcasted per cm^2 were kept the same for all the substrates (details in the SI). From the faradaic efficiency toward HCOOH, given in Figure 6.1a, it is observed that the substrate has a significant influence on the selectivity of CO_2RR on immobilized InPP. The PG substrate is the most selective toward HCOOH, and the GC substrate the least selective. These effects cannot be ascribed to the activity of the bare substrate as shown by control experiments in Figure C.17a, which show that bare PG, GC and BDD are not active for CO_2RR. In Figure 6.1b-d, the absolute total and partial current densities are shown for CO_2RR on the different substrates. For a correct comparison of the activity, the current density was also normalized by the real amount of InPP adsorbed on the substrate. As will be discussed in detail later, the electroactive coverage of InPP is not the same for the different substrates. It can be seen that there is an order of magnitude difference in j_{total} and j_{HCOOH} on PG compared to GC and BDD. Note that this difference is not associated to a difference in electrochemical active surface area (ECSA), as shown in Figure C.8(a). The fact that GC and BDD both perform worse compared to PG, indicates that the enhancement in CO_2RR selectivity and activity cannot be ascribed to either the high content of sp^2 or sp^3 carbon atoms present in respectively GC and BDD.

The results in Figure 6.1 are in line with the online mass spectrometry and online HPLC experiments, depicted in Figure 6.2a and b respectively, from which we confirm that significantly more H_2 is produced on InPP-GC, and significantly more HCOOH on InPP-PG. The CO_2 consumption on InPP-PG is also much

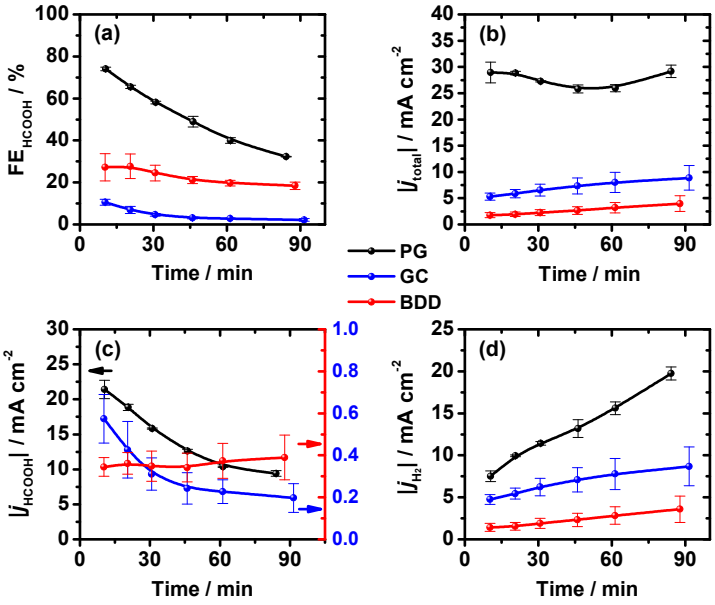

Figure 6.1 (a) Faradaic efficiency toward HCOOH, (b) absolute total current density, (c) absolute partial current density for HCOOH, and (d) absolute partial current density for H_2 during CO_2 reduction on immobilized InPP on different substrates in 0.1 M phosphate buffer of pH 9.6. Lines to guide the eye.

higher compared to the other substrates, in agreement with higher j_{total}, and the higher HCOOH production rate observed on PG compared to the other substrates. Although difficult to quantify, the onset potential for H_2 and HCOOH on InPP-BDD is at more negative potential compared to PG and GC, which is a general characteristic of BDD. Moreover, in Figure 6.2b we can observe differences in the peak potentials of HCOOH formation between the different substrates, which is related to the competition of the hydrogen evolution reaction (HER).

Besides a change in selectivity and activity, there is a clear difference in stability between the substrates, since a slight decrease is observed in j_{HCOOH} as a function of time on PG and GC, accompanied with an increase in j_{H_2}. We define the relative FE with respect to the initial value (Equation 6.1) as a measure for the stability of the system. From a graph of this relative FE versus time (Figure 6.3a), we can compare experiments with different values of FE. A more horizontal trend indicates a higher stability as the FE does not decrease significantly in time.

$$\frac{FE_t}{FE_{initial}} \times 100\% \tag{6.1}$$

The tendency of the FE to decrease with time has been observed before, and was associated with the detachment of InPP from the surface or deactivation of the

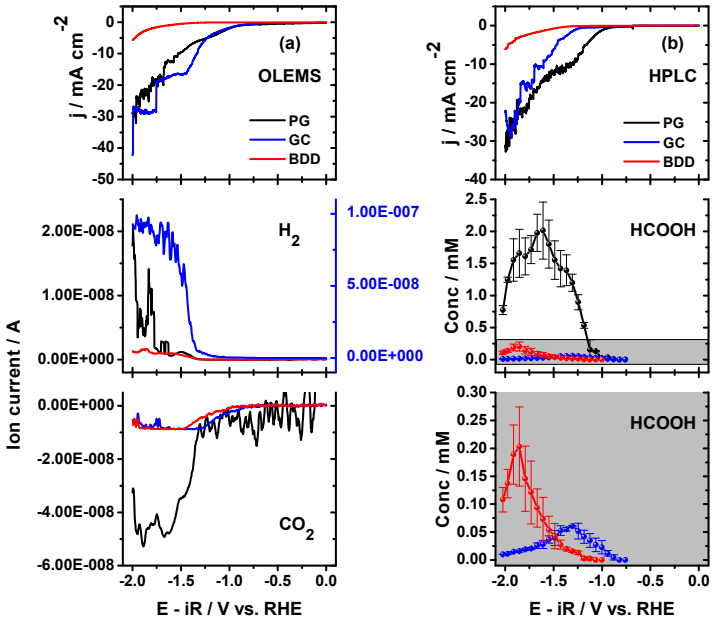

Figure 6.2 (a) Online Electrochemical Mass Spectrometry and (b) online HPLC during CO_2 reduction on immobilized InPP on different substrates in 0.1 M phosphate buffer of pH 9.6.

porphyrin.[12] We have performed x-ray photoelectron spectroscopy on InPP-PG before and after electrolysis, as shown in Figure 6.3b. We observed that the indium content on the electrode, which is a measure of the actual amount of InPP adsorbed on PG, is substantially decreased after 10 minutes, with a negligible further decrease after 1 hour, which is in agreement with the decreasing trend of FE as a function of time. Additionally, we performed experiments under homogeneous conditions of InPP (Figure C.4), in which we do not observe a decrease in selectivity with time. Therefore we confirm that the destabilization of immobilized indium protoporphyrin is related to detachment from the surface. Moreover, the detachment from the surface takes place in the first 10 minutes of electrolysis. The adsorption of the porphyrin on the substrate is through noncovalent π-π interactions,[30,38,39] which is believed to be important for enhanced CO_2RR performance, and strongly dependent on the carbon substrate.

We believe that the substrate morphology plays an important role as evidenced by the higher CO_2 consumption observed with OLEMS, which can be explained by efficient mass transport effects due to the more porous structure of PG compared to GC or BDD (Figure C.8a), which may also suppress the HER. These observations are similar to mass transport effects recently reported for heterogeneous electrocatalysts, showing that the mesostructure can affect the selectivity and activity of

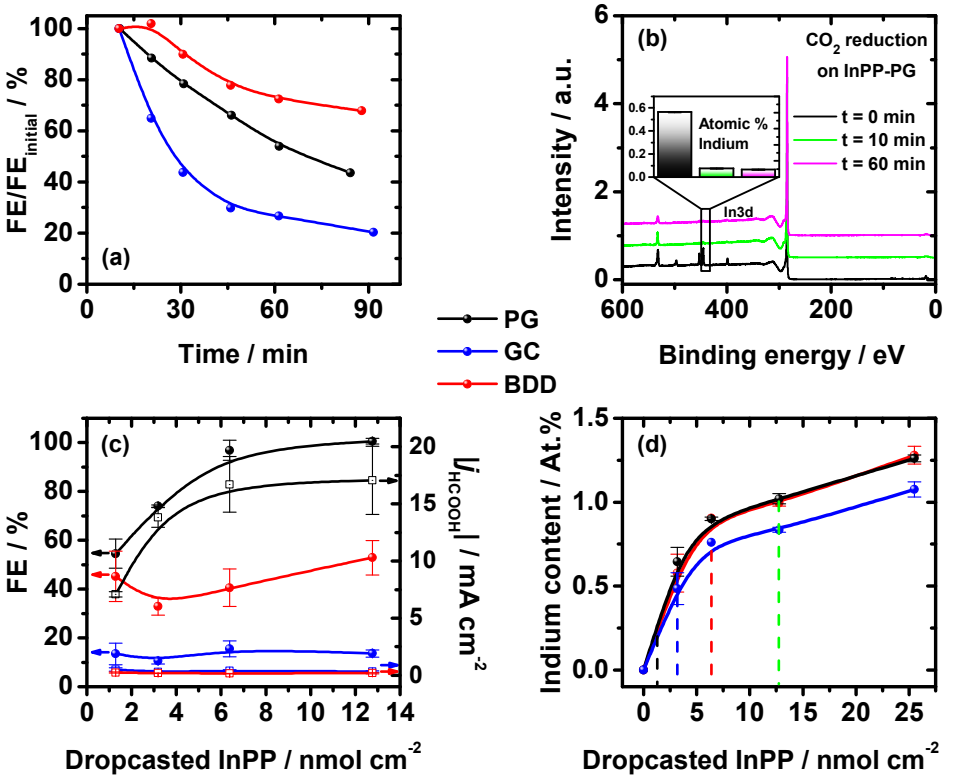

Figure 6.3 (a) Stability of immobilized InPP on different substrates (lines to guide the eye), (b) XPS spectra of InPP-PG electrodes before electrolysis and after electrolysis (t = 10 min and t = 1 h) with in the inset the indium content (at.%), (c) faradaic efficiency toward HCOOH (left axis) and partial current density for HCOOH (right axis) as a function of the amount InPP dropcasted on the different substrates (lines to guide the eye), and (d) indium content of the InPP immobilized on the substrates, as estimated from XPS, as a function of the amount InPP dropcasted (lines to guide the eye).

CO_2RR.[40,41] Additionally, a typical characteristic of GC is its poor permeability for gases, which likely affects the mass transport.[42] X-ray diffractometry and Raman spectroscopy of our substrates (Figure C.9a and C.10) indicate typical characteristics in agreement with the literature. PG and BDD exhibit sharp XRD peaks, and GC weak and broad peaks, indicating a high degree of crystallinity for PG and BDD, and a somewhat amorphous structure for GC.[43] The Raman spectra indicate the characteristic D- and G bands for sp^2 carbons in PG, and a specific peak associated to sp^3 carbon in BDD. The Raman bands for GC are weaker and less sharp, which indicate disorder of the graphite lattice for GC.[44,45] The low

activity and selectivity on GC may be associated with its poor crystallinity, as a high crystallinity infers enhanced charge transport, as observed in covalent organic frameworks.[29,46] Recently, crystallinity has been shown to play an important role on the selectivity of CO_2RR on copper phthalocyanine catalysts.[47] However, high crystallinity alone is not sufficient for improved CO_2RR catalysis, based on the significant differences in CO_2RR performance between PG and BDD, which are both highly crystalline.

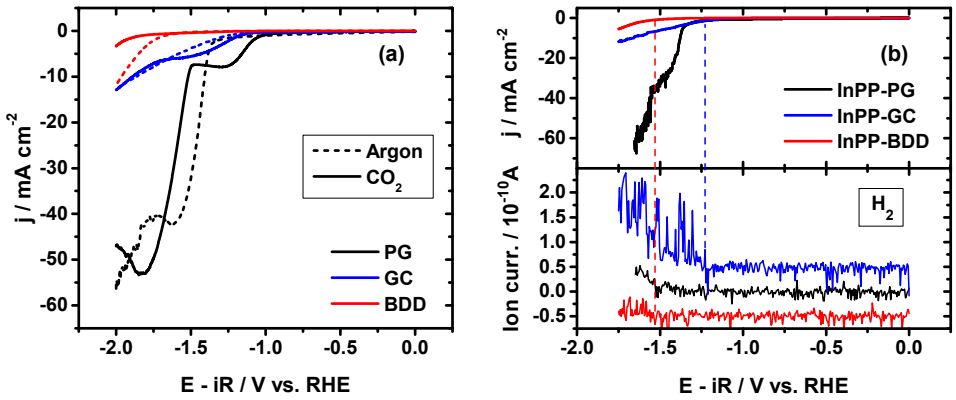

Figure 6.4 (a) Linear sweep voltammetry on immobilized InPP on different substrates in 0.1 M phosphate buffer of pH 9.6 under argon and CO_2 atmosphere, scan rate: 20 mV s^{-1} and (b) Online Electrochemical Mass Spectrometry measurement of hydrogen evolution on InPP immobilized on different substrates

Apart from the substrate morphology and surface structure, a plausible explanation for the enhanced selectivity and activity on PG may be related to a difference in the effective amount of the porphyrin on the three substrates. As can be seen in Figure 6.3c, a difference in the amount of immobilized InPP on the substrate leads to a difference in activity and selectivity (details of the corresponding experiments are provided in Figures C.1-C.3). In case of PG this concentration effect is more pronounced, and in case of GC almost completely absent, which can be interpreted as a "InPP saturation limit" that is reached earlier for GC compared with PG. In other words, PG substrate can accommodate more catalyst compared to GC and BDD. These conclusions are in agreement with quantitative information obtained from XPS spectra of InPP immobilized on the different substrates (Figure C.12). We also varied the amount of InPP dropcasted on the different substrates and plotted the indium content as estimated by XPS vs. the amount dropcasted in Figure 6.3d. The vertical dashed lines indicate the InPP amounts used for the qualitative study shown in Figure 6.3c and C.1-C.3. It can be seen that the indium content is the highest for PG and the lowest for GC, which is in agreement with our conclusion that a PG substrate can accommodate more catalyst compared to GC. Furthermore, we used the indium content of InPP immobilized on different

substrates (PG, GC, BDD = 0.65, 0.49, 0.58) to normalize the activity to real amount of adsorbed InPP (Figure 6.1b-d).

Another cause of the improved CO_2RR selectivity may be a difference in HER activity between the substrates instead of solely an intrinsic substrate effect specifically related to CO_2RR. In Figure 6.4a, a comparison between the substrates for HER and CO_2RR is shown. The high overpotential for HER on the BDD substrate does not favor CO_2RR, since the CO_2RR onset potential is shifted toward more negative potentials, and the current is suppressed on InPP-BDD with CO_2 in solution. The HPLC results (Figure 6.2b) confirm the formation of HCOOH at more negative potentials on BDD compared to GC and PG. Under argon, where only hydrogen evolution takes place, the current density on InPP-GC is smaller compared to InPP-PG. However, as shown by OLEMS measurements in Figure 6.4b, more H_2 is produced on GC. Moreover, in the presence of CO_2, the onset potential is shifted positively for InPP-PG, but is almost unchanged for InPP-GC, which indicates a more efficient catalysis of CO_2RR on PG with respect to GC, in agreement with the online experiments in Figure 6.2. Consequently, the GC substrate is more active toward HER compared to PG. These results indicate that the competition between CO_2RR and HER strongly depends on the nature of the substrate, which in turn affects HCOOH selectivity.

In order to increase the impact and generality of our findings, we studied the substrate effect on protoporphyrins with Rh and Sn metal centers, which previously were found to produce HCOOH.[12] Although the HCOOH selectivity for these porphyrins is much lower than for InPP (which is an intrinsic catalytic effect), a similar trend can be observed for the different substrates as found for InPP (Figure C.5). Pyrolytic graphite substrate leads to the highest FE, while glassy carbon substrate is the least selective toward HCOOH.

The above results demonstrate the important influence of the substrate, which is believed to be the result of an interplay of several factors influencing the selectivity and reactivity of CO_2RR, such as morphology/mesostructure (and thereby optimized mass transport effects), crystallinity, electrostatic interaction with the molecular catalyst, and activity for HER.

6.3.2 Effect of substrate pretreatment

Besides the nature of the substrate, modification or treatment of the substrate surface offers a means to influence the CO_2 selectivity, reactivity, and stability. We investigated the influence of a cathodic and anodic electrochemical pretreatment ("Cat-PG" and "An-PG"), and a H_2 and O_2 plasma treatment ("H_2-PG" and "O_2-PG") of the PG substrate. In Figure 6.5, it is shown that O_2 plasma treatment increases the FE and j_{HCOOH}. These effects can be attributed to a change in chemical functionality as discussed later, instead of an increased surface area as evidenced by similar C_{dl} before and after O_2 plasma treatment (Figure C.8b). Furthermore, the exposure time of O_2 plasma seems to play a role as shown in Figure C.6, since a mild O_2 plasma treatment (3 and 6 min. exposure) slightly

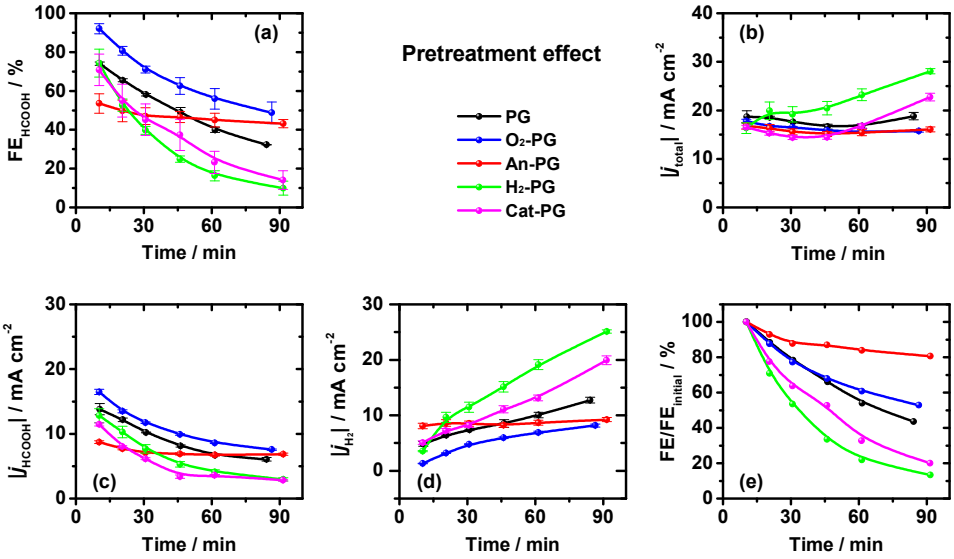

Figure 6.5 (a) Faradaic efficiency toward HCOOH, (b) absolute total current density, (c) absolute partial current density for HCOOH, (d) absolute partial current density for H_2, (e) stability during CO_2 reduction on immobilized InPP on different pretreated PG substrates. Electrolyte: 0.1 M phosphate buffer of pH 9.6. Lines to guide the eye.

improves CO_2RR, while a harsh O_2 plasma treatment (12 min exposure) worsens CO_2RR performance. In Figure 6.5e, it is shown that O_2 plasma treatment has negligible influence on the stability. Anodization of PG leads to lower initial FE, but improves the stability dramatically. Moreover, both hydrogen treatments, cathodic and H_2 plasma, decrease the selectivity, reactivity and stability of CO_2RR significantly. Since H_2-PG has a lower C_{dl} and thus a smaller surface area (Figure C.8b), but a higher j_{total}, the observed changes in selectivity and reactivity do not result from a change in surface area of PG after H_2 plasma treatment.

The observed differences for the investigated pretreated PG substrates, highlight the role of oxygenated and hydrogenated functional groups of the substrate's surface on the immobilization of InPP and subsequently on the CO_2RR. Our results imply that hydrogen functional groups on the PG surface strongly decrease CO_2RR selectivity, reactivity and stability, and oxygen functionalities increase CO_2RR performance. H_2 plasma consists of a large amount of H atoms, which reacts with surface oxides leading to C-H bonds and a decreased O/C ratio on the surface.[24,48] The chemisorbed hydrogen on the surface promotes HER with respect to CO_2RR, which is reflected in a decrease in FE and j_{HCOOH}, and increase in j_{H_2}. On the other hand, O_2 plasma treatment increases the amount of oxygen functional groups (e.g. hydroxyl, carbonyl, carboxylate) on the surface, which generally leads to a more polar and hydrophilic surface and stronger adsorbate-substrate interaction.

O_2 plasma treated PG shows an improvement in CO_2RR selectivity. A similar influence of O_2 plasma treatment of the substrate has been reported before for the oxygen reduction reaction.[49]

On anodically treated PG we expected similar behavior as after O_2 plasma treatment, due to the introduction of oxygenated species, but no improvement in activity or selectivity has been observed. However, a remarkable increase in the stability is observed. Based on blank voltammograms of the pretreated PG (Figure C.7), there is a significant difference in An-PG compared to the untreated and other pretreated PG electrodes. Application of strong anodic pretreatment causes a destruction of the carbon surface, and formation of a thick graphite oxide layer, which contains a high amount of anionic sites and interior void volume, leading to high surface area, in agreement with the dramatic increase in C_{dl} for An-PG in Figure C.8b.[24,50] Complementary information was obtained by x-ray diffractometry, Raman spectroscopy, and x-ray photoelectron spectroscopy. As shown in Figure C.9b, the crystalline nature of PG remains intact upon electrochemical pretreatment. However, anodization of PG leads to a significant increase in the Raman peak at $\approx$ 1352 cm^{-1}, and a slight increase in the D' peak around 1620 cm^{-1} (Figure C.10b). The peak at 1352 cm^{-1} is attributed to the presence of graphitic edges, which increases in intensity upon anodic treatment as observed in our spectra, and the peak at 1620 cm^{-1} indicates delamination of graphitic planes. Formation of graphite oxide increases the strain on the PG lattice, leading to fracturization.[51] In Figure C.11 the ratio of the D- and G band intensity for the different substrates and pretreated PG is depicted, which clearly shows a high ratio of I_D/I_G in case of An-PG. Anodization of PG leads to an increase in the edge plane density. Note that GC also exhibits a relatively high I_D/I_G, but showed a poor stability as seen before. Therefore, we believe a high edge plane density in combination with high crystallinity to be the reason for the strongly improved stability. The XPS spectra of the plasma- and electrochemically treated pyrolytic graphite electrodes, shown in Figure C.13, provide a quantitative basis for our conclusions about chemical functionality on CO_2RR performance. The oxygen content is significantly higher on An-PG and O_2-PG compared to untreated PG. Moreover, the H_2 plasma- and cathodically treated PG exhibit less surface oxygenated species compared to untreated PG. These results are in agreement with our interpretation of the CO_2RR results and our Raman spectroscopy experiments.

6.3.3 Effect of polymer encapsulation

In addition to pretreating the substrate, another strategy aimed at improving CO_2RR selectivity, reactivity and stability, is by incorporation of the porphyrin in polymeric matrices. In this work, we compare the influence of didodecyldimethylammonium bromide (DDAB), nafion®, poly(4-vinylpyridine) (P4VP), and poly(3,4-ethylenedioxythiophene) polystyrene sulfonate (PEDOT:PSS). Details about the immobilization in these polymeric matrices are given in the SI. The concentration of InPP in the polymer films, and the amount of polymer dropcasted per cm^2 surface

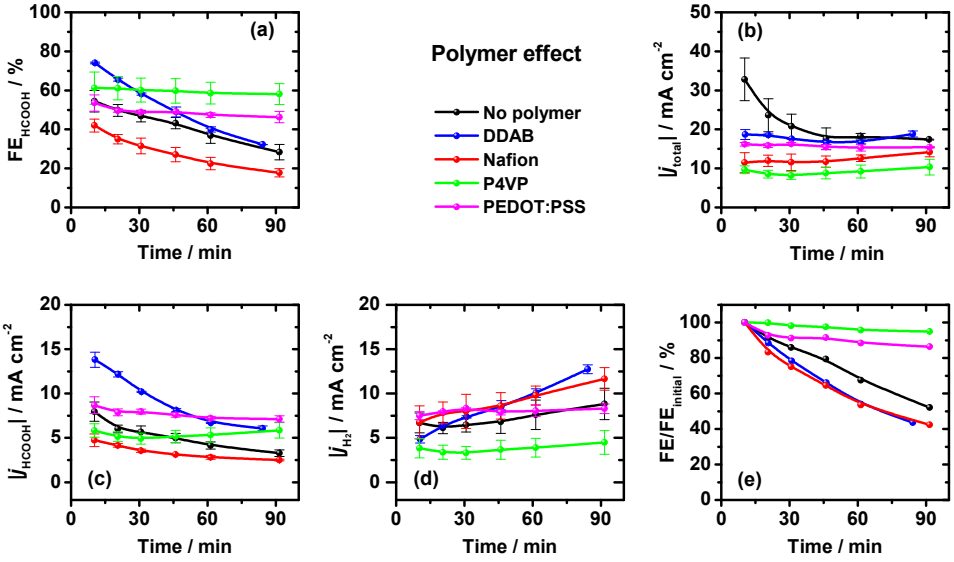

Figure 6.6 (a) Faradaic efficiency toward HCOOH, (b) absolute total current density, (c) absolute partial current density for HCOOH (d) absolute partial current density for H_2, (e) stability during CO_2 reduction on immobilized InPP in different polymer membranes. Electrolyte: 0.1 M phosphate buffer of pH 9.6. Lines to guide the eye.

were always kept the same. As depicted in Figure 6.6, interesting differences are observed between the polymer membranes. Compared with polymer-free InPP (InPP-PG), encapsulation in DDAB, P4VP, and PEDOT:PSS shows enhanced selectivity and activity, whereas nafion negatively impacts the selectivity and activity. From Figure 6.6d it can be seen that the HER activity with P4VP is drastically decreased. A striking observation in Figure 6.6e is the enhanced stability when using P4VP or PEDOT:PSS compared to the other polymers. These results underscore the importance of the nature of the polymer as seen before for a modified bulk silver electrode.[52] Enhanced CO_2RR performance by P4VP has been reported before for cobalt phthalocyanine, where the authors explain the observed effects by the presence of pyridine residues in the polymer, which influences the coordination to the catalyst.[35,36] Although nafion coated catalysts are widely used for various electrocatalytic systems, negative effects of nafion on the catalytic activity have been observed previously.[53,54]

Differences in polymer-dispersed catalysts are generally associated with the introduction of a hydrophobic environment, leading to the suppression of the HER.[28,34,55] However, the differences in CO_2RR performance in our investigation are likely to be explained by the different chemical structures of the polymers (Figure C.14), leading to different substrate/adsorbate interactions. As can be seen in the blank CVs in Figure C.15, the typical InPP peaks are masked or

shifted for nafion, P4VP and PEDOT:PSS. Changes in the voltammetric behavior after immobilization of porphyrins in DDAB have been reported before, in which the authors also suggest the possibility of porphyrin dimer formation in DDAB vesicles.[55] The absence of InPP redox peaks in the investigated potential window indicates a change in electrochemical behavior, but does not rule out the presence of InPP on the surface since reasonable amounts of HCOOH are produced. The CV of PEDOT:PSS coated PG shows a much larger double layer, which indicates the strong influence of the polymer on the chemical environment near the electrode surface. The polymers without InPP exhibit reasonable CO_2RR activity as can be seen in Figure C.17b, where the same trend is observed as for InPP encapsulated in the different polymers. A detailed investigation of the electrocatalytic activity of polymers for CO_2RR is beyond the aim of this work. Nonetheless, it can be concluded that the observed effects are partly due to the activity of the polymer for CO_2RR, which is higher with P4VP and PEDOT:PSS. The pyridine group in P4VP and aromatic moieties in PEDOT:PSS are assumed to play an important role in this respect, since Dunwell et al. very recently reported CO_2RR toward HCOOH mediated by pyridine.[56] The porphyrin exhibits a planar macrocycle with large π-conjugation, which facilitates electrostatic interactions with the polymer. We believe that the increased stability is a result of the presence of aromatic building blocks as present in P4VP and PEDOT:PSS, which facilitates axial coordination to the indium metal center by electron donation. This effect is known for pyridine or imidazole ligands which are used for (covalently) anchoring catalysts to electrodes, and are found to stabilize the coordination of CO_2.[34] This interaction is absent in case of Nafion and DDAB, leading to a inferior stability compared to the polymer-free InPP, P4VP and PEDOT:PSS. DDAB shows an increase in selectivity and activity, which is associated with the suppression of the HER similar to previous work.[52] The poor CO_2RR performance with nafion is tentatively ascribed to the low mobility of the porphyrin in the polymer, and a disordered structure of the nafion layer.[53,54] We performed electrochemical impedance spectroscopy on the different polymer dispersed catalysts to investigate the kinetics of electron-transfer processes (Figure C.16). As discussed in the SI, the charge transfer resistance between the polymer films is in agreement with the observed activity in Figure 6.6b. We conclude that the nature of the polymer affects the rate of electron transfer during CO_2RR rather than mass transport of active species, leading to different activity amongst the polymer films.

The results in the present work demonstrate that the hydrophobic environment, induced by the polymer membrane in general, not always leads to suppression of the HER activity and subsequent improvement of CO_2RR. Additional effects related to the chemical structure, allowing for electrostatic interactions with the porphyrin or activity towards CO_2RR by the polymer itself, play an important role. Note that the current findings strongly depend on the (molecular) catalyst under study, and one should be careful to generalize the observed polymer effects for other electrocatalytic systems. Nonetheless, we emphasize the possible negative influence

of nafion on CO_2RR, as nafion is very often used to immobilize catalysts, or as binder in the preparation of ink containing nanoparticulate electrocatalysts.

6.4 Conclusions

This work has shown the importance of the nature of the substrate for immobilized indium(III) protoporphyrin IX for CO_2RR toward formic acid. For this particular system, a pyrolytic graphite substrate outperforms glassy carbon and boron doped diamond in terms of CO_2RR selectivity and reactivity, while boron doped diamond shows the best stability. The enhanced activity and selectivity of PG are assigned to a combination of different factors. First, to a more porous surface structure, leading to efficient mass transport. Furthermore, to an optimal interaction between substrate and InPP, and a favorably low HER activity.

We have investigated two strategies to improve or alter the selectivity, reactivity, and stability of CO_2RR. Pretreatment of the substrate before catalyst immobilization, and immobilization in polymeric matrices have shown to be practical tools to fine-tune CO_2 reduction performance. Hydrogenated functional groups on the surface decrease the selectivity, activity, and stability, while (mild) oxygen functionalization positively influences the CO_2 reduction performance. Anodization of the graphite surface substantially increases the stability, which is believed to be related to the thick graphite oxide layer containing high edge plane density. Both P4VP and PEDOT:PSS, increase the stability, which is believed to be due to axial coordination of their aromatic moieties to the indium metal center. DDAB, P4VP and PEDOT:PSS improve the performance of CO_2RR, while nafion impacts CO_2RR negatively. These strategies are assumed to be applicable to similar macrocyclic catalysts immobilized on carbon materials.

It should be noted that the CO_2RR performance is often a trade-off between selectivity, activity, and stability, each of which can be modified by substrate pretreatment and catalyst encapsulation in polymers. Although complete mechanistic insight in the pretreatment- and polymer effects is still missing, the results obtained here, may help to design heterogenized molecular catalytic systems for CO_2 reduction with specifically optimized properties. Other molecular catalysts may behave differently, hence one should be careful generalizing the results obtained in this study. However, it is very likely that the substrate, its pretreatment, and catalyst dispersion in polymers will have an influence on CO_2RR performance, and the insight obtained herein may be used as starting point for further optimization of the system.

6.5 References

[1] D. T. Whipple, P. J. A. Kenis, *J. Phys. Chem. Lett.* **2010**, *1*, 3451–3458.

[2] J.-P. Jones, G. K. S. Prakash, G. A. Olah, *Isr. J. Chem.* **2014**, *54*, 1451–1466.

[3] J. Durst, A. Rudnev, A. Dutta, Y. Fu, J. Herranz, V. Kaliginedi, A. Kuzume, A. A. Permyakova, Y. Paratcha, P. Broekmann, T. J. Schmidt, *Chimia* **2015**, *69*, 769–776.

[4] R. Kortlever, J. Shen, K. J. P. Schouten, F. Calle-Vallejo, M. T. M. Koper, *J. Phys. Chem. Lett.* **2015**, *6*, 4073–4082.

[5] J. P. Collin, J. P Sauvage, *Coord. Chem. Rev.* **1989**, *93*, 245–268.

[6] E. E. Benson, C. P. Kubiak, A. J. Sathrum, J. M. Smieja, *Chem. Soc. Rev.* **2009**, *38*, 89–99.

[7] C. Finn, S. Schnittger, L. J. Yellowlees, J. B. Love, *Chem. Commun.* **2012**, *48*, 1392–1399.

[8] J. Bonin, A. Maurin, M. Robert, *Coord. Chem. Rev.* **2017**, *334*, 184–198.

[9] J.-M. Savéant, *Chem. Rev.* **2008**, *108*, 2348–2378.

[10] N. Furuya, K. Matsui, *J. Electroanal. Chem.* **1989**, *271*, 181–191.

[11] L. Chen, Z. Guo, X.-G. Wei, C. Gallenkamp, J. Bonin, E. Anxolabéhère-Mallart, K.-C. Lau, T.-C. Lau, M. Robert, *J. Am. Chem. Soc.* **2015**, *137*, 10918–10921.

[12] Y. Y. Birdja, J. Shen, M. T. M. Koper, *Catal. Today* **2017**, *288*, 37–47.

[13] S. Yamazaki, Y. Yamada, S. Takeda, M. Goto, T. Ioroi, Z. Siromaa, K. Yasuda, *Phys. Chem. Chem. Phys.* **2010**, *12*, 8968–8976.

[14] C. Costentin, S. Drouet, M. Robert, J.-M. Savéant, *Science* **2012**, *338*, 90–94.

[15] A. Lü, Y. Fang, M. Zhu, S. Huang, Z. Ou, K. M. Kadish, *J. Porphyrins Phthalocyanines* **2012**, *16*, 310–315.

[16] I. Azcarate, C. Costentin, M. Robert, J.-M. Savéant, *J. Am. Chem. Soc.* **2016**, *138*, 16639–16644.

[17] Z. N. Zahran, E. A. Mohamed, Y. Naruta, *Scientific Reports* **2016**, *6*, 1–12.

[18] J. L. Inglis, M. T. MacLean, B. J. Pryce, J. G. Vos, *Coord. Chem. Rev.* **2012**, *256*, 2571–2600.

[19] G. F. Manbeck, E. Fujita, *J. Porphyrins Phthalocyanines* **2015**, *19*, 45–64.

[20] J. Shen, R. Kortlever, R. Kas, Y. Y. Birdja, O. Diaz-Morales, Y. Kwon, I. Ledezma-Yanez, K. J. P. Schouten, G. Mul, M. T. M. Koper, *Nat. Commun.* **2015**, *6*, 8177.

[21] S. A. Yao, R. E. Ruther, L. Zhang, R. A. Franking, R. J. Hamers, J. F. Berry, *J. Am. Chem. Soc.* **2012**, *134*, 15632–15635.

[22] A. Morozan, S. Campidelli, A. Filoramo, B. Jousselme, S. Palacin, *Carbon* **2011**, *49*, 4839–4847.

[23] S. Navalón, J. R. Herance, M. Álvaro, H. García, *Chem. Eur. J.* **2017**, *23*, 1–33.

[24] R. L. McCreery, *Chem. Rev.* **2008**, *108*, 2646–2687.

[25] M. L. Rigsby, D. J. Wasylenko, M. L. Pegis, J. M. Mayer, *J. Am. Chem. Soc.* **2015**, *137*, 4296–4299.

[26] T. V. Magdesieva, T. Yamamoto, D. A. Tryk, A. Fujishima, *J. Electrochem. Soc.* **2002**, *149*, D89–D95.

[27] R. W. Murray, *Acc. Chem. Res.* **1980**, *13*, 135–141.

[28] R. W. Murray, A. G. Ewing, R. A. Durst, *Anal. Chem.* **1987**, *59*, 379A–390A.

[29] S. Lin, C. S. Diercks, Y.-B. Zhang, N. Kornienko, E. M. Nichols, Y. Zhao, A. R. Paris, D. Kim, P. Yang, O. M. Yaghi, C. J. Chang, *Science* **2015**, *349*, 1208–1213.

[30] Z. Sun, L. Kong, X. Ding, C. Du, X. Zhao, J. Chen, H. Fu, X. Yang, T. Cheng, *Phys. Chem. Chem. Phys.* **2016**, *18*, 9367–9376.

[31] C. W. Li, M. W. Kanan, *J. Am. Chem. Soc.* **2012**, *134*, 7231–7234.

[32] Y. Chen, C. W. Li, M. W. Kanan, *J. Am. Chem. Soc.* **2012**, *134*, 19969–19972.

[33] H. Mistry, A. S. Varela, C. S. Bonifacio, I. Zegkinoglou, I. Sinev, Y.-W. Choi, K. Kisslinger, E. A. Stach, J. C. Yang, P. Strasser, B. R. Cuenya, *Nat. Commun.* **2016**, *7*, 12123.

[34] T. Abe, T. Yoshida, S. Tokita, F. Taguchi, H. Imaya, M. Kaneko, *J. Electroanal. Chem.* **1996**, *412*, 125–132.

[35] T. Yoshida, K. Kamato, M. Tsukamoto, T. Iida, D. Schlettwein, D. W. M. Kaneko, *J. Electroanal. Chem.* **1995**, *385*, 209–225.

[36] W. W. Kramer, C. C. L. McCrory, *Chem. Sci.* **2016**, *7*, 2506–2515.

[37] J.-M. Savéant, *ChemElectroChem* **2016**, *3*, 1967–1977.

[38] J.-H. Fuhrhop, *Langmuir* **2014**, *30*, 1–12.

[39] A. Maurin, M. Robert, *J. Am. Chem. Soc.* **2016**, *138*, 2492–2495.

[40] R. Kas, K. K. Hummadi, R. Kortlever, P. de Wit, A. Milbrat, M. W. Luiten-Olieman, N. E. Benes, M. T. Koper, G. Mul, *Nat. Commun.* **2016**, *7*, 10748.

[41] Y. Yoon, A. S. Hall, Y. Surendranath, *Angew.Chem. Int.Ed.* **2016**, *55*, 15282–15286.

[42] F. C. Cowlard, D. C. Lewis, *J. Mater. Sci.* **1967**, *2*, 507–512.

[43] Y. Hishiyama, M. Nakamura, *Carbon* **1995**, *33*, 1399–1403.

[44] R. Bowling, R. T. Packard, R. L. McCreery, *Langmuir* **1989**, *5*, 683–688.

[45] Y. Wang, D. C. Alsmeyer, R. L. McCreery, *Chem. Mater.* **1990**, *2*, 557–563.

[46] S. Wan, F. Gándara, A. Asano, H. Furukawa, A. Saeki, S. K. Dey, L. Liao, M. W. Ambrogio, Y. Y. Botros, X. Duan, S. Seki, J. F. Stoddart, O. M. Yaghi, *Chem. Mater.* **2011**, *23*, 4094–4097.

[47] S. Kusama, T. Saito, H. Hashiba, A. Sakai, S. Yotsuhashi, *ACS Catal.* **2017**, *7*, 8382–8385.

[48] J. Xu, Q. Chen, G. M. Swain, *Anal. Chem.* **1998**, *70*, 3146–3154.

[49] K. Vaik, D. J. Schiffrin, K. Tammeveski, *Electrochem. Commun.* **2004**, *6*, 1–5.

[50] R. S. Kelly, D. J. Weiss, S. H. Chong, T. Kuwana, *Anal. Chem.* **1999**, *71*, 413–418.

[51] R. Bowling, R. T. Packard, R. L. McCreery, *J. Am. Chem. Soc.* **1989**, *111*, 1217–1223.

[52] F. Quan, M. Xiong, F. Jia, L. Zhang, *Appl. Surf. Sci.* **2017**, *399*, 48–54.

[53] D. A. Buttry, F. C. Anson, *J. Am. Chem. Soc.* **1984**, *106*, 59–64.

[54] A. Jarzębińska, P. Rowiński, I. Zawisza, R. Bilewicz, L. Siegfried, T. Kaden, *Analytica Chimica Acta* **1999**, *396*, 1–12.

[55] M. T. de Groot, M. T. M. Koper, *Phys. Chem. Chem. Phys.* **2008**, *10*, 1023–1031.

[56] M. Dunwell, Q. Lu, J. M. Heyes, J. Rosen, J. G. Chen, Y. Yan, F. Jiao, B. Xu, *J. Am. Chem. Soc.* **2017**, *139*, 3774–3783.

CHAPTER 7

Optimization of Electrolyte Composition for Electrocatalytic CO_2 Reduction on Immobilized Indium(III) protoporphyrin

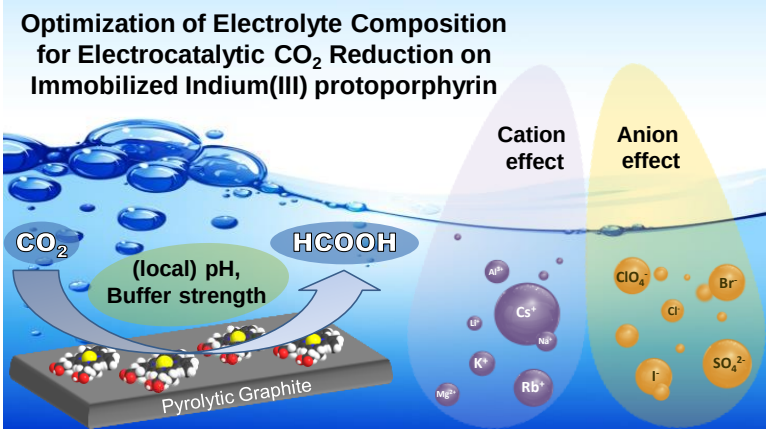

This chapter is based on the article:
Yuvraj Y. Birdja, Olha Nahorna and Marc T. M. Koper, in preparation

Abstract

In this work, we investigate the performance of CO_2 electroreduction on indium(III) protoporphyrin IX immobilized on pyrolytic graphite in different electrolyte solutions. We demonstrate the importance of the electrolyte composition and buffer capacity for high selectivity and reactivity toward formic acid. A significant enhancement of the faradaic efficiency in unbuffered electrolytes is obtained, reaching values of FE $\approx 96 \pm 3$ % toward formic acid, which is the result of a combined effect of the electrolyte pH and buffering strength. A cation- or anion effect as has been observed for heterogeneous electrocatalysts or homogeneous molecular catalysts in aprotic solvents, is absent, which indicates the relevance of the nature of the solvent, type of catalysis and reaction path for the impact of electrolyte composition on the selectivity and activity of electrochemical CO_2 reduction. Moreover, we found that the destabilization of the immobilized indium(III) protoporphyrin IX may be more pronounced depending on the electrolyte composition and buffering strength.

7.1 Introduction

Electrocatalytic CO_2 reduction (CO_2RR) is an attractive way toward a sustainable carbon cycle, utilizing renewable energy sources. Decarbonization and electrification of the current energy systems, and intermittency of renewable energy sources can be addressed simultaneously.[1,2] In the last couple of decades, research activity has focused primarily on the design, synthesis and optimization of various electrocatalysts aimed at high selectivity, reactivity and stability of CO_2RR. Additionally, reaction- and process parameters such as the nature of the solvent, ionic species in the electrolyte, buffering strength of the electrolyte, and CO_2 partial pressure, have been identified to play an important role on CO_2RR performance, but have received little systematic attention.

In the late '80s, the electrolyte was shown to impact CO_2 reduction on metal electrodes.[3,4] However, the exact cause of this influence is still not clear, since the effects cannot conclusively be ascribed to pH changes, buffering effects, or cationic/anionic species in solution. Recently, systematic studies have been initiated on these specific factors.[5–14] Kas et al. and Varela et al. demonstrated the change in product selectivity of CO_2RR on copper electrodes by changing the buffer strength.[6,7] Although ionic species also have been shown to influence CO_2RR, there is no consensus yet in the literature about the actual cause of these effects.[8–13] Moreover, we recently found that liquid CO_2RR products can be observed from Cannizzaro-type reactions instead of from direct CO_2RR, due to a local alkaline pH in the vicinity of the electrode, manifested in weakly- or unbuffered electrolytes.[15] Studies regarding the aforementioned parameters have mainly been performed on heterogeneous electrocatalysts.

Savéant and coworkers reported improved catalyst stabilization and a promoting effect by specific ionic species on CO_2RR by iron porphyrins under homogeneous conditions in DMF.[16,17] Heterogenized molecular catalysts have gained in popularity due to the small amount of catalyst needed, the absence of solubility issues in aqueous media, and the more attractive prospects for industrial scale up of the CO_2RR process compared to dissolved catalysts.[18,19] The influence of the electrolyte composition, ionic species, buffer strength has not been studied systematically for heterogenized molecular catalysts to date. Recently, we found that metalloprotoporphyrins immobilized on pyrolytic graphite (PG) are able to efficiently reduce CO_2 to CO or HCOOH depending on the metal center, applied potential and electrolyte pH.[20,21] Moreover, we found that the selectivity, activity and stability are strongly affected by the nature of the substrate, its pretreatment and the catalyst chemical environment.[22]

In this work, we study the effects of electrolyte composition on the selectivity and reactivity of CO_2RR on heterogenized molecular catalysts. As a model system we use indium(III) protoporphyrin IX (InPP) immobilized on PG, which previously has been found to produce formic acid with high faradaic efficiency. In this comparative

study, we demonstrate the influence of the electrolyte, ionic species, and buffering effects on the CO_2RR performance.

7.2 Experimental

For the electrochemical experiments, we used a conventional two-compartment cell ("H-cell") in a three-electrode configuration, where a nafion membrane (Nafion 115) separated the working electrode (WE) and counter electrode (CE) compartments. Pyrolytic graphite was used as WE on which indium(III) protoporphyrin IX was immobilized. Details can be found in the SI and in our previous work.[21] A platinum gauze and reversible hydrogen electrode were used as CE and reference electrode respectively. Current densities reported in this work are normalized by the geometric surface area of the WE, and potentials are corrected for ohmic drop. Generally, potentiostatic bulk electrolysis was performed at E = -1.5 V vs. RHE for 90 minutes, with analysis of collected samples at specific times by High Performance Liquid Chromatography. In this work we distinguish between initial and final pH, which refer to the bulk pH measured respectively before and after CO_2 saturation.

7.3 Results and Discussion

We compare the selectivity and activity of CO_2RR on immobilized InPP on PG in four electrolyte solutions with different anions and buffer capacities, *viz.* phosphate buffer, bicarbonate buffer, borate buffer and potassium chloride electrolyte, each with an initial pH $\approx$ 8.7 and similar concentration of 0.1 M. As shown in Figure 7.1a, very significant differences in faradaic efficiency (FE) can be observed. Bicarbonate buffer and borate buffer solutions lead to respectively the most and least selective HCOOH formation. Although the initial pH was kept the same, the bulk pH after CO_2 saturation is slightly different between the electrolyte solutions as shown in Figure D.1a. Interestingly, the trend in the final pH between the three electrolytes ($pH_{borate} < pH_{phosphate} < pH_{bicarbonate}$) is similar to the trend in faradaic efficiency between these electrolytes ($FE_{borate} < FE_{phosphate} < FE_{bicarbonate}$), which would indicate a possible pH effect, where higher FE is favored by more alkaline final pH. However, the KCl electrolyte does not follow this trend, since the final pH is much lower than that of the remaining electrolytes (Figure D.1b), while the HCOOH selectivity in KCl is higher compared to phosphate and borate buffers. The lower final pH for the KCl electrolyte is obvious, since KCl is not a buffer. For comparison of the stability, we looked at the FE normalized by the initial value, as shown in Figure 7.1e. Besides lowest selectivity, borate buffer also has the lowest stability, while the stability is similar in the other electrolytes. Furthermore, we observe in Figure 7.1b-d that the CO_2RR activity also depends on the electrolyte composition. The bicarbonate electrolyte facilitates the highest activity, while borate buffer leads to very low activity for CO_2RR. Moreover, the HER current

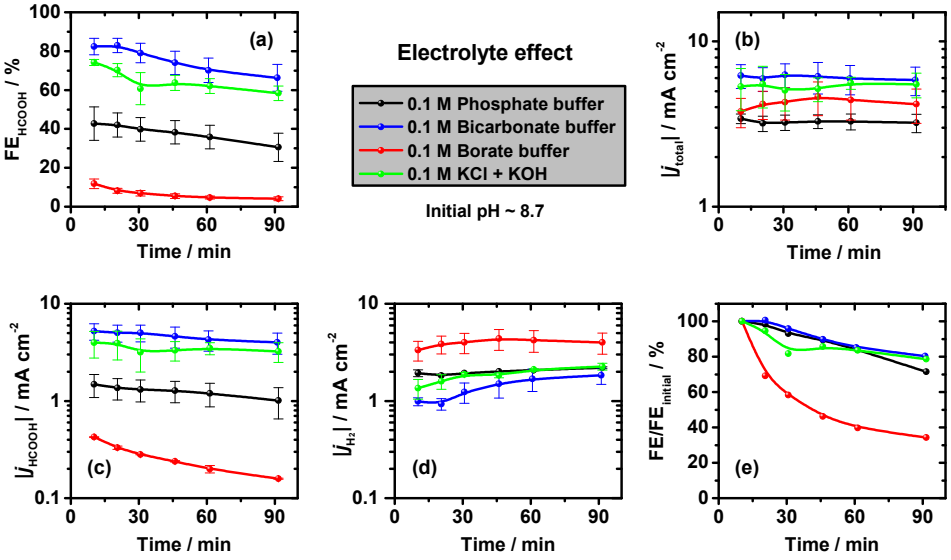

Figure 7.1 (a) Faradaic efficiency toward HCOOH, (b) absolute total current density, (c) absolute partial current density for HCOOH, (d) absolute partial current density for H_2, (e) stability during CO_2 reduction on immobilized InPP in different electrolytes of initial pH $\approx$ 8.7. Lines to guide the eye.

is suppressed in $KHCO_3$, which suggests an additional influence of bicarbonate as reported before.[23,24] Dunwell et al. argued that bicarbonate increases the concentration of CO_2 dissolved in the electrolyte by forming a so-called bicarbonate-CO_2 equilibrium complex.[23] Note that they do not imply that bicarbonate is the active species. Experiments and simulations performed by Hashiba et al., showed an improvement in the limiting CO_2 flux to the electrode surface in bicarbonate buffer compared to KCl and phosphate buffer.[24] Wuttig et al. reported on the sluggish buffering capability of bicarbonate, which acts as a proton donor past the rate-limiting step of CO_2RR on gold.[25] Since borate buffer also performs much worse compared to the unbuffered KCl electrolyte, it is unlikely that the buffering capability of the electrolyte is a necessity for high CO_2RR selectivity.

Due to the interesting performance in KCl electrolytes, and the possible influence of the pH on the performance, we investigated CO_2RR in different KCl electrolytes, where the initial pH was varied by addition of KOH to the solution. As shown in Figure 7.2a, a similar possible correlation is observed as for the three buffer electrolytes, where a more alkaline final pH leads to higher HCOOH selectivity. Figure 7.2b shows that the activity also follows a similar pH dependence as the faradaic efficiency. However, it is clear that a highly alkaline pH is not the key to high selectivity, since a 0.1 M KOH solution leads to lower HCOOH selectivity. Therefore we believe that the pH is an important, but not the only factor influencing

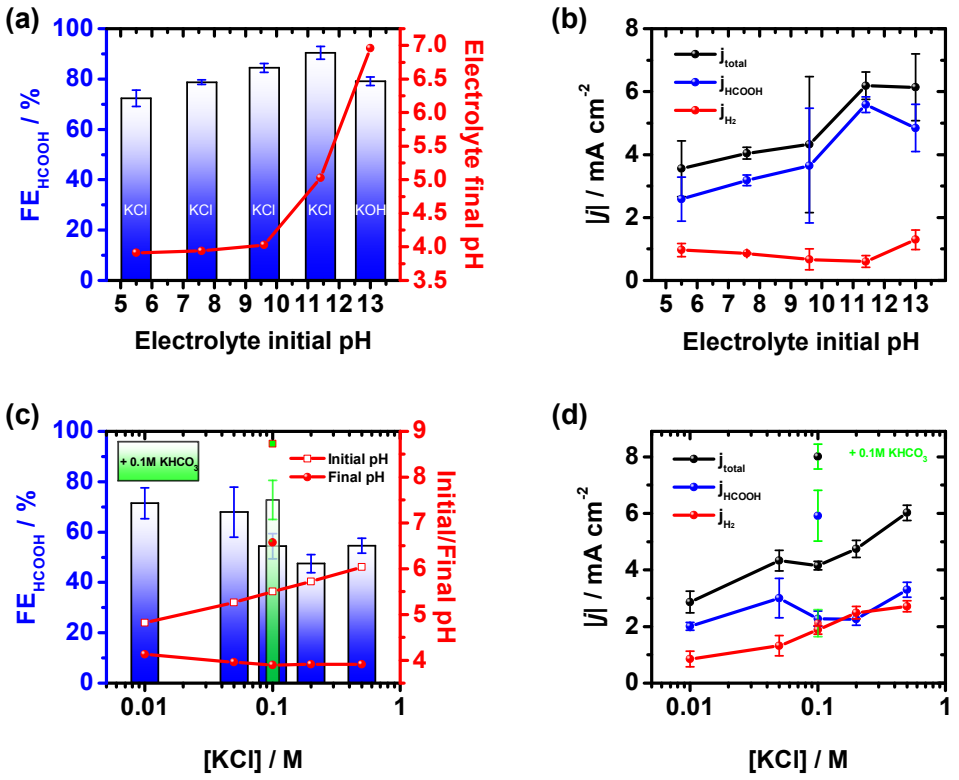

Figure 7.2 Faradaic efficiency toward HCOOH during 10 minute CO_2 reduction on immobilized InPP in (a) 0.1 M KCl electrolyte of different initial pH by addition of KOH and (c) KCl electrolytes of different concentrations. Corresponding total current density and partial current densities for HCOOH and H_2 in (b) and (d).

the selectivity toward HCOOH. Moreover, we studied the influence of different KCl concentrations on the selectivity and activity of CO_2RR as shown in Figure 7.2c-d. These different concentrations of KCl affect the pH of the electrolyte, and it can be seen that the FE again follows the trend of final pH of these electrolytes, which is in agreement with the KCl electrolytes as shown in Figure 7.2a. Interestingly, when 0.1 M $KHCO_3$ is added to 0.1 M KCl (shown in green in Figures 7.2c-d), the selectivity and activity are significantly increased, in agreement with the presumed promoting effect of bicarbonate as discussed before. It is noteworthy that in principle, after CO_2 saturation, a bicarbonate buffer is formed regardless of the electrolyte composition, albeit with different buffering strength or pH.

In our previous work, we observed a difference in the amount of HCOOH formed in phosphate buffers depending on the concentration of the phosphate buffer.[21] In Figure 7.3, we look more closely at the influence of the buffer capacity on

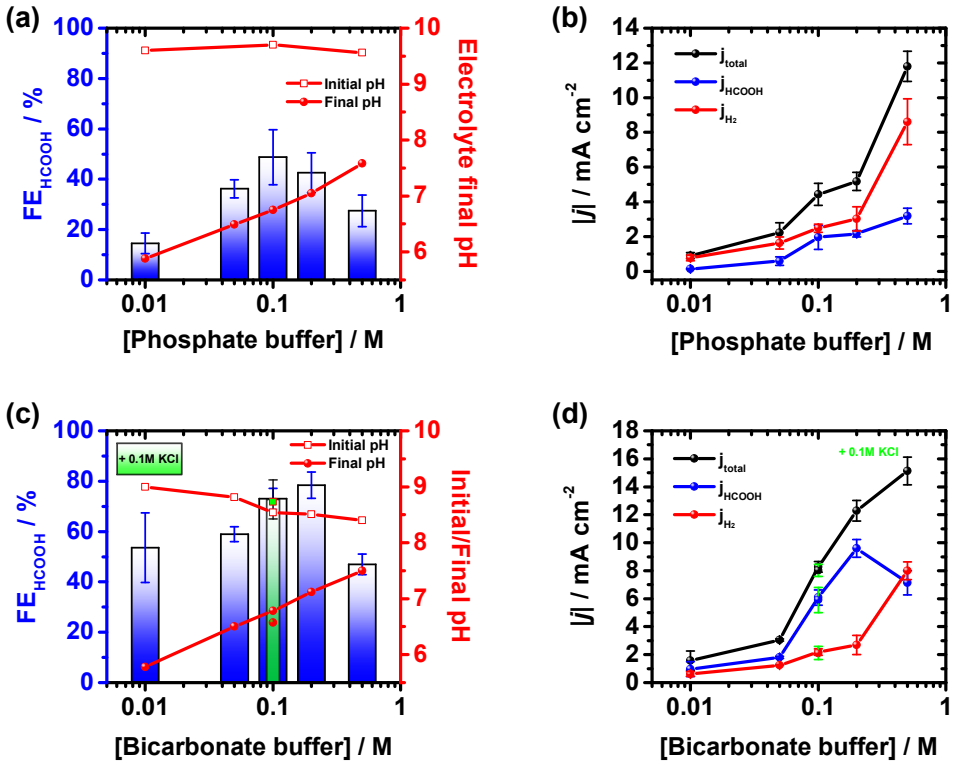

Figure 7.3 Faradaic efficiency toward HCOOH during 10 minute CO_2 reduction on immobilized InPP in (a) phosphate buffer and (c) bicarbonate buffer electrolytes with different buffering strenghts. Corresponding total current density and partial current densities for HCOOH and H_2 in (b) and (d).

the selectivity and activity of CO_2RR. We observe that an intermediate buffer capacity of 0.1 - 0.2 M leads to the highest CO_2RR selectivity in phosphate and bicarbonate buffers. This observation is different compared to the buffer capacity effect reported for copper electrodes,[6,7] which can be explained by the relatively simple product spectrum of our immobilized InPP compared to the product spectrum of copper, since the path toward either CH_4 or C_2H_4 on copper is known to be pH dependent.[26] Note that addition of 0.1 M KCl (in green in Figure 7.3c-d) does not lead to an improvement of the selectivity or activity. When studying the selectivity and activity as a function of time (Figure D.2), we find that a low buffer strength leads to an initial increase and eventually stable FE, while a high buffer strength is accompanied with a monotonic decrease in FE, and increase of hydrogen partial current (Figure D.2d), indicating the important role of local concentrations of protons and carbonaceous species. The presence of an optimum

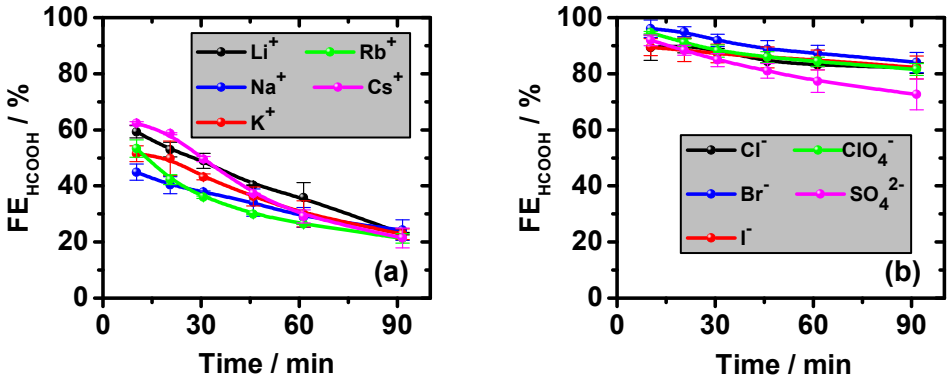

Figure 7.4 Faradaic efficiency toward HCOOH during CO_2 reduction on immobilized InPP in (a) phosphate buffer (pH 9.6) with 25 μM alkali cations in solution, and (b) 0.1 M KX electrolyte brought to pH $\approx$ 9.6, where X stands for different anions. Lines to guide the eye.

buffer capacity suggests at least two factors with opposite effects on the FE toward HCOOH. Moreover, these effects are likely to be time dependent, such as a stability issue or the settling of a new (local) equilibrium. A high buffer capacity reflects small local pH changes. The results indicate that small local pH changes negatively influence the stability and promote HER, while large pH changes suppress the HER and improve the stability. We believe that the enhanced rate of hydrogen evolution may affect the stability of the system, and a higher local pH is beneficial for high HCOOH selectivity. Differences in bulk pH after CO_2 saturation can be observed for the different buffer capacities shown in Figure 7.3a and c with red symbols. The trend of final pH between the different buffer solutions is as expected, and the possible correlation of final pH and FE is not similar to the trend observed before for the different buffer solution (higher final pH favors higher HCOOH selectivity). Deviation from this presumed correlation is observed for high final pH, which is similar to the KOH electrolyte as observed before. Therefore, we conclude that high selectivity toward HCOOH is not solely determined by the pH nor the buffer capacity, although both parameters seem to influence the faradaic efficiency toward HCOOH. Given the differences in selectivity and activity between the buffer electrolytes (Figure 7.1), we believe that also the pK_a of the buffer solution is important, influencing the CO_2 transport through the electrolyte, in agreement with recent work.[24]

In Figure 7.4a, we show that alkali cations do not significantly affect the CO_2 reduction performance on immobilized InPP, which is in contrast to the recent literature for heterogeneous electrocatalysts,[8–10,12] but in agreement with the different behavior of buffer capacity on CO_2RR for our system compared with heterogeneous electrocatalysts. Again, this could be due to the formation of only

HCOOH instead of C_1 and C_2 products, which is believed to be insensitive to differences in hydration number or pK_a value of the different cations as reported before.[11,12] Although Lewis acids such as Mg^{2+} were reported to positively impact CO_2RR under homogeneous conditions in DMF, we found that Mg^{2+} and Al^{3+} significantly worsen the selectivity toward HCOOH (Figure D.3). The promoting effect under homogeneous conditions in DMF is explained by electrophilic assistance, which helps the cleavage of C-O bonds.[16,17] Hence, it is reasonable that a similar effect is absent in our system, since the formation of HCOOH does not require C-O bond cleavage. Additionally, we observed a decrease in the electrolyte pH after addition of Al^{3+} ions, leading to promotion of HER and low FE toward HCOOH. These observations indicate the importance of the solvent, the reaction path (dominant product), and type of catalysis (homogeneous or heterogeneous) for the investigation of reaction- or process parameters on the CO_2RR selectivity and activity.

It was found in Figure 7.1 that KCl leads to higher FE compared to phosphate or borate buffer of similar pH. This enhancement could possibly be related to the presence of Cl^- ions in solution, since low buffer capacity does not lead to higher FE (Figure 7.3 and D.2a). Therefore, we systematically studied the influence of halide ions in solution. In Figure 7.4b, we compare the FE in electrolytes containing different anionic species brought to an initial pH of 9.6 by addition of KOH. Although no significant difference in selectivity is observed between the various anions, the FE is generally much higher compared to those observed earlier. An initial faradaic efficiency of 96 ± 3 % is even obtained in KBr electrolyte. Note, that there is no significant difference in the HCOOH selectivity between the typical adsorbing (halide and SO_4^{2-}) and non-adsorbing anions (ClO_4^-), which excludes an active site blockage effect.

7.4 Conclusions and Outlook

It can be concluded that the impact of electrolyte composition strongly depends on the type of catalysis, nature of the solvent and product distribution, and variations in the electrolyte composition can significantly affect the selectivity and activity of the CO_2RR. Although a cation or anion effect is absent, slight differences in the concentration or nature of ionic species in the electrolyte can affect the final pH, and consequently the performance of CO_2RR. The impact on the CO_2RR performance is believed to be a synergistic effect of various parameters such as pH after CO_2 saturation, buffering strength and pK_a of the electrolyte, which makes it difficult or even impossible to predict a priori the influence of a specific parameter on the CO_2RR performance.

The investigated system in this work, indium(III) protoporphyrin IX immobilized on pyrolytic graphite, behaves differently compared to homogeneous and heterogeneous electrocatalysts, since it does not show a typical cation nor anion effect for CO_2RR selectivity or reactivity. However, we show a strong influence of

the electrolyte composition and buffer strength on the selectivity of CO_2RR, where even the highest HCOOH selectivity for this system measured so far (FE $\approx 96 \pm 3$ %), is obtained in unbuffered electrolytes. Furthermore, the detachment of the porphyrin, leading to instability of the catalyst, is most likely associated to the low local pH and high hydrogen evolution activity.

7.5 References

[1] D. T. Whipple, P. J. A. Kenis, *J. Phys. Chem. Lett.* **2010**, *1*, 3451–3458.

[2] E. V. Kondratenko, G. Mul, J. Baltrusaitis, G. O. Larrazábal, J. Pérez-Ramírez, *Energy Environ. Sci.* **2013**, *6*, 3112–3135.

[3] Y. Hori, A. Murata, R. Takahashi, S. Suzuki, *J. Chem. Soc. Chem. Commun.* **1988**, *0*, 17–19.

[4] Y. Hori, A. Murata, R. Takahashi, *J. Chem. Soc. Faraday Trans. 1* **1989**, *85*, 2309–2326.

[5] S. Verma, X. Lu, S. Ma, R. I. Masel, P. J. A. Kenis, *Phys. Chem. Chem. Phys.* **2016**, *18*, 7075–7084.

[6] R. Kas, R. Kortlever, H. Yilmaz, M. T. M. Koper, G. Mul, *ChemElectroChem* **2015**, *2*, 354–358.

[7] A. S. Varela, M. Kroschel, T. Reier, P. Strasser, *Catal. Today* **2016**, *260*, 8–13.

[8] J. Resasco, L. D. Chen, E. Clark, C. Tsai, C. Hahn, T. F. Jaramillo, K. Chan, A. T. Bell, *J. Am. Chem. Soc.* **2017**, *139*, 11277–11287.

[9] O. Ayemoba, A. Cuesta, *ACS Appl. Mater. Interfaces* **2017**, *9*, 27377–27382.

[10] E. Pérez-Gallent, G. Marcandalli, M. C. Figueiredo, F. Calle-Vallejo, M. T. M. Koper, *J. Am. Chem. Soc.* **2017**, *139*, 16412–16419.

[11] A. Murata, Y. Hori, *Bull. Chem. Soc. Jpn.* **1991**, *64*, 123–127.

[12] M. R. Singh, Y. Kwon, Y. Lum, I. Joel W. Ager, A. T. Bell, *J. Am. Chem. Soc.* **2016**, *138*, 13006–13012.

[13] M. R. Thorson, K. I. Siil, P. J. A. Kenis, *J. Electrochem. Soc.* **2013**, *160*, F69–F74.

[14] A. S. Varela, W. Ju, T. Reier, P. Strasser, *ACS Catal.* **2016**, *6*, 2136–2144.

[15] Y. Y. Birdja, M. T. M. Koper, *J. Am. Chem. Soc.* **2017**, *139*, 2030–2034.

[16] M. Hammouche, D. Lexa, M. Momenteau, J.-M. Savéant, *J. Am. Chem. Soc.* **1991**, 8455–8466.

[17] I. Bhugun, D. Lexa, J.-M. Savéant, *J. Phys. Chem.* **1996**, *100*, 19981–19985.

[18] J. L. Inglis, M. T. MacLean, B. J. Pryce, J. G. Vos, *Coord. Chem. Rev.* **2012**, *256*, 2571–2600.

[19] G. F. Manbeck, E. Fujita, *J. Porphyrins Phthalocyanines* **2015**, *19*, 45–64.

[20] J. Shen, R. Kortlever, R. Kas, Y. Y. Birdja, O. Diaz-Morales, Y. Kwon, I. Ledezma-Yanez, K. J. P. Schouten, G. Mul, M. T. M. Koper, *Nat. Commun.* **2015**, *6*, 8177.

[21] Y. Y. Birdja, J. Shen, M. T. M. Koper, *Catal. Today* **2017**, *288*, 37–47.

[22] Y. Y. Birdja, R. E. Vos, T. A. Wezendonk, L. Jiang, F. Kapteijn, M. T. M. Koper, *ACS Catal.* **under revision**.

[23] M. Dunwell, Q. Lu, J. M. Heyes, J. Rosen, J. G. Chen, Y. Yan, F. Jiao, B. Xu, *J. Am. Chem. Soc.* **2017**, *139*, 3774–3783.

[24] H. Hashiba, L.-C. Weng, Y. Chen, H. K. Sato, S. Yotsuhashi, C. Xiang, A. Z. Weber, *J. Phys. Chem. C* **2018**, *in press*.

[25] A. Wuttig, Y. Yoon, J. Ryu, Y. Surendranath, *J. Am. Chem. Soc.* **2017**, *139*, 17109–17113.

[26] K. J. P. Schouten, E. P. Gallent, M. T. M. Koper, *J. Electroanal. Chem.* **2014**, *716*, 53–57.

Summary and Future Perspectives

Summary

Global energy challenges have received unprecedented attention and recognition in recent decades, which is associated with the increase in carbon dioxide emissions from fossil fuel combustion, global warming, climate change, and consequently the aim to decarbonize the current energy system. Electrification and renewable energy utilization are acknowledged to play an important role in future energy systems. In this respect, electrocatalysis is of paramount importance, since it facilitates the incorporation of renewable electricity in future energy systems. Renewable electricity is then stored in chemical bonds as fuels or commodity chemicals by sustainable processes. An additional advantage is the ability to tackle the intermittency problem of renewable energy sources. The production of energy carriers from CO_2 is a promising strategy to aid in the aforementioned energy and CO_2 related issues. Since the current energy infrastructure is optimized for liquid fuels, which are easier to handle and to store compared to gaseous fuels, the production of liquid products from CO_2 is preferred. This thesis focuses on the use of heterogeneous electrocatalysts and heterogenized molecular catalysts for the electrocatalytic conversion of CO_2 toward liquid products.

First, we give the conspectus from a broad perspective, briefly discussing the current status of the carbon cycle, and the role and relevance of electrocatalytic CO_2 reduction herein.

In chapter 2, we review recent breakthroughs and remaining obstacles in the research field of electrocatalytic CO_2 reduction. We highlight progress on important mechanistic topics such as the initial activation of CO_2, and carbon-carbon bond formation. Moreover, we discuss the influence of the electrode morphology and process- and reaction conditions such as mass transport, local pH gradients and cationic/anionic species on CO_2 electroreduction. Lastly, we discuss two important techniques often employed in electrochemical CO_2 reduction research: in situ spectroelectrochemistry and computational techniques.

In chapter 3, we shed light on local phenomena in the vicinity of the electrode surface, which influence the product spectrum of electrocatalytic CO_2 reduction. We demonstrate the involvement of disproportionation reactions, promoted by

the local alkaline environment near the electrode surface during electrocatalytic CO_2 reduction, caused by the concomitant hydrogen evolution reaction. These Cannizzaro-type reactions are found to be independent of the electrode material, and lead to disproportionation of aldehydes into acids and alcohols, which should be distinguished from those formed by direct CO_2 reduction. Especially for the formation of liquid products such as methanol and ethanol, where the corresponding aldehyde is often proposed as a reaction intermediate, one should keep the presence of these phenomena in mind, and be careful with the attribution of alcohols or acids observed. Lastly, we show that the occurrence of these disproportionation reactions is strongly influenced by the electrolyte pH and buffering strength.

We shift to electrochemical CO_2 reduction on molecular catalysts, which is introduced in chapter 4. First we give an overview of molecular catalysts often used for electrochemical CO_2 reduction. Next we briefly review the work done on metalloporphyrins for CO_2 reduction. We conclude this chapter with a discussion of heterogenized systems of molecular catalysts, since the remainder of this thesis is devoted to electrochemical CO_2 reduction on heterogenized metalloporphyrins.

In chapter 5, we study the electrocatalytic reduction of CO_2 toward formic acid on different metalloprotoporphyrins immobilized on pyrolytic graphite. We reveal the formic acid selectivity dependence on the metal center of metalloprotoporphyrins. Based on their metal center, we show that the investigated metalloprotoporphyrins can be divided in active (Rh, Sn, In centers), poorly active (Ni, Cu, Ga, Pd centers) and inactive (Cr, Mn, Fe, Co centers) porphyrins for formic acid formation. Moreover, we investigate the influence of the overpotential and electrolyte pH, which strongly affects the selectivity toward formic acid. Sn- and In-protoporphyrins are shown to be weakly coupled to the hydrogen evolution reaction, while Rh-protoporphyrin is strongly coupled to the hydrogen evolution reaction, leading to lower faradaic efficiency toward formic acid for rhodium protoporphyrin. Indium protoporphyrin was found to be the most active, the most stable, and most selective toward formic acid (faradaic efficiency up to ≈ 70 %). Finally, an attempt was made to qualitatively study the influence of bicarbonate in formic acid formation.

Chapter 6 builds upon the findings of chapter 5, by studying immobilized indium protoporphyrins in more detail. Although heterogenized molecular catalysts have gained more attention recently, experimental procedures and choices are often still based on empirical considerations, without underlying mechanistic rationale. In this chapter, we made an attempt to gain insight into factors related to heterogenization of molecular catalysts. We investigate the influence of the nature of the substrate, its chemical functionality, and the catalyst chemical environment on the electrocatalytic CO_2 reduction performance. We show that there is a significant effect of the substrate, where pyrolytic graphite outperforms glassy carbon and boron doped diamond substrates with respect to the selectivity and activity of CO_2 electroreduction. This superior performance is ascribed to a combination of factors such as a more porous surface structure, leading to more efficient mass transport, an optimal interaction between substrate and catalyst, and a favorably low hydrogen evolution activity. Moreover, we modify the surface chemical functionality by plasma- and

electrochemical pretreatment of the pyrolytic graphite substrate. We show that hydrogenated functional groups negatively influence the selectivity, activity and stability of CO_2 electroreduction, while oxygen functionalization slightly improves the CO_2 reduction performance. Anodization of the pyrolytic graphite surface leads to a substantial enhancement in stability, which is associated with the formation of a thick graphite oxide layer with high edge plane density. Lastly, we immobilize the indium protoporphyrin in polymeric membranes. We show that encapsulation of the catalyst in polymeric membranes cannot be described simply by introducing a hydrophobic environment, which suppresses the hydrogen evolution. We found that dispersion in poly(4-vinylpyridine) and poly(3,4-ethylenedioxythiophene) polystyrene sulfonate improve the selectivity, activity and stability of CO_2 reduction, while encapsulation in nafion negatively impacts the CO_2 reduction. Although other molecular catalysts may behave differently, we strongly believe that there will be an influence of the substrate, its pretreatment, and catalyst encapsulation in polymers on the selectivity, reactivity and stability of CO_2 electroreduction. The insights obtained here, can be used to fine-tune and optimize heterogenized molecular systems for the electrocatalytic CO_2 reduction beyond the empirical level.

In chapter 7, we continue with the study of indium protoporphyrins immobilized on pyrolytic graphite for the electrochemical reduction of CO_2 toward formic acid. Herein, we investigate extrinsic factors to the porphyrin catalyst, which affect the CO_2 reduction performance. We focus on the effects of electrolyte composition on the activity and selectivity of CO_2 reduction, such as the influence of ionic species in solution, buffering strength and initial (bulk) pH of the electrolyte. Moreover, we look into the cause of instability observed for the heterogenized indium protoporphyrin system.

Future Perspectives

Electrochemical reduction of carbon dioxide will play a prominent role in future energy systems. However, in order to ultimately contribute to a more sustainable carbon cycle, simultaneous implementation of various processes is required. Most importantly, we need to move from laboratory scale to industrial scale, which leads to additional research topics that need to be addressed, not only from a fundamental point of view, but from an engineering perspective as well e.g. integration with a CO_2 capture system, large-scale production and regeneration of catalysts, product separation, and economic viability of the whole industrial system.

Zooming in on the electrocatalytic CO_2 reduction itself, to date, research has mostly focused on the fundamental and mechanistic aspects of electrochemical CO_2 reduction. Firstly, attention should also be given to the anode side of the system, since this can significantly affect the efficiency of the complete system. Moreover, instead of merely finding or improving highly active/selective electrocatalysts, CO_2 reduction research should be directed toward the inclusion of extrinsic factors

such as mass transport phenomena, fluid flow, electrode morphology, process- and reaction conditions, and catalyst stability.

Samenvatting en Toekomstperspectieven

Samenvatting

Wereldwijde energiegerelateerde uitdagingen hebben in de afgelopen decennia ongekende aandacht en erkenning gekregen, wat geassocieerd wordt met onder andere de toename in kooldioxide uitstoot door verbranding van fossiele brandstoffen, opwarming van de aarde, klimaatverandering en hieruit voortvloeiend het streven om het huidige energiesysteem koolstofvrij te maken. Men is het erover eens dat elektrificatie en het gebruik van hernieuwbare energie een belangrijke rol zullen spelen in toekomstige energiesystemen. Hierbij is elektrokatalyse uitermate belangrijk, aangezien zij de integratie van hernieuwbare elektriciteit in toekomstige energiesystemen mogelijk maakt. Hernieuwbare elektriciteit wordt dan door duurzame processen opgeslagen in chemische bindingen als brandstoffen of grondstoffen. Een bijkomend voordeel is de mogelijkheid om het probleem van onbalans tussen productie en afname van hernieuwbare elektriciteit aan te pakken. De productie van energiedragers uit CO_2 is een veelbelovende strategie om bij te dragen aan de oplossing van bovengenoemde energie en CO_2 gerelateerde problemen. Aangezien de huidige energie infrastructuur geoptimaliseerd is voor vloeibare brandstoffen, welke makkelijker zijn voor gebruik en opslag dan gasvormige brandstoffen, geniet de productie van vloeibare producten uit CO_2 de voorkeur. In dit proefschrift ligt de focus op heterogene elektrokatalysatoren en geheterogeniseerde moleculaire katalysatoren voor de elektrokatalytische omzetting van CO_2 in vloeibare producten.

Eerst geven wij de synopsis vanuit een breed perspectief, waarin we kort de huidige status van de koolstofcyclus bespreken, evenals de rol en relevantie van elektrokatalytische CO_2 reductie hierin.

In hoofdstuk 2 laten we recente doorbraken en resterende obstakels in het onderzoeksgebied van elektrokatalytische CO_2 reductie de revue passeren. Hierbij benadrukken we de vooruitgang in belangrijke mechanistische onderwerpen zoals de initiële activering van CO_2 en de vorming van de koolstof-koolstof binding. Verder bespreken we de invloed van de elektrode morfologie en proces- en reactie omstandigheden waaronder massa transport, lokale pH gradiënten en kationen/anionen op de elektroreductie van CO_2. Ten slotte bediscussiëren we twee belangrijke

technieken die vaak toegepast worden in onderzoek binnen de elektrochemische CO_2 reductie: in situ spectroelektrochemie en computationele technieken.

In hoofdstuk 3 belichten we lokale verschijnselen in de nabijheid van het elektrode oppervlak, die het product spectrum van de elektrokatalytische CO_2 reductie beïnvloeden. We tonen de betrokkenheid van disproportioneringsreacties aan, welke bevorderd worden door het lokale alkalisch milieu nabij het elektrode oppervlak tijdens de elektrokatalytische CO_2 reductie, wat veroorzaakt wordt door de gelijktijdige waterstof evolutie reactie. Deze Cannizzaro-type reacties blijken onafhankelijk te zijn van het elektrode materiaal en leiden tot de disproportionering van aldehyden in zuren en alcoholen, wat onderscheiden moet worden van zuren en alcoholen gevormd door directe CO_2 reductie. Vooral bij de vorming van vloeibare producten zoals methanol en ethanol, waar het corresponderende aldehyde vaak als tussenproduct wordt voorgesteld, moet men terdege rekening houden met deze verschijnselen en voorzichtigheid betrachten bij het toeschrijven van de vorming van waargenomen alcoholen en zuren. Ten slotte laten wij zien dat het voorkomen van deze disproportioneringsreacties sterk wordt beïnvloed door de pH en buffersterkte van het elektrolyt.

Vervolgens wordt er overgeschakeld op de elektrochemische CO_2 reductie aan moleculaire katalysatoren, wat ingeleid wordt in hoofdstuk 4. Allereerst geven we een overzicht van de moleculaire katalysatoren die vaak gebruikt worden voor de elektrochemische CO_2 reductie. Vervolgens bediscussiëren we de studies uitgevoerd aan metalloporfyrines voor de CO_2 reductie. We sluiten dit hoofdstuk af met een discussie over geheterogeniseerde systemen van moleculaire katalysatoren, aangezien het vervolg van dit proefschrift gewijd is aan de elektrochemische CO_2 reductie aan geheterogeniseerde metalloporfyrines.

In hoofdstuk 5 bestuderen we de elektrokatalytische reductie van CO_2 tot mierenzuur aan verschillende metalloprotoporfyrines geïmmobiliseerd aan pyrolytisch grafiet. We onthullen dat de selectiviteit van mierenzuur afhankelijk is van het metaal centrum van de metalloprotoporfyrine en dat op basis van het metaal centrum, de onderzochte metalloprotoporfyrines in te delen zijn in actieve (Rh, Sn, In centra), weinig actieve (Ni, Cu, Ga, Pd centra) en inactieve (Cr, Mn, Fe, Co centra) porfyrines voor de vorming van mierenzuur. Verder onderzoeken we de invloed van de overpotentiaal en de pH van het elektrolyt, wat de selectiviteit naar mierenzuur sterk beïnvloedt. Er wordt aangetoond dat Sn- en In-protoporfyrines zwak gekoppeld zijn aan de waterstof evolutie reactie, terwijl Rh-protoporfyrine sterk gekoppeld is aan de waterstof evolutie reactie, wat leidt tot een lagere faraday efficiëntie voor mierenzuur aan rhodium protoporfyrine. Indium protoporfyrine bleek de meest actieve, meest stabiele en meest selectieve van de onderzochte porfyrines te zijn met betrekking tot de vorming van mierenzuur (faraday efficiëntie tot wel ≈ 70 %). Uiteindelijk is ook een begin gemaakt om de invloed van bicarbonaat op de mierenzuur vorming kwalitatief te onderzoeken.

Hoofdstuk 6 borduurt voort op de bevindingen van hoofdstuk 5 door de geïmmobiliseerde indium protoporfyrines in meer detail te onderzoeken. Hoewel geheterogeniseerde moleculaire katalysatoren recent steeds meer aandacht krijgen,

zijn experimentele procedures en keuzes vaak nog gebaseerd op empirische overwegingen zonder onderliggende mechanistische redeneringen. In dit hoofdstuk proberen wij inzicht te krijgen in factoren betrokken bij de heterogenisering van moleculaire katalysatoren. Wij onderzoeken de invloed van het soort substraat, zijn chemische functionaliteit en het chemische milieu van de katalysator op de prestaties van de elektrokatalytische CO_2 reductie. Wij tonen een significant effect van het substraat aan, waarbij pyrolytisch grafiet beter presteert in termen van selectiviteit en activiteit van CO_2 elektroreductie, vergeleken met glasachtig koolstof ("glassy carbon") en boor-gedoteerd diamant ("boron doped diamond") substraten. Deze betere prestatie wordt toegeschreven aan een combinatie van factoren zoals een poreuzere oppervlaktestructuur wat een beter massa transport tot gevolg heeft, een optimale interactie tussen substraat en katalysator, en een gunstige lage waterstof evolutie activiteit. Bovendien modificeren we de chemische functionaliteit van het substraat door plasma- en elektrochemische voorbehandelingen van het pyrolytisch grafiet substraat. We tonen aan dat gehydrogeneerde functionele groepen een negatieve invloed hebben op de selectiviteit, activiteit en stabiliteit van CO_2 elektroreductie, terwijl zuurstof functionalisering de CO_2 reductie prestaties enigszins verbetert. Anodisatie van het pyrolytisch grafiet oppervlak leidt tot een substantiële verbetering van de stabiliteit, wat gerelateerd is aan de vorming van een dikke grafiet oxidelaag met hoge randvlakdichtheid ("edge-plane density"). Ten slotte immobiliseren we de indium protoporfyrine in polymere membranen. We laten zien dat het inkapselen van de katalysator in polymere membranen niet simpelweg beschreven kan worden als het introduceren van een hydrofobe omgeving wat de waterstof evolutie onderdrukt. Dispersie in poly(4-vinylpyridine) en poly(3,4-ethyleendioxythiopheen) polystyreen sulfonaat bleek de selectiviteit, activiteit en stabiliteit van CO_2 reductie te verbeteren, terwijl inkapseling in nafion een negatieve invloed heeft op de CO_2 reductie. Hoewel andere moleculaire katalysatoren zich anders kunnen gedragen, geloven we er sterk in dat er een invloed zal zijn van het substraat, zijn voorbehandeling en inkapseling van de katalysator in polymeren op de selectiviteit, reactiviteit en stabiliteit van CO_2 elektroreductie. De inzichten die hier zijn verkregen, kunnen worden gebruikt voor het verfijnen en optimaliseren van geheterogeniseerde moleculaire systemen voor de elektrokatalytische CO_2 reductie op basis van meer dan alleen het empirisch niveau.

In hoofdstuk 7 vervolgen we de studie van indium protoporfyrines, geïmmobiliseerd aan pyrolytisch grafiet, voor de elektrochemische reductie van CO_2 naar mierenzuur. Hierin onderzoeken we extrinsieke factoren ten opzichte van de porfyrine katalysator, die de prestatie van CO_2 reductie beïnvloeden. We concentreren ons op de effecten van de samenstelling van het elektrolyt op de activiteit en selectiviteit van CO_2 reductie, zoals de invloed van ionen in de oplossing, buffersterkte en initiële (bulk) pH van het elektrolyt. Verder richten wij ons ook op oorzaken van de waargenomen instabiliteit van het geheterogeniseerde indium protoporfyrine systeem.

Toekomstperspectieven

Elektrochemische reductie van kooldioxide zal een prominente rol vervullen in toekomstige energiesystemen. Echter, om uiteindelijk bij te dragen aan een duurzamere koolstofcyclus, is een gelijktijdige implementatie van verschillende processen noodzakelijk. Het belangrijkste is de overgang van laboratoriumschaal naar industriële schaal, wat leidt tot aanvullende onderzoeksthema's die niet alleen vanuit fundamenteel oogpunt, maar ook vanuit een technisch oogpunt benaderd moeten worden. Voorbeelden zijn de integratie met een CO_2 opvangsysteem, grootschalige productie en regeneratie van katalysatoren, scheiding van producten en economische haalbaarheid van het complete industriëel systeem.

Als wordt ingezoomd op de elektrokatalytische CO_2 reductie, blijkt dat het onderzoek zich heden ten dage vooral heeft geconcentreerd op fundamentele en mechanistische aspecten van de elektrochemische CO_2 reductie. Allereerst moet ook aandacht besteed worden aan de kant van de anode, aangezien dit de efficiëntie van het totale systeem aanzienlijk kan beïnvloeden. Verder moet CO_2 reductie onderzoek meer gericht worden op het betrekken van extrinsieke factoren zoals massa transportverschijnselen, vloeistofstroming, elektrode morfologie, proces- en reactie omstandigheden en stabiliteit van de katalysator in plaats van alleen te zoeken naar of verbeteren van zeer actieve/selectieve elektrokatalysatoren.

Appendices

Appendix A

Supporting Information to Chapter 3

The Importance of Cannizzaro-Type Reactions during Electrocatalytic Reduction of Carbon Dioxide

A.1 Characterization of the BDD electrode

Figure A.1 displays the spectra of the Boron Doped Diamond and Pyrolytic Graphite (PG) electrodes, indicating the sp^3 and sp^2 bonded carbon atoms. In Figure A.2 (a) the blank voltammograms and (b) CO_2 reduction and hydrogen evolution on the BDD electrode are shown in 0.001 M $HClO_4$ + 0.099M $NaClO_4$ electrolyte.

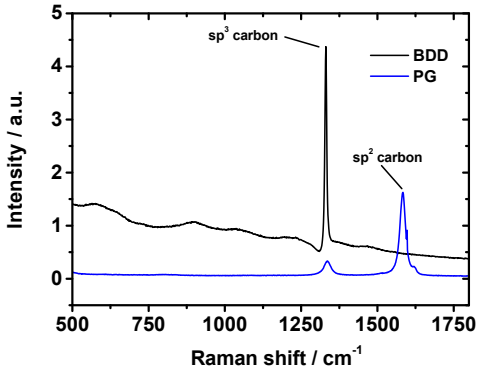

Figure A.1 Raman spectra of the BDD electrode and the PG electrode

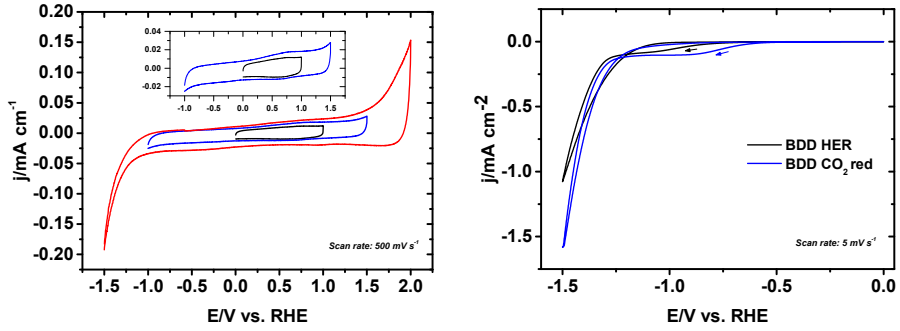

(a) (b)

Figure A.2 (a) Blank voltammograms on BDD in 0.001 M $HClO_4$ + 0.099M $NaClO_4$ electrolyte. Scan rate: 500 mV s^{-1} and (b) CO_2 reduction & hydrogen evolution on BDD in 0.001 M $HClO_4$ + 0.099M $NaClO_4$ electrolyte. Scan rate: 5 mV s^{-1}.

A.2 Faradaic efficiency liquid products

Potentiostatic bulk electrolysis experiments are performed for 90 minutes to determine the faradaic efficiency of the major liquid products from CO_2 reduction,

HCHO and HCOOH. 100 μl samples are taken at specific times and analyzed with HPLC. The faradaic efficiency is calculated using equation A.1, where z_i is the number of electrons needed for the formation of product i, n_i the amount of product i formed (in moles), F the Faraday constant and Q the total charge calculated by the integration of the measured (IR corrected) current with respect to time.

$$FE_i = \frac{z_i n_i F}{Q} \cdot 100\% \tag{A.1}$$

The faradaic efficiency towards HCHO and HCOOH are shown in Figure A.3 for E = -0.95 V and E = -2.1 V. These values are lower compared to the results of Nakata et al.,[1] which is ascribed to the use of an electrolyte with higher proton concentration in our experiments. The total faradaic efficiency of HCHO and HCOOH is less than 100 %, where the remaining charge is assumed to be used for the production of H_2 and CO as detected by OLEMS. As described in chapter 3, the concomitant hydrogen evolution leads to a local alkaline environment and since the aim of this paper is to elucidate the effects of this local pH gradient and not on optimizing catalyst efficiency, we have not determined the faradaic efficiency at other reaction conditions (pH, potential etc.). At E = -2.1 V, HCHO was not detected, which is in agreement with our online HPLC measurement (Figure 3.1C). Moreover, the faradaic efficiency for HCHO decreases with time, while the faradaic efficiency towards HCOOH increases in time. This could be due to disproportionation of formaldehyde as discussed in chapter 3.

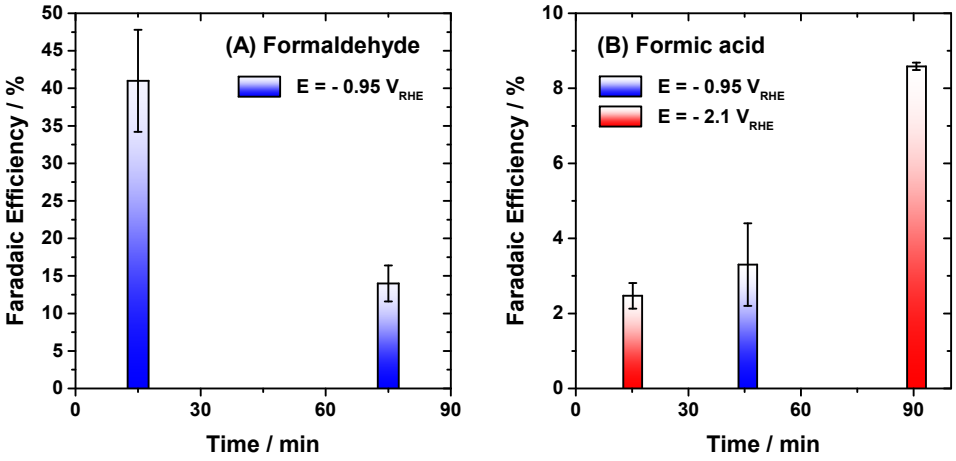

Figure A.3 Faradaic efficiency towards (A) formaldehyde and (B) formic acid at E = -0.95 V_{RHE} and E = -2.1 V_{RHE} on BDD in 0.001 M $HClO_4$ + 0.099M $NaClO_4$ electrolyte

A.3 Methanol formation during formaldehyde reduction

In addition to the online HPLC measurements, Online Electrochemical Mass Spectrometry has been utilized to investigate the products formed by reduction of formaldehyde on BDD in 0.001 M $HClO_4$ + 0.099M $NaClO_4$ electrolyte. As seen in Figure A.4a, m/z = 31 is observed with an onset potential similar to H_2. This mass fragment is associated with methanol (CH_2OH^+). The reason why no methanol was detected with HPLC (Figure 3.2A) is due to the very low concentrations of methanol formed. In order to prove this, a higher concentration of formaldehyde was reduced and methanol was detected as shown in Figure A.4b. Now formic acid is not observed which is due to overlap in the chromatograms of the large formaldehyde peak with that of formic acid.

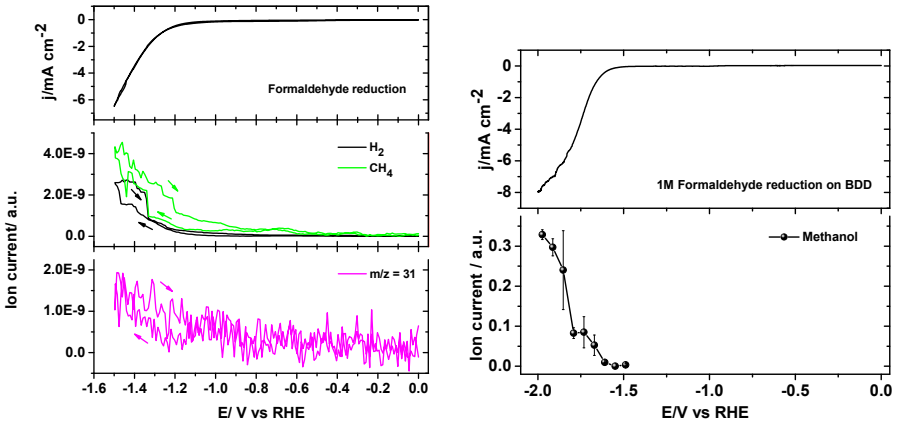

(a) OLEMS **(b)** Online HPLC

Figure A.4 (a) Formation of H_2 and methanol during 100 mM formaldehyde reduction and (b) formation of methanol during 1 M formaldehyde reduction in 0.001 M $HClO_4$ + 0.099M $NaClO_4$ electrolyte. Scan rate: 1 mV s^{-1}.

A.4 Formation of Cannizzaro products from C_1-C_3 aldehydes and NaOH

Experiments were performed to investigate the products formed by the C_1-C_3 aldehydes treated with OH^-. 50 mM of the aldehydes was mixed with different concentrations of NaOH and analyzed with HPLC. In all cases the carboxylic acids and primary alcohols were detected as shown in Figure A.5. The higher

the hydroxide concentration, the higher the concentration of carboxylic acid and primary alcohol.

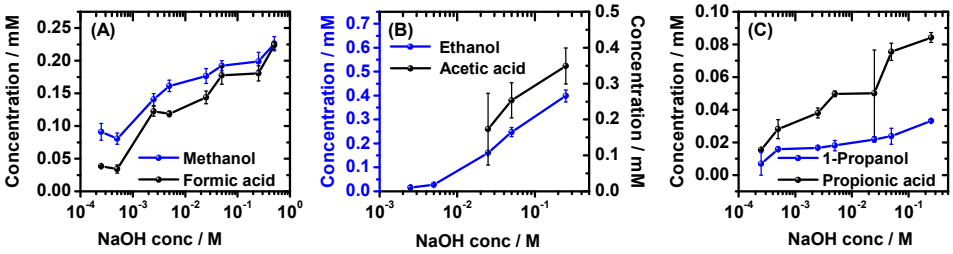

Figure A.5 Formation of carboxylic acids and alcohols during reduction of (A) Formaldehyde, (B) Acetaldehyde and (C) Propionaldehyde as function of OH^- concentration

A.5 Liquid product formation on other electrodes

The formation of the carboxylic acids and primary alcohols during reduction of the C_1-C_3 aldehydes on a Pyrolytic Graphite electrode in perchloric acid of pH 3 is shown in Figure A.6. Figure A.7 displays the reduction of formaldehyde on gold and copper in 0.001 M $HClO_4$ + 0.099M $NaClO_4$ electrolyte, leading to formic acid and methanol. In both figures the onset of the carboxylic acid and alcohol is similar to the HER onset potential.

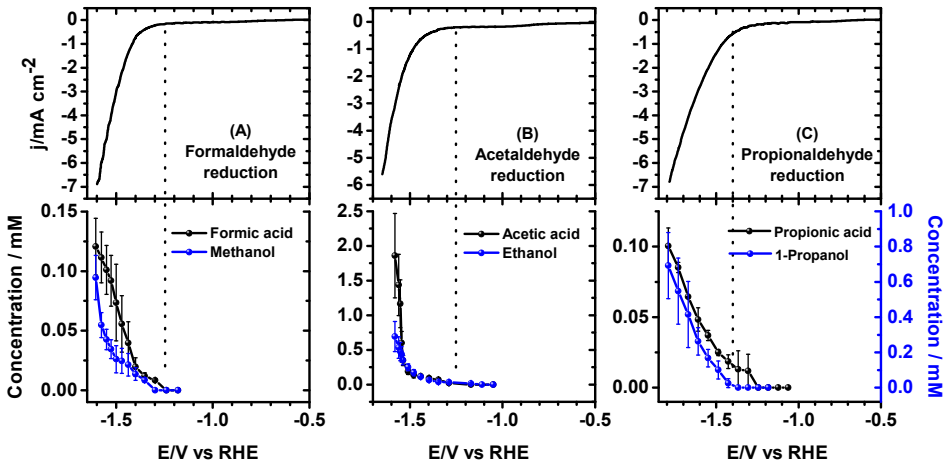

Figure A.6 Liquid products detected during reduction of (A) 50 mM Formaldehyde, (B) 100 mM Acetaldehyde and (C) 100 mM Propionaldehyde on pyrolytic graphite in 0.001 M $HClO_4$ + 0.099M $NaClO_4$ electrolyte. Scan rate: 1 mV s^{-1}

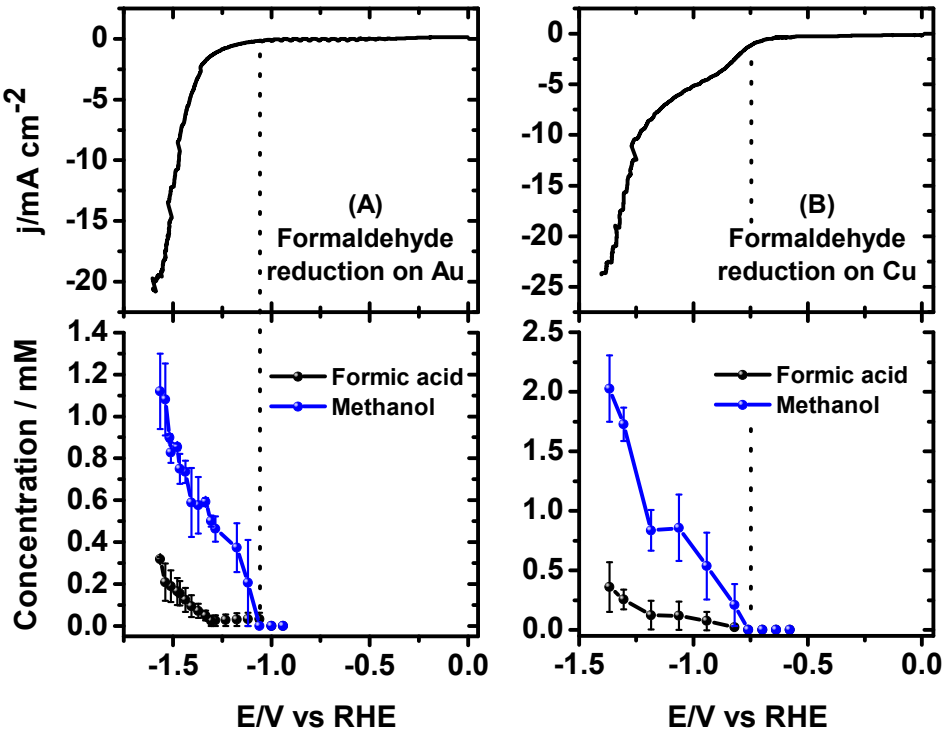

Figure A.7 Liquid products detected during reduction of 50 mM Formaldehyde on (A) gold and (B) copper in 0.001 M $HClO_4$ + 0.099M $NaClO_4$ electrolyte. Scan rate: 1 mV s^{-1}

A.6 References

[1] K. Nakata, T. Ozaki, C. Terashima, A. Fujishima, Y. Einaga, *Angew. Chem. Int. Ed.* **2014**, *53*, 871–874.

APPENDIX B

Supporting Information to Chapter 5

Influence of the Metal center of Metalloprotoporphyrins on the Electrocatalytic CO_2 reduction to Formic acid

B.1 Blank voltammograms

Before each experiment, the immobilization of the MPP is qualitatively verified by measuring a cyclic voltammogram in the potential range of -0.5 and 1.3 V_{RHE} before and after immobilization. The presence of additional redox waves ensures the immobilization of the MPP. In Figure B.1 the voltammograms for RhPP, InPP and SnPP are shown. It can be seen that PG itself already shows redox peaks (between 0.5-0.7 V) and a reduction peak (around -0.3 V). These peaks are ascribed to electron transfer processes of surface functional groups on PG as studied extensively by Compton and coworkers.[1–4] The extra peaks which become visible after immobilization of the MPP are associated to redox transitions of the metal center itself. The exact nature of the redox transition is not investigated herein as only a qualitative proof of immobilization is desired.

In Figure B.2a the formation of volatile products on pristine PG in $HClO_4$, pH = 3 is depicted. As can be seen only H_2 is produced on PG. In Figure B.2b the CO_2 reduction on pristine PG is measured and again only significant amounts of H_2 are observed. As the m/z = 44 and m/z = 28 signals decrease at negative potentials it is assumed that CO_2 is consumed at these potentials (CO follows the CO_2 signal, unless the signal is much higher compared to CO_2). As no other mass signals were found to increase it is likely that CO_2 reduction on PG does not produce significant amounts of products and the current is mainly due to HER. The CO_2 consumption at negative potentials is ascribed to an increase in local pH at the electrode surface, converting CO_2 into HCO_3^-.

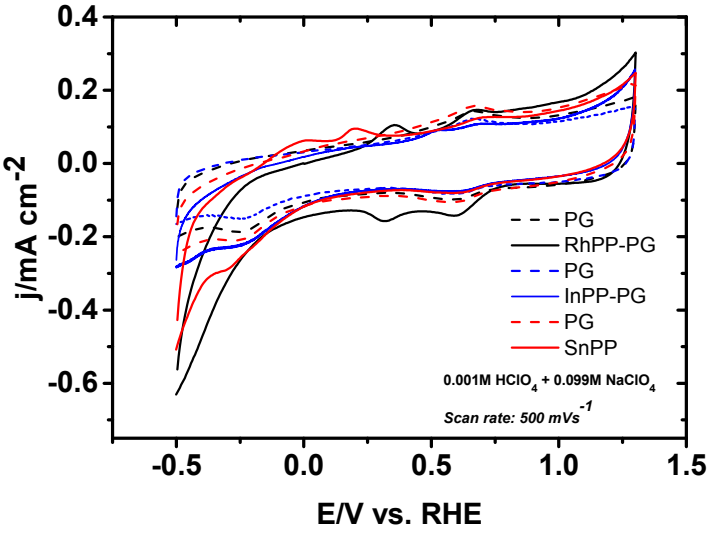

Figure B.1 Blank CV's on (immobilized MPPs on) PG in 0.001 M $HClO_4$ + 0.099 M $NaClO_4$. Scan rate: 500 mV s^{-1}.

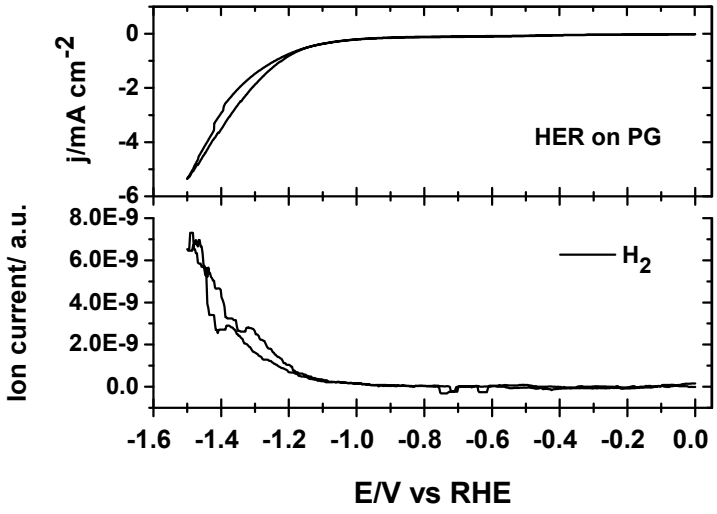

(a)

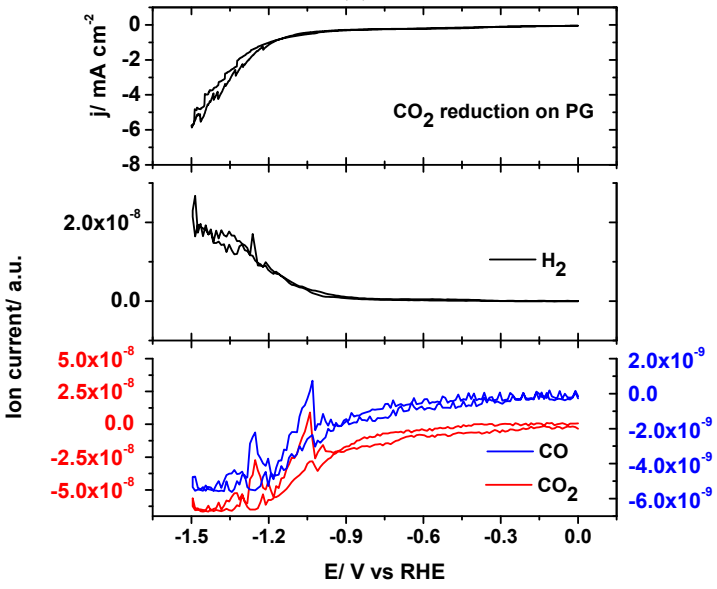

(b)

Figure B.2 HER (a) and CO_2 reduction (b) on pristine pyrolytic graphite in 0.001 M $HClO_4$ + 0.099 M $NaClO_4$. Scan rate 1 mV s^{-1}.

B.2 IR compensation

In this work the electrolysis experiments were IR corrected by the potentiostat's IR compensation function, while voltammetric experiments on the 10 mm diameter PG electrode were corrected mathematically afterwards. For the latter experiments, the voltammograms sometimes show unrealistic behavior (more than one datapoint corresponding to a single potential) which is caused by the combination of current fluctuations at negative potentials (H_2 bubbles) and IR correction after the measurement. Before each electrolysis experiment the uncompensated resistance was determined by potentiostatic electrochemical impedance spectroscopy (Iviumstat or Compactstat, Ivium Technologies) on the pristine PG electrode in the blank electrolyte at E = 0.2 V_{RHE} which is a potential within the doublelayer region. The frequency range was usually between 20 kHz and 10 Hz. In a ideal system the limiting case of inifinite frequency would lead to the uncompensated resistance. In the Nyquist plot, a line is fitted through the datapoints corresponding to higher frequencies and the intercept with the real axis is obtained. To avoid overcompensation and instabilities in the potentiostat control, 85% of this value is used in the potentiostat's IR compensation function. An example of a typical Nyquist plot for a PG electrode is shown in Figure B.3. In table B.1 the used electrolytes are shown together with their solution resistance in the one-compartment electrochemical cell.

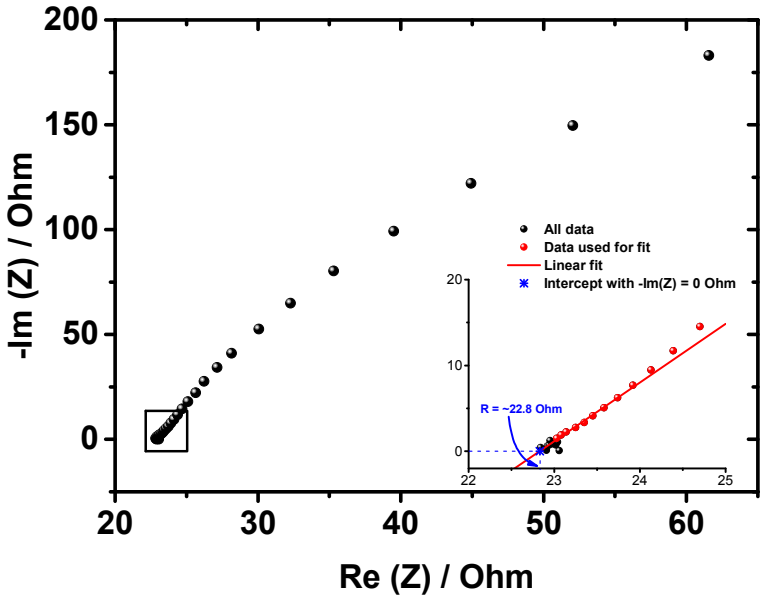

Figure B.3 Example of Nyguist plot from which the cell resistance is derived

Table B.1 Composition of the used electrolytes and their solution resistance

pH	Electrolyte solution			Resistance
1	0.1 M $HClO_4$			≈ 19.8 Ω
3	0.001 M $HClO_4$	+	0.099M $NaClO_4$	≈ 71.1 Ω
4.0-4.1	0.001 M H_3PO_4	+	0.1 M KH_2PO_4	≈ 82.2 Ω
5.8	0.1 M KH_2PO_4	+	0.01 M K_2HPO_4	≈ 59.7 Ω
6.8	0.1 M KH_2PO_4	+	0.1 M K_2HPO_4	≈ 27.2 Ω
7.8	0.01 M KH_2PO_4	+	0.1 M K_2HPO_4	≈ 37.9 Ω
9.6-9.8	0.1 M K_2HPO_4	+	0.001 M K_3PO_4	≈ 38.7 Ω
11.6	0.1 M K_2HPO_4	+	0.1 M K_3PO_4	≈ 17.9 Ω

B.3 OLEMS on different MPPs

In this section the OLEMS results for CO_2 reduction on the different MPPs are shown, indicating the volatile products that have been formed. Formation of CO is hard to see, since the CO signal (m/z = 28) follows the CO_2 (m/z = 44) signal due to fragmentation of CO_2 in the mass chamber. CO can be detected when large amounts are produced as seen for NiPP. For the HCOOH producing porphyrins (RhPP, SnPP and InPP), we confirmed the absence of CO production with gas chromatography.

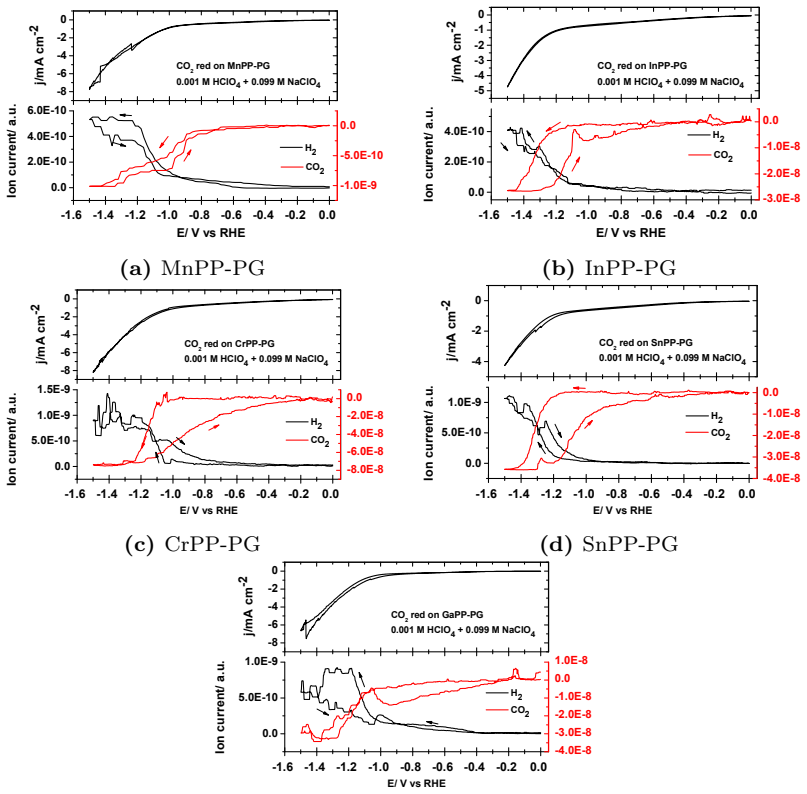

(a) MnPP-PG **(b)** InPP-PG

(c) CrPP-PG **(d)** SnPP-PG

(e) GaPP-PG

Figure B.4 OLEMS results during CO_2 reduction on different MPPs in 0.001 M $HClO_4$ + 0.099 M $NaClO_4$. Scan rate: 1 mV s^{-1}.

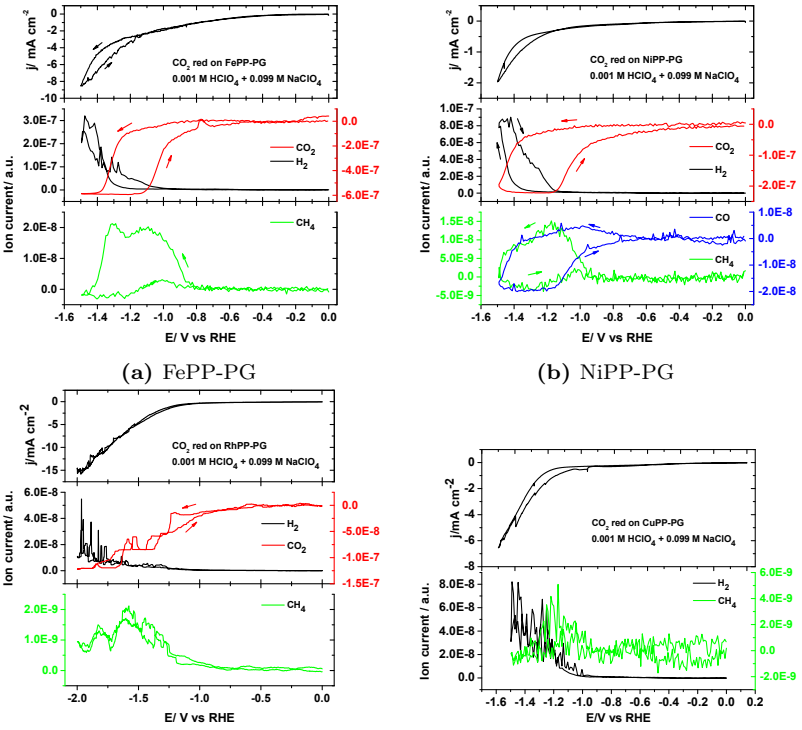

(a) FePP-PG **(b)** NiPP-PG

(c) RhPP-PG **(d)** CuPP-PG

Figure B.5 OLEMS results during CO_2 reduction on different MPPs in 0.001 M $HClO_4$ + 0.099 M $NaClO_4$. Scan rate: 1 mV s^{-1}.

B.4 Normalized concentration profiles

The graphs shown in Figures 5.7a, 5.8a and 5.9a are normalized by the maximum concentration and shown in Figure B.6 to show the shift of the concentration profiles of RhPP with pH. This shift is less prominent for InPP and SnPP.

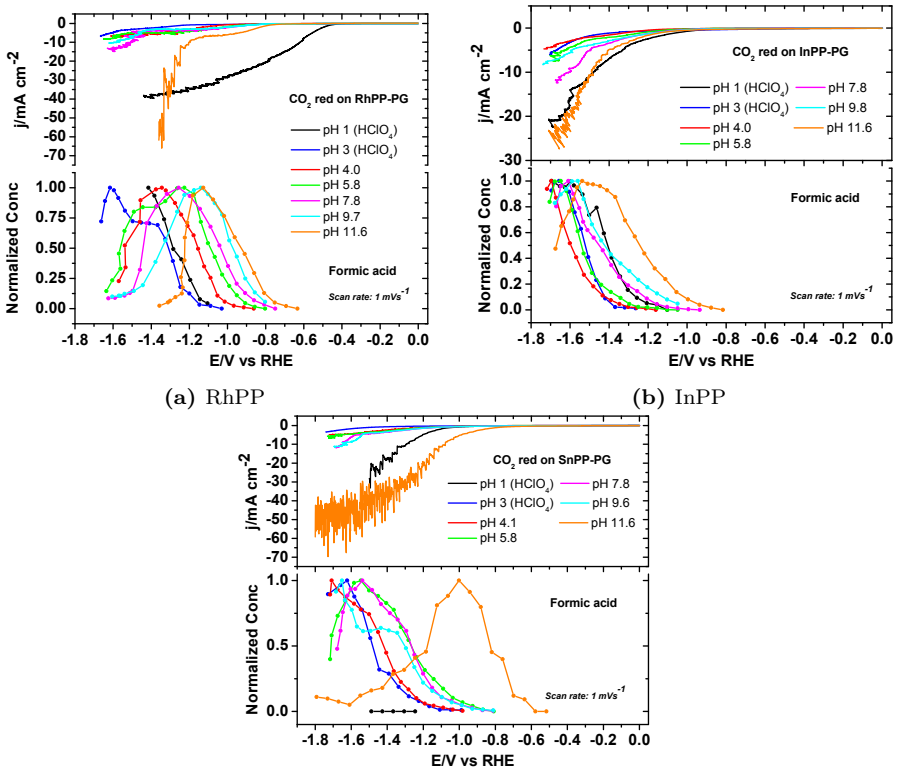

(a) RhPP **(b)** InPP

(c) SnPP

Figure B.6 CO_2 reduction on formic acid producing MPP at different pH's

B.5 Comparison definition of onset potential

As the definition of the onset potential is somewhat arbitrary, a different definition could lead to different results. However, in Figure B.7 it is shown that for both, the concentration profile and the current profile, the trend of the onset potential as a function of pH is the same irrespective of the method used. The onset potentials shown in Figure 5.10 are based on an average of different definitions.

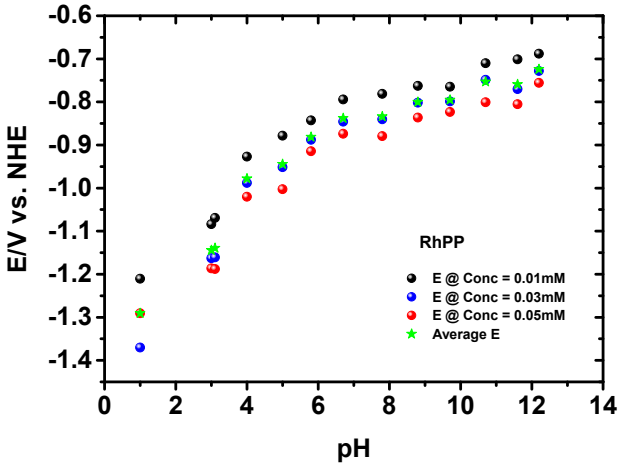

(a) Onset potential of concentration profile

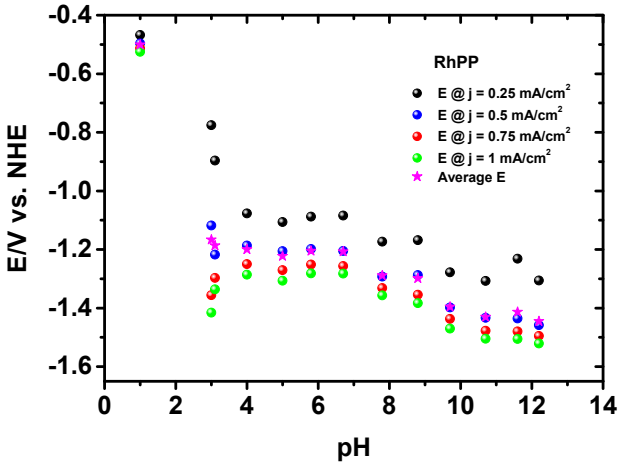

(b) Onset potential of current profile

Figure B.7 Comparison of different definitions of the onset potentials

B.6 Faradaic efficiency

The faradaic efficiencies determined for RhPP, InPP and SnPP in different electrolytes at a potential of E = -1.5 V_{RHE}.

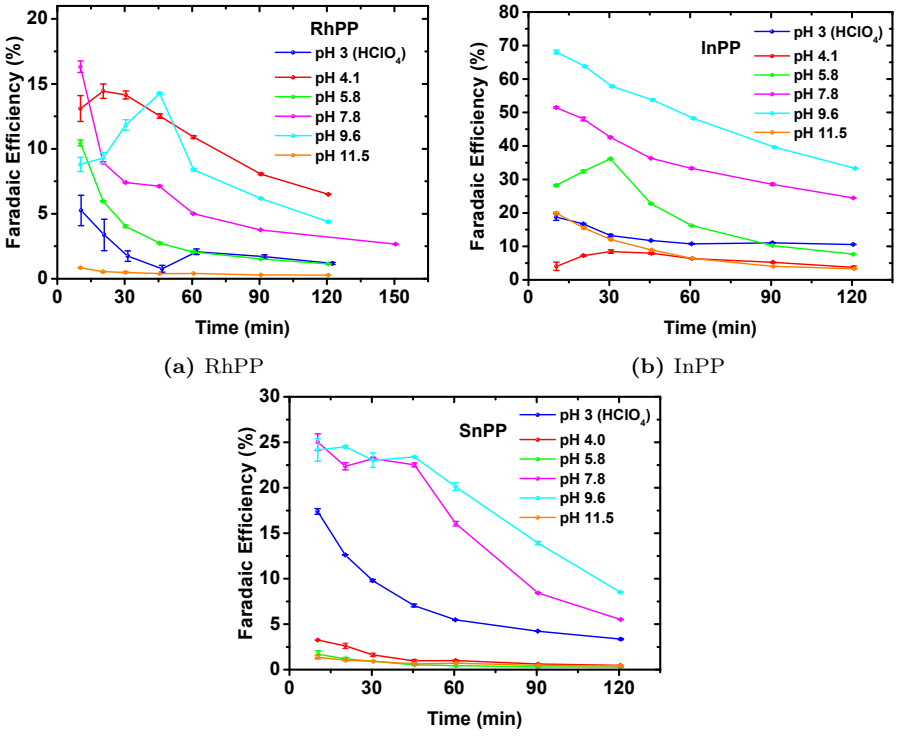

(a) RhPP (b) InPP

(c) SnPP

Figure B.8 Faradaic efficiencies in different electrolytes at E = -1.5V versus time

B.7 Deactivation of the catalyst

The deactivation of the catalyst is looked into by comparing the blank voltammograms of the immobilized porphyrins before and after the HER or CO_2 reduction as shown in Figure B.9. It can be seen that the porphyrin-specific redox peaks have disappeared after HER and CO_2 reduction. As this observation is found for all the different MPPs and for both, HER and CO_2 reduction, the deactivation is believed to be associated to the destruction of the porphyrin structure or immobilization of the porphyrin on PG as a result of the very negative potentials.

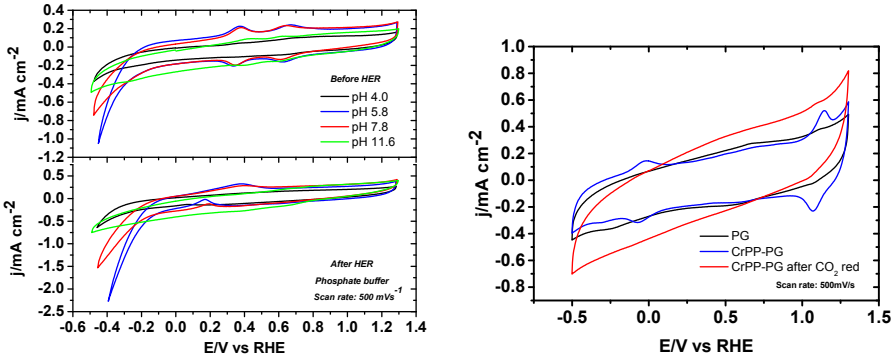

Figure B.9 Blank voltammograms before and after (a) HER on immobilized RhPP in different phosphate buffers and (b) CO_2 reduction on immobilized CrPP in 0.001 M $HClO_4$ + 0.099 M $NaClO_4$

B.8 Influence of the buffer capacity

The buffer capacity may have an influence on the catalytic activity as it affects the local pH during CO_2 reduction. As shown in Figure B.10, a higher buffer capacity leads to a higher current. The formation of formic acid is also dependent on the buffer capacity. These results may indicate that the local pH may play a role in the catalytic activity of the immobilized porphyrins.

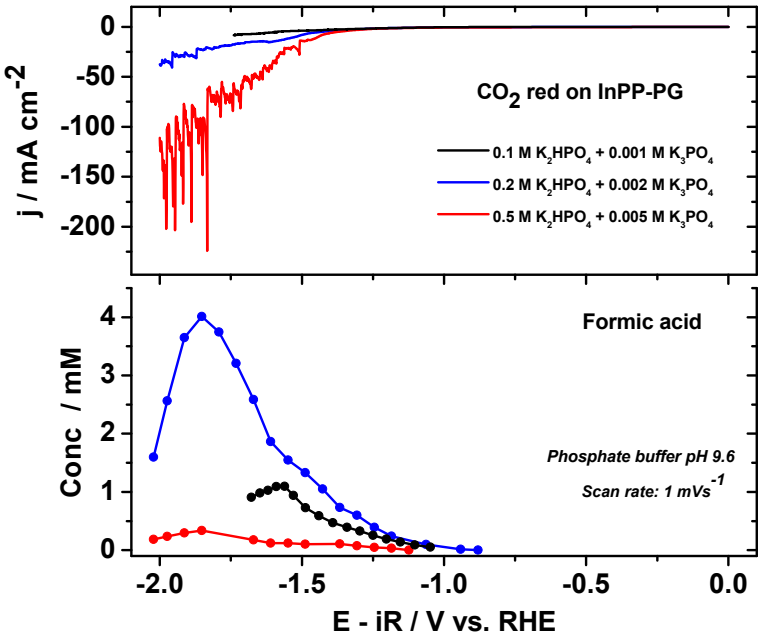

Figure B.10 CO_2 reduction on InPP-PG in phosphate buffers of pH 9.6 with different buffer capacities. Scan rate: 1 mV s^{-1}.

B.9 References

[1] G. G. Wildgoose, P. Abiman, R. G. Compton, *J. Mater. Chem.* **2009**, *19*, 4875–4886.

[2] X. Ji, C. E. Banks, A. Crossley, R. G. Compton, *ChemPhysChem* **2006**, *7*, 1337–1344.

[3] C. A. Thorogood, G. G. Wildgoose, A. Crossley, R. M. J. Jacobs, J. H. Jones, R. G. Compton, *Chem. Mater.* **2007**, *19*, 4964–4974.

[4] C. A. Thorogood, G. G. Wildgoose, J. H. Jones, R. G. Compton, *New J. Chem.* **2007**, *31*, 958–965.

APPENDIX C

Supporting Information to Chapter 6

Effects of Substrate and Polymer encapsulation on CO_2 Electroreduction by Immobilized Indium(III) protoporphyrin

C.1 Materials and Experimental procedures

Materials

Pyrolytic graphite (PY001009, Graphite Store, USA), cut in 5 mm diameter discs such that the basal planes are exposed, glassy carbon (5 mm diameter) and boron doped diamond (10 mm diameter, Windsor Scientific Ltd., UK) were used as working electrode.

Potassium phosphate dibasic TraceSELECT ≥99.999% (Honeywell) and potassium phosphate tribasic (Sigma Aldrich) were used for the preparation of the phosphate buffer solution of pH = 9.6 ± 0.1. The pH was measured with a SI Analytics Lab 855 pH meter. The Indium(III) protoporphyrin IX was purchased from Frontier Scientific and used without further purification.

The chemicals used for immobilization in polymer membranes were didodecyldimethylammonium bromide (98 %, Sigma Aldrich), Nafion® perfluorinated resin solution (5 wt. % in lower aliphatic alcohols and water, contains 15-20% water, Sigma Aldrich), poly(4-vinylpyridine) (average Mw ≈ 60,000, Sigma Aldrich) and poly(3,4-ethylenedioxythiophene)-poly(styrenesulfonate) (0.54% in H_2O, high-conductivity grade, Sigma Aldrich).

Electrochemical experiments

Glassware was cleaned as in our previous work.[1] Prior to each experiment, the PG and GC electrodes were polished and ultrasonicated in water for approximately 5 min in water. PG was polished with sandpaper (first P600 and then P1000), and GC with alumina slurry (1μm, 0.3μm and 0.05μm particle size). BDD was first ultrasonicated in concentrated nitric acid for 5 min and then in water. The subsequent procedures (deaeration of the cell, voltammetric procedures before and after InPP immobilization) are akin to the procedures reported previously.[1]

Product analysis

High Performance Liquid Chromatography (Prominence HPLC, Shimadzu) was utilized for the analysis of non-volatile reaction products. The samples were placed in an auto-sampler (SIL-20A) which injects 20 μl of the sample into the column. An Aminex HPX 87-H (Bio-Rad) column with a Micro-Guard Cation H Cartridge (Bio-Rad) in front were used. The eluent was 5 mM H_2SO_4 and the eluent flow rate 0.6 ml min^{-1}. The column and the refractive index detector (RID-10A) were maintained at a temperature of 45 °C. The setup utilized for online HPLC experiments has been described before.[2]

OnLine Electrochemical Mass Spectrometry (OLEMS) was utilized for the detection of volatile reaction products. A tip, containing a hydrophobic membrane is placed close (≈10 μm) to the electrode surface, and continuously collects volatile

reaction products from the electrode interface. The setup has been described previously.[3]

Immobilization of InPP

The immobilization of InPP onto the substrate was performed by dropcasting 2.5 μl 0.25 mM InPP solution per 0.196 cm^2 geometric surface area, followed by evaporation of the solvent under an argon stream. The preparation of the InPP solution has been described by de Groot et al.[4] For the experiments on the substrate effect and pretreatment effect the immobilization was consistently carried out with InPP in DDAB layers, as this resulted in higher activity. For investigation of the polymer effect, InPP was also dropcasted without polymer from the solution reported by de Groot et al. The immobilization using Nafion, P4VP and PEDOT:PSS were carried out similarly with minor modifications. The InPP-Nafion and InPP-PEDOT:PSS solutions were prepared by mixing equivolumes of 0.5 mM InPP stock solution with respectively 2 wt.% Nafion solution or 0.54 wt.% PEDOT:PSS solution. Due to the insolubility of P4VP in the InPP stock solution, we first dropcasted 0.5 mM InPP solution on PG, followed by an equal volume of 2 wt.% P4VP solution (in 0.1 M acetic acid). For a correct comparison, it was made sure that the amount of dropcasted InPP per cm^2 is always the same.

Pretreatment of pyrolytic graphite

The electrochemical pretreatments of the pyrolytic graphite surface were carried out in a conventional one-compartment three electrode cell with 0.1 M perchloric acid (Merck Suprapure) electrolyte. A platinum wire was used as counter electrode and reversible hydrogen electrode as reference. For the anodic pretreatment, chronoamperometry at E = 2.25 V vs. RHE for t = 5 minutes was performed, and for the cathodic pretreatment, chronoamperometry at E = -1.8 V vs. RHE for t = 5 minutes.

For the plasma treatment of the pyrolytic graphite electrodes a capacitively coupled plasma system with the Radio-Frequency (RF) of 40 kHz and 200W power from Diener electronic was employed at room temperature. The base pressure of this system is less than 0.02 mbar. The parameters were 10 W power/1.0 mbar pressure for H_2 plasma and 30 W power/0.5 mbar pressure for O_2 plasma. For H_2 the exposure time was 3 minutes, and for the O_2 plasma we varied the exposure time (3, 6 and 12 minutes) to achieve mild and harsh plasma treated PG.

Apparatus

X-ray diffraction data were collected on a Philips X'Pert diffractometer, equipped with the X'Celerator, using Cu-Kα radiation in steps of 0.02° (2θ) with 10 s counting time in the range from 10° to 80° (2θ).

Raman spectra were recorded with a WITEC alpha300 R âĂŞ Confocal Raman Imaging spectrometer with a laser wavelength of 532 nm at ambient conditions and room temperature.

X-ray photoelectron spectroscopy (XPS) measurements were performed on a K-alpha Thermo Fisher Scientific spectrometer using a monochromated Al Kα X-ray source. The measurements were carried out using point analysis with auto-height signal optimization, with each point having a spot size of 300 micron at ambient temperature and chamber pressure of about 10^{-8} mbar. A flood gun was used for charge compensation. All the measured spectra were corrected by setting the reference binding energy of C*1s* at 284.8 eV. The electron energy analyzer was operated with pass energy of 200 eV and 0.25 eV energy spacing for the survey spectrum, and pass energy of 50 eV and 0.1 eV energy spacing for the high-resolution spectrum. Each reported spectrum is the statistic average of 10 measured scans. To ensure homogeneity of the immobilized InPP, different spots of the samples were analyzed. The spectra were analyzed and processed using Thermo Avantage v5.903 software (Thermo Fisher Scientific). Smart background subtraction, derived from the Shirley background, was used over the peak width. By applying full width integration over the core-level signals and using tabulated atomic sensitivity factors, relative atomic contributions on the surface were calculated.

C.2 Substrate effect

In the Figures C.1-C.3 we compare the influence of different amounts of InPP on PG, GC, and BDD on the selectivity and activity of CO_2RR. The amount InPP per cm^2 is kept the same for all the substrates. For PG we observe that a higher amount of InPP on the surface leads to a significant increase in FE and j_{HCOOH}, and decrease in j_{H_2}, while j_{total} remains unchanged. These observations are associated with the higher amount of active sites available, where even an initial FE of approximately 100 % can be obtained. Conversely, as can be seen in Figure C.2, on GC a higher amount of InPP has negligible influence on CO_2RR selectivity and activity. In terms of FE, BDD is somewhat in between PG and GC, but the HCOOH activity seems to be inhibited for higher InPP concentrations. These results show the different behavior of the substrates with increasing amounts of dropcasted InPP, which is interpreted as the capacity of PG to accommodate more InPP compared to GC and BDD. In order to draw more quantitative conclusions, we performed XPS measurements on the different substrates with immobilized InPP. XPS is a very useful and sensitive technique to study the surface species. In Figure C.12, the XPS spectra of the different substrates with and without InPP are shown. As reference for the indium protoporphyrin, the spectrum of $In_2(SO_4)_3$ is included as well. Analysis of the XPS spectra of InPP containing substrates and $In_2(SO_4)_3$ indicate a clear In(III) contribution with peak broadening of In*3d* core level binding energy. No loss of features at higher binding energy is observed, indicative of absent

metallic In species. The indium content extracted from the XPS spectra is used as a quantitative measure for the real amount of adsorbed InPP on the substrates.

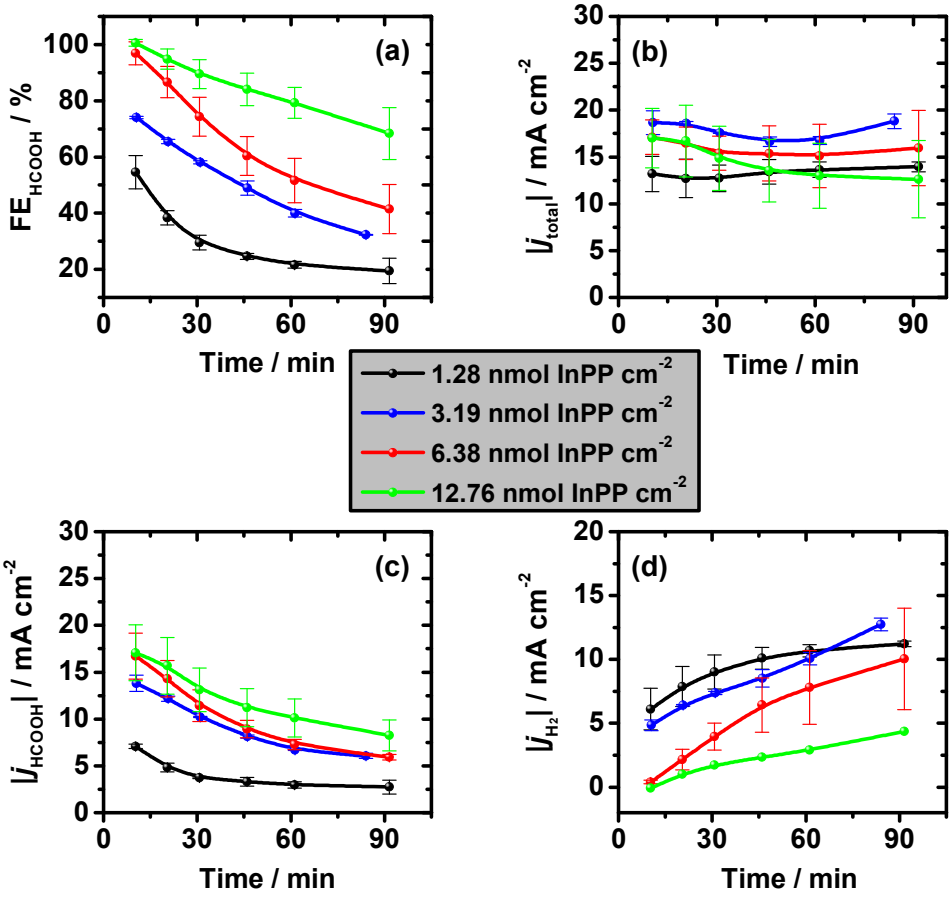

Figure C.1 (a) Faradaic efficiency toward HCOOH, (b) absolute total current density, (c) absolute partial current density for HCOOH, (d) absolute partial current density for H_2 during CO_2 reduction on different amounts of immobilized InPP on PG in 0.1 M phosphate buffer of pH 9.6. Lines to guide the eye.

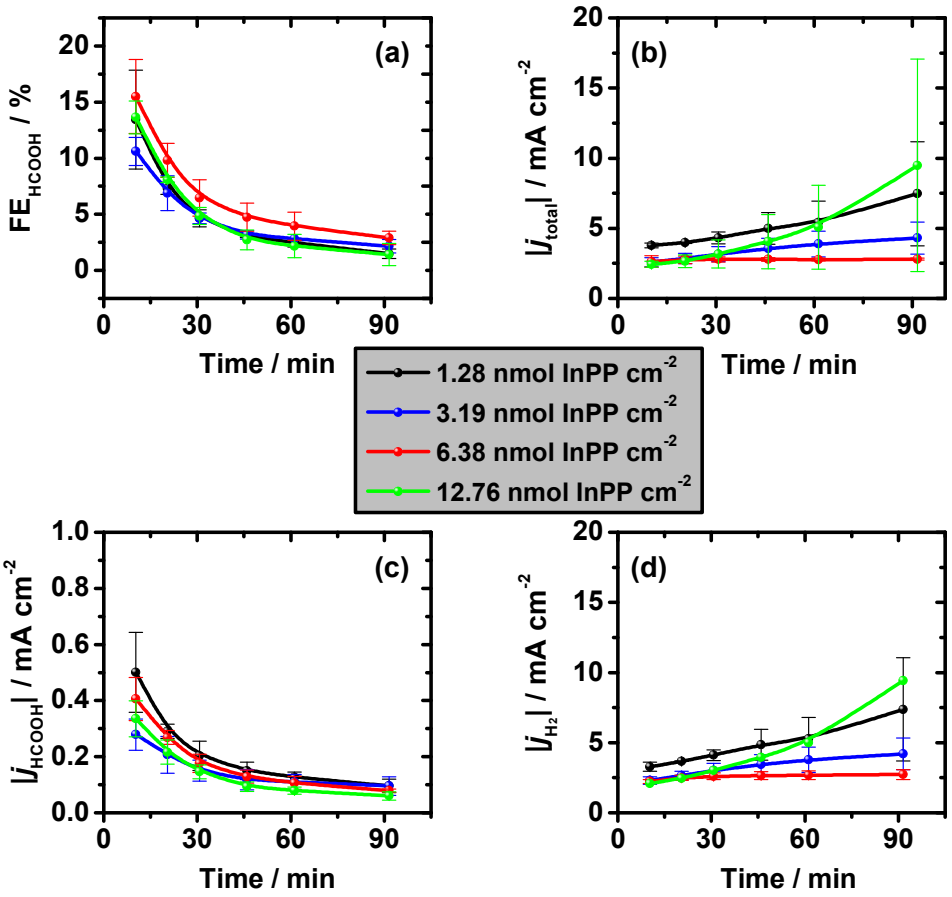

Figure C.2 (a) Faradaic efficiency toward HCOOH, (b) absolute total current density, (c) absolute partial current density for HCOOH, (d) absolute partial current density for H_2 during CO_2 reduction on different amounts of immobilized InPP on GC in 0.1 M phosphate buffer of pH 9.6. Lines to guide the eye.

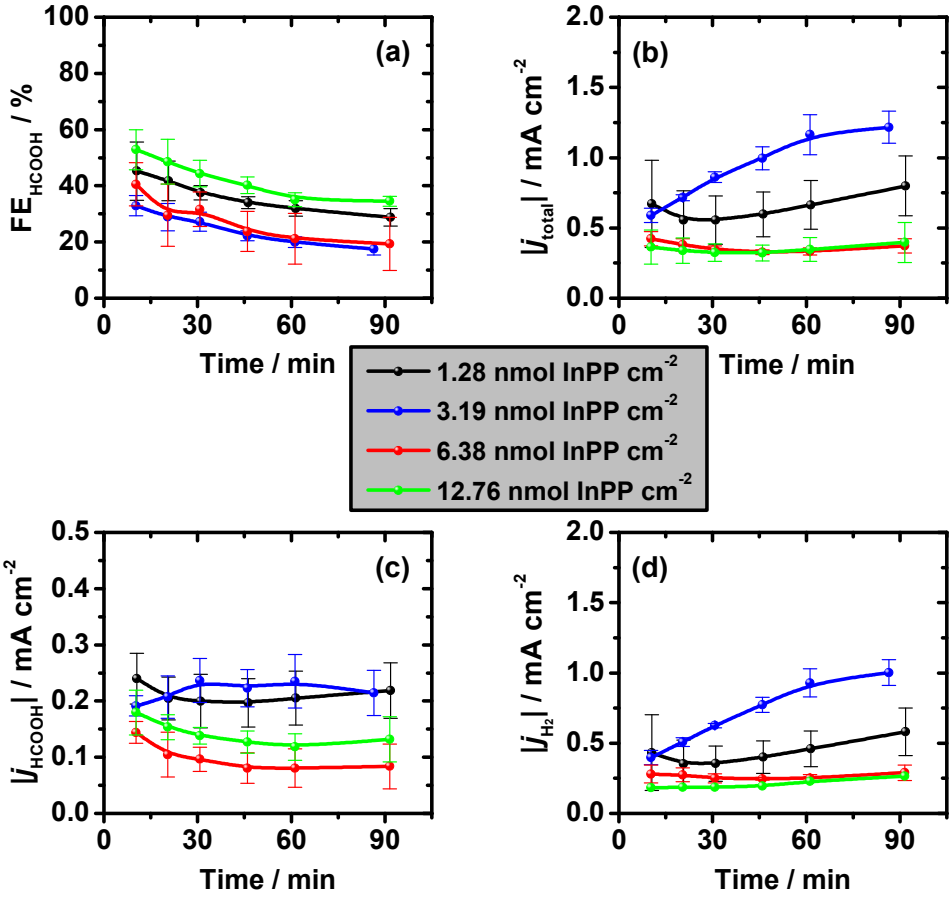

Figure C.3 (a) Faradaic efficiency toward HCOOH, (b) absolute total current density, (c) absolute partial current density for HCOOH, (d) absolute partial current density for H_2 during CO_2 reduction on different amounts of immobilized InPP on BDD in 0.1 M phosphate buffer of pH 9.6. Lines to guide the eye.

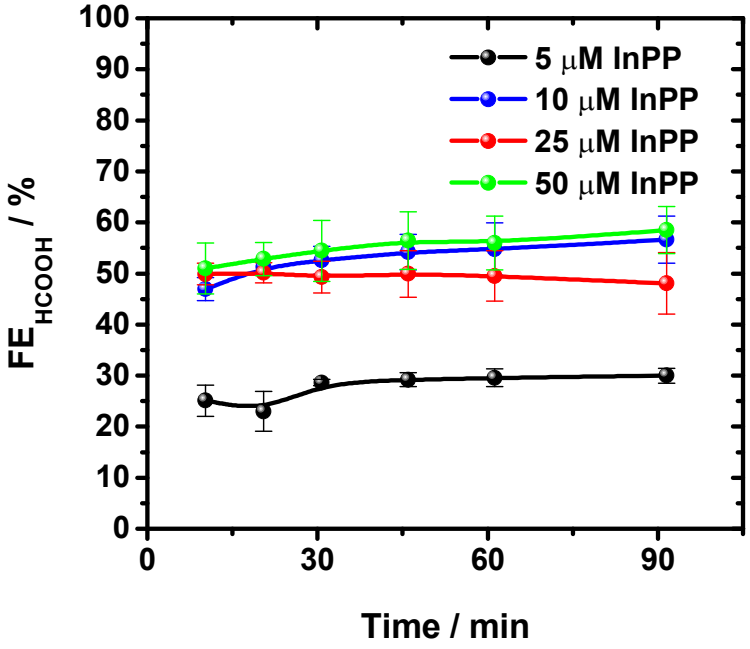

Figure C.4 Faradaic efficiency toward HCOOH during CO_2 reduction on PG in phosphate buffer of pH ≈ 9.6 containing different concentrations of InPP. Lines to guide the eye.

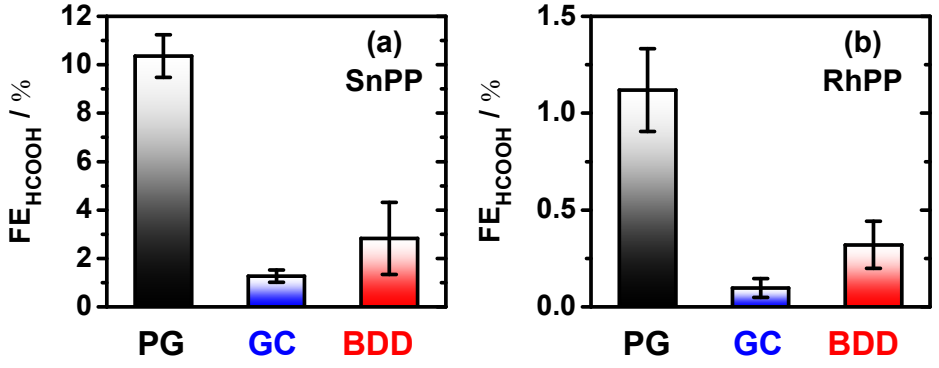

Figure C.5 Faradaic efficiency toward HCOOH during CO_2 reduction at E = -1.5 V vs. RHE in 0.1 M phosphate buffer of pH 9.6 on (a) immobilized SnPP after 10 minutes, and (b) immobilized RhPP after 30 minutes on different substrates.

C.3 Pretreatment effect

In Figure C.6 the CO_2RR performance of O_2 plasma treated PG with different exposure time is compared. The FE decreases, and j_{H_2} increases for 12 minutes O_2 plasma treatment. J_{total} does not show a clear trend as a function of exposure time. In Figure C.7 we characterize the PG surface before and after pretreatment, by means of cyclic voltammetry. Significant difference is observed with the anodic treatment, whereas the other treatments lead to similar voltammograms. This observation is in agreement with the increased double layer capacitance shown in Figure C.8(b).

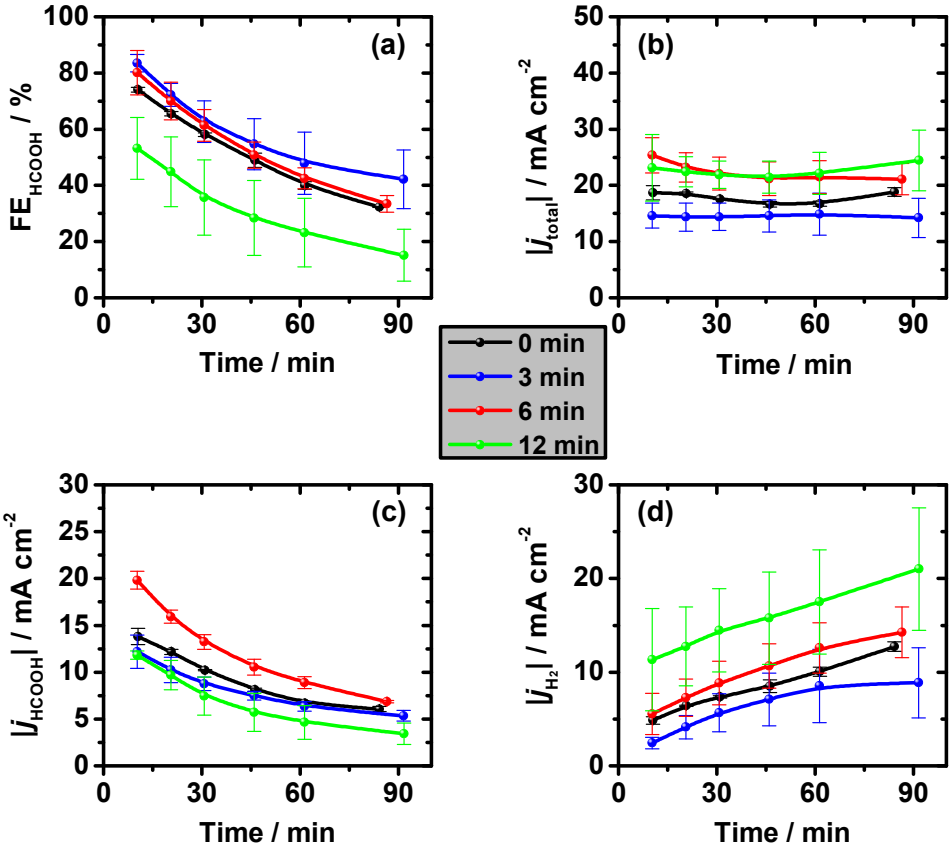

Figure C.6 (a) Faradaic efficiency toward HCOOH, (b) Absolute total current density, (c) Absolute partial current density for HCOOH (d) Absolute partial current density for CO_2 reduction on immobilized InPP on PG with different exposure times of O_2 plasma in 0.1 M phosphate buffer of pH 9.6. Lines to guide the eye.

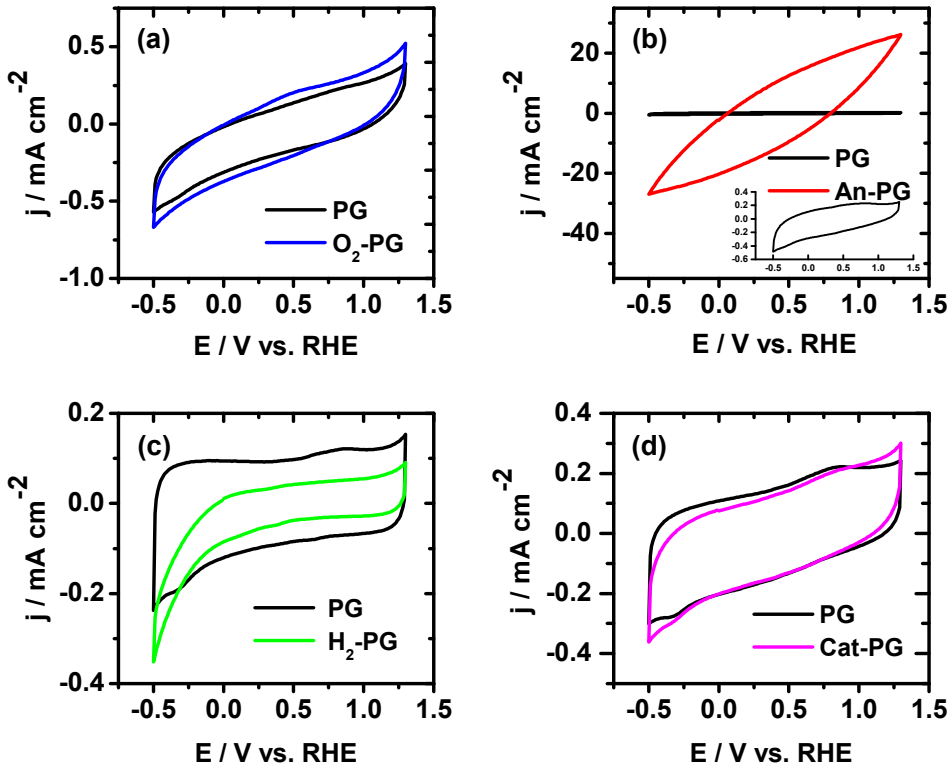

Figure C.7 Blank voltammograms before and after pretreatment of PG: (a) O_2 plasma treatment (6 min), (b) Anodic treatment, (c) H_2 plasma treatment, (d) Cathodic treatment. Electrolyte: 0.1 M phosphate buffer of pH 9.6. Scan rate: 500 mV s^{-1}

C.4 Characterization

In Figure C.8, the double layer capacitance (C_{dl}) in μF cm^{-2} is shown for the investigated substrates, and pretreated PG. C_{dl} is derived from voltammograms measured in the double layer region at different scan rates. The slope of I vs. scan rate at a fixed potential is the capacity, which is normalized by the geometric area of the electrode. C_{dl} is proportional to the electrochemical active surface area or roughness of the electrode ($C = \frac{\epsilon A}{d}$). The ratio between C_{dl} of the investigated substrates is different from the ratio between j_{total} of the investigated substrates (Figure 6.1(b)), which indicates that the difference in activity observed between the substrates is not the result of a difference in active surface area.

The XRD patterns for the investigated substrates, electrochemical pretreated PG, and polymer coated PG are shown in Figure C.9. The electrochemical pretreatments and InPP encapsulation in polymers do not affect the crystallinity of the PG.

In Figure C.10a, the Raman spectra are depicted for the investigated substrates PG, GC, and BDD revealing the peaks related to the sp^2 (D, G, 2D) and sp^3 carbon atoms. The peak at 1330 cm^{-1} observed in BDD is associated to the σ bonds between the C atoms. Graphite shows the G-band at 1580 cm^{-1}, which is characteristic for crystalline graphite (hence GC exhibits a weak and broad G-band), and the D-band at 1352 cm^{-1}, which is typically assigned to disorder of the graphite lattice by edge planes. It should be noted that discrimination of the D-band with the sp^3 carbon peak is difficult in case a laser with a wavelength of 632 nm is used. Hence we used a laser with a wavelength of 532 nm. The peaks between 2400 and 3300 cm^{-1} are second order features attributed to overtones of fundamental modes.[5] Figure C.10b shows the Raman spectra for PG and after the various pretreatments. Based on the intensities obtained here for the D and G peaks, the ratios of I_D/I_G are depicted in Figure C.11.

As discussed before, XPS measurements were carried out to obtain more quantitative information about the surface species. The indium content is used to compare the real amount of indium adsorbed on the various substrates, and to compare the stability between the different substrates. Additionally, the oxygen content is used to provide a quantitative basis for the conclusions related to the pretreatment effect.

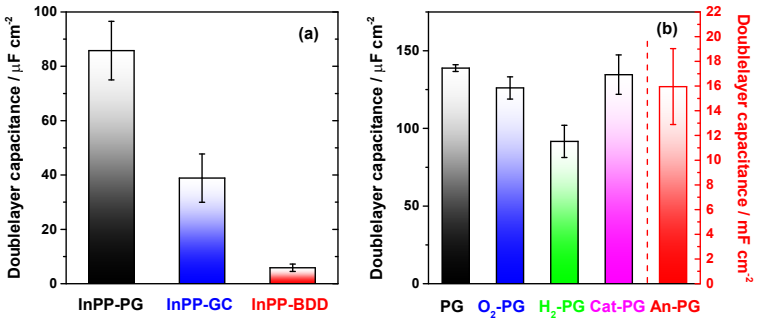

Figure C.8 Double layer capacitance of (a) investigated substrates and (b) different pretreatments of PG.

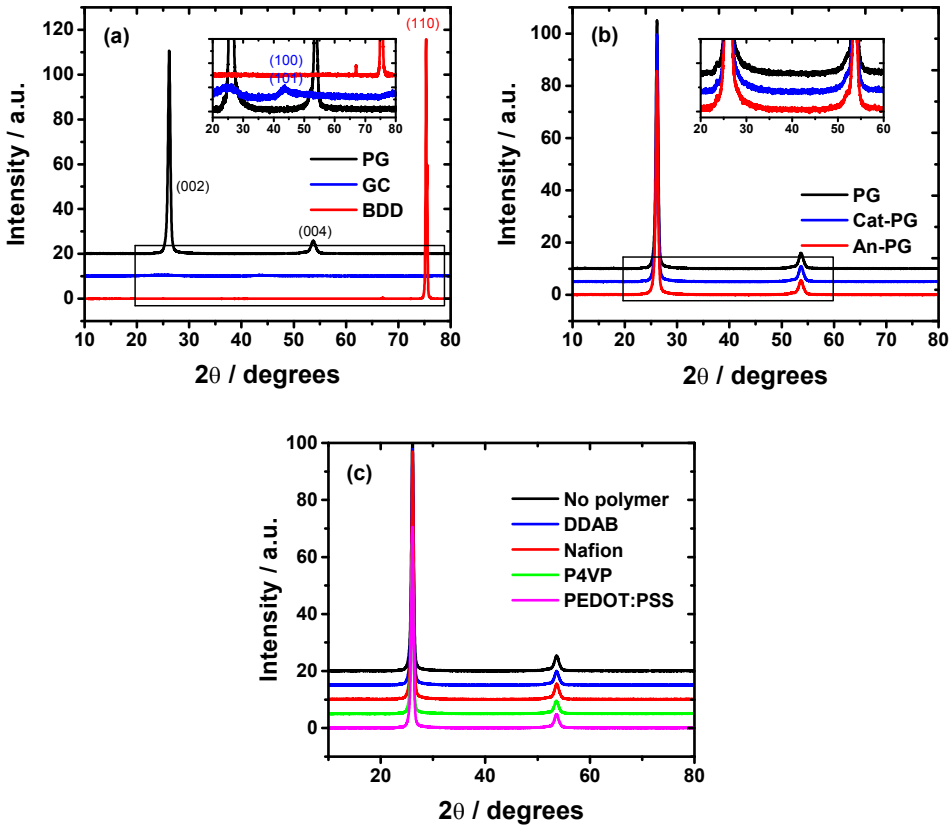

Figure C.9 XRD patterns of (a) different substrates, (b) untreated, anodically treated and cathodically treated PG and (c) PG coated with InPP in different polymer films.

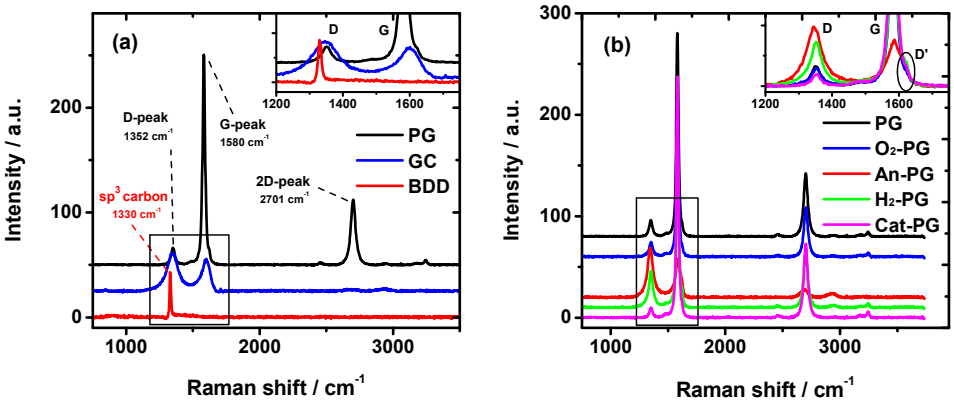

Figure C.10 Raman spectra of (a) the different substrates and (b) the different pretreatments of PG.

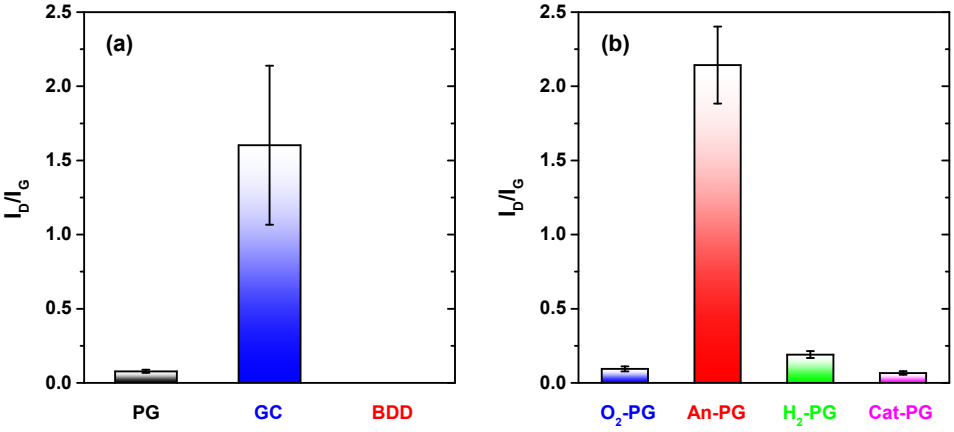

Figure C.11 Ratio of D-peak and G-peak intensity of (a) the different substrates and (b) the different pretreatments of PG.

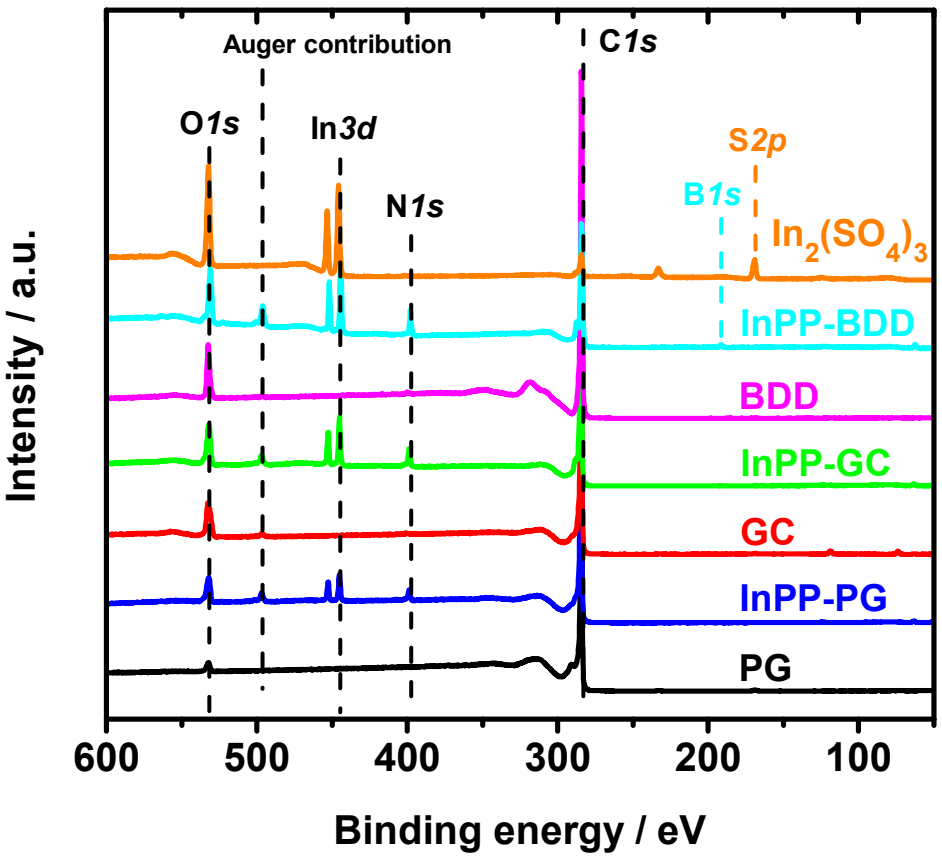

Figure C.12 XPS spectra of the different substrates with and without immobilized InPP, and $In_2(SO_4)_3$.

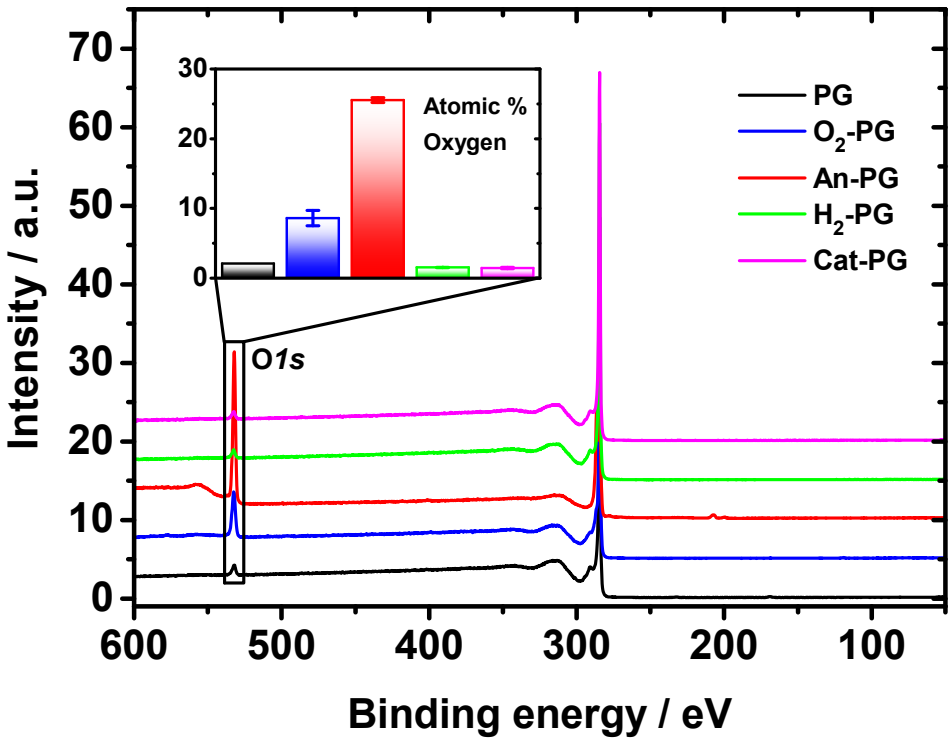

Figure C.13 XPS spectra of plasma- and electrochemically pretreated pyrolytic graphite. Inset: comparison of the oxygen content (at.%) between the pretreated PG.

C.5 Effect of polymer encapsulation

In Figure C.14, the chemical structures of the investigated polymers are depicted. In Figure C.15, we compare the blank cyclic voltammograms of InPP immobilized on PG using different polymers. The typical peaks observed after InPP immobilization without polymer or with DDAB (denoted by the arrows) are not always visible (P4VP and Nafion), possibly due to a shift of the redox peaks as observed before.[4] In case of PEDOT:PSS a larger double layer and additional peaks are observed, which is assumed to be related with the polymer chemical structure. The differences in the CVs are believed to be the result of a different chemical environment in vicinity of the electrode as observed before.[4]

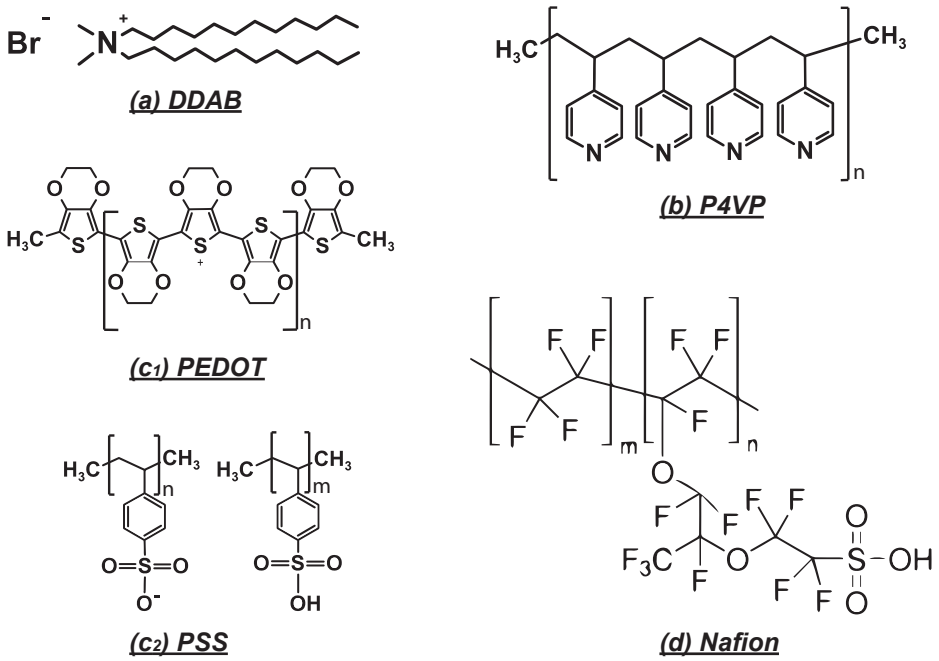

Figure C.14 Chemical structures of the investigated polymers for InPP immobilization: (a) DDAB, (b) P4VP, (c) PEDOT:PSS and (d) Nafion

We performed Electrochemical Impedance Spectroscopy experiments on the different polymer dispersed catalysts to investigate the kinetics of electron-transfer processes. The Nyquist plots were obtained in CO_2-saturated and blank (argon saturated) 0.1 M phosphate buffer solution of pH 9.6 in a frequency range from 10 kHz to 1 Hz with an amplitude of 10 mV at a potential of -1.5 V vs. RHE, similar to the potential at which we performed the CO_2RR electrolysis experiments. From the Nyquist plots (Figure C.16a-b), we observe only one semicircle, and the absence

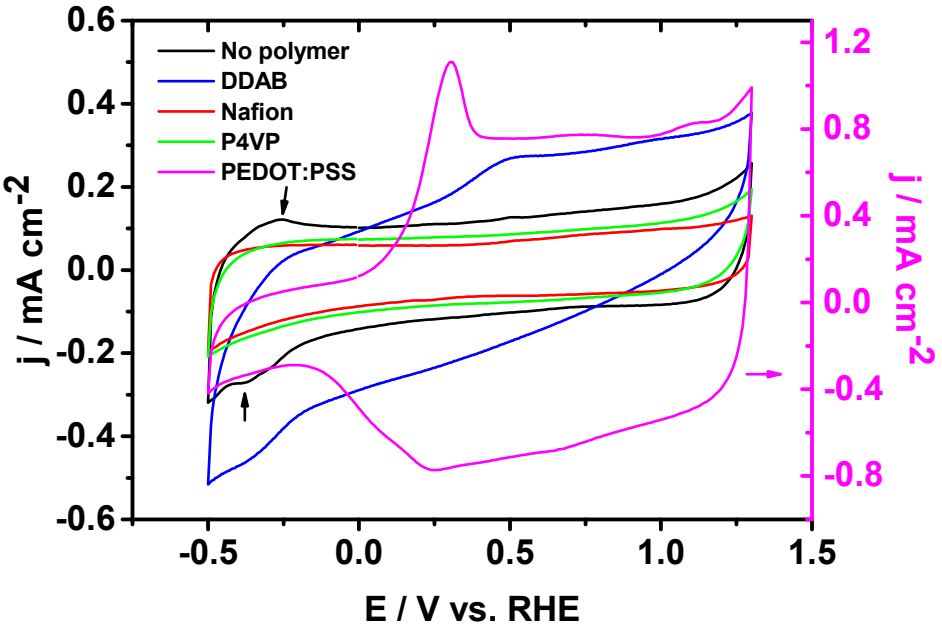

Figure C.15 Blank voltammograms InPP immobilized on PG using different polymers. Electrolyte: 0.1 M phosphate buffer of pH 9.6. Scan rate: 500 mV s^{-1}

of a mass transfer controlled regime, which generally indicates that the impedance is determined by slow electron transfer kinetics. The diameter of the semicircle is a measure of the charge transfer resistance (R_{ct}), which is different for the various polymer films and different in the blank vs. CO_2 saturated electrolyte. The data is fitted with typical Randles equivalent circuits in series, modified by replacing the capacitor with a constant phase element and omitting the diffusion element (Figure C.16c), which leads to a better fit for our data, and which has been used for polymer-modified electrodes.[6,7] Fitting was performed with the software provided by potentiostat manufacturer (IviumSoft). We also tried more complex equivalent circuits reported in the literature, which turned out to be incompatible with our Nyquist plots due to the absence of a diffusion controlled region.[8,9]

The relevant fitting parameters obtained, are the ohmic bulk solution resistance (R_s), charge transfer resistance (R_{ct}), and double layer capacitance (C_{dl}). C_{dl} values were not included in the analysis, since EIS was measured at potentials much more negative than the double layer region. Hence, the C_{dl} values obtained in Figure C.8 are more accurate. In Figure C.16 d-e, we plotted the obtained values of R_s (left panels) and R_{ct} (right panels) in blank and CO_2-purged electrolyte for the different polymer films.

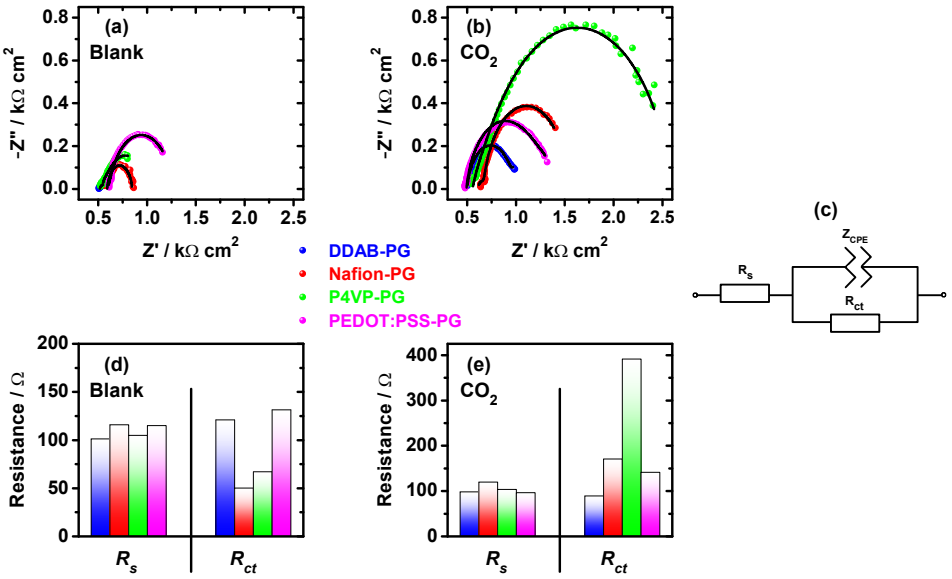

Figure C.16 Nyquist impedance plots of polymer encapsulated InPP on PG in (a) argon-purged, and (b) CO_2-purged electrolyte in a frequency range of 10 kHz to 1 Hz with 10 mV amplitude at E = -1.5 V vs. RHE. (c) a single (modified) Randles equivalent circuit. Parameters of the fitted equivalent circuit in (d) argon-purged, and (e) CO_2-purged solution: solution resistance (R_s) in the left panels and charge transfer resistance (R_{ct}) in the right panels.

R_s is found to be similar between the different polymers, which is expected since the electrolyte composition is unchanged. Furthermore, the difference in R_s between the polymers does not affect the CO_2RR performance, since we corrected for Ohmic drop during electrolysis. The relevant parameter is the charge transfer resistance (R_{ct}). It can be seen from the right panels in Figures C.16c-d, that R_{ct} is increased under CO_2 atmosphere for all polymers, which indicates a lower rate of electron transfer for CO_2RR compared to HER. Additionally, we observe a relatively high R_{ct} for P4VP under CO_2 atmosphere, indicating a lower electron transfer rate, which is in agreement with the lower current density observed for P4VP in Figure 6.6b. The trend of R_{ct} between the polymers is in line with the current density for the different polymers, but given the single semicircle nature of the EIS data, the additional information obtained from the EIS with respect to the CV data is unfortunately very limited. From these results, we conclude that the nature of the polymer affects the rate of electron transfer during CO_2RR rather than mass transport of active species, leading to different activity. Note that this EIS analysis does not allow us to draw conclusions about the difference in CO_2RR selectivity between the different polymers used for encapsulation of InPP.

C.6 Control experiments

For a correct ascription of the observed substrate effects and influence of polymer encapsulation, control experiments were performed. CO_2 reduction was investigated under the same conditions, but without InPP present. The faradaic efficiency after 20 minutes is shown in Figure C.17. As can be seen in Figure C.17a, PG exhibit little activity for CO_2RR (FE $< 4\%$), while GC and BDD are not active for CO_2RR (FE $< 0.5\%$).

In Figure C.17b, it can be seen that the polymer itself is active for CO_2RR. This trend is comparable with the mutual differences in FE observed in Figure 6.6. Therefore we believe that the influence of the polymer is partly caused by the intrinsic activity of the polymer towards HCOOH.

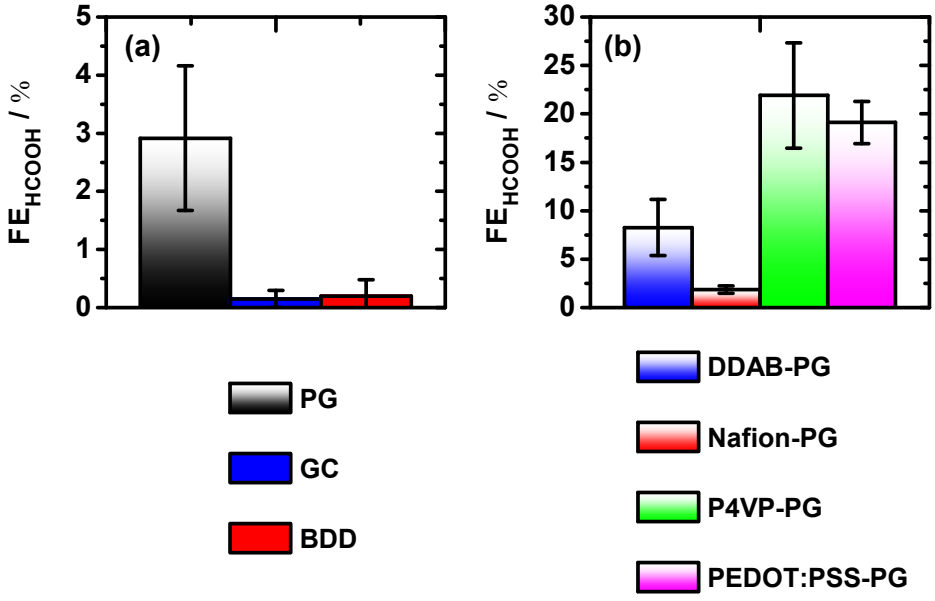

Figure C.17 Control experiments for (a) the substrate effect and (b) the effect of polymer encapsulation

C.7 References

[1] Y. Y. Birdja, J. Shen, M. T. M. Koper, *Catal. Today* **2017**, *288*, 37–47.

[2] Y. Kwon, M. T. M. Koper, *Anal. Chem.* **2010**, *82*, 5420–5424.

[3] A. H. Wonders, T. H. M. Housmans, V. Rosca, M. T. M. Koper, *J. Appl. Electrochem.* **2006**, *36*, 1215–1221.

[4] M. T. de Groot, M. T. M. Koper, *Phys. Chem. Chem. Phys.* **2008**, *10*, 1023–1031.

[5] Y. Wang, D. C. Alsmeyer, R. L. McCreery, *Chem. Mater.* **1990**, *2*, 557–563.

[6] J. Bisquert, G. Garcia-Belmonte, P. Bueno, E. Longo, L. Bulhões, *J. Electroanal. Chem.* **1998**, *452*, 229–234.

[7] Z. Chen, S. Yao, L. Liu, *J. Mater. Chem. A* **2017**, *5*, 24651–24656.

[8] M. Sharp, B. Lindholm-Sethson, E.-L. Lind, *J. Electroanal. Chem.* **1993**, *345*, 223–242.

[9] K. Calfumán, J. Honores, D. Guzmán, M. Ohlbaum, F. Armijo, R. D. Río, M. Isaacs, *ChemElectroChem* **2017**, *4*, 3314–3321.

APPENDIX D

Supporting Information to Chapter 7

Optimization of Electrolyte Composition for Electrocatalytic CO_2 Reduction on Immobilized Indium(III) protoporphyrin

D.1 Materials and Experimental procedures

The experimental procedures are similar to those reported before.[1,2] High purity chemicals were used for the preparation of the electrolyte solutions: KH_2PO_4, K_2HPO_4, $KHCO_3$, KI (TraceSELECT, Honeywell), K_2SO_4, $KClO_4$, KCl, KBr (EMSURE, Merck), KOH (semiconductor grade, Honeywell) and NaB_2O_7 (trace metal basis, Sigma Aldrich). The pH was measured with a SI Analytics Lab 855 pH meter. Indium(III) protoporphyrin IX was purchased from Frontier Scientific and used without further purification.

High Performance Liquid Chromatography (Prominence HPLC, Shimadzu) was utilized for the analysis of non-volatile reaction products. The samples were placed in an auto-sampler (SIL-20A) which injects 20 μl of the sample into the column. An Aminex HPX 87-H (Bio-Rad) column with a Micro-Guard Cation H Cartridge (Bio-Rad) in front were used. The eluent was 5 mM H_2SO_4 and the eluent flow rate 0.6 ml min^{-1}. The column and the refractive index detector (RID-10A) were maintained at a temperature of 45 °C. The setup utilized for online HPLC experiments has been described before.[3] The reported concentrations of liquid products or subsequently calculated faradaic efficiency (FE) are an average of at least two independent experiments. Additionally, the data points for each experiment were obtained by the average of three injections of the same sample. The dominant contribution of the uncertainty in concentration/FE resulted from the different experiments.

D.2 Electrolyte effect

It can be seen in Figure D.1a, that the bulk pH of the different buffer electrolytes after CO_2 saturation is as follows: $pH_{borate} < pH_{phosphate} < pH_{bicarbonate}$. The pH after CO_2 saturation for the KCl electrolytes is higher for the electrolytes with higher initial pH, as shown in Figure D.1b.

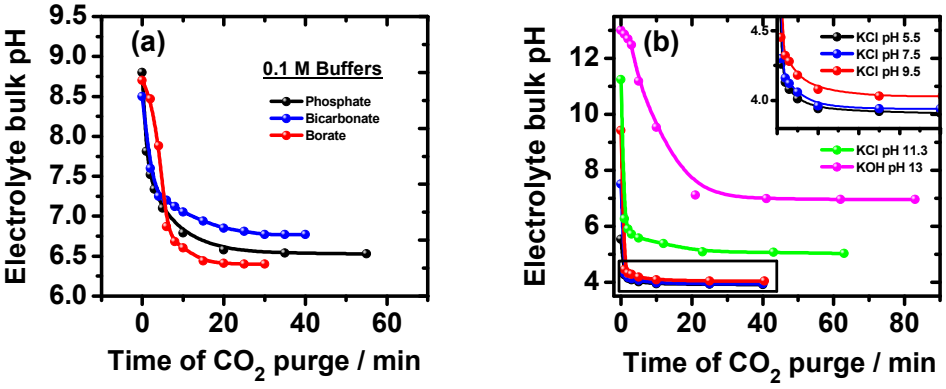

Figure D.1 (a) pH of the different buffer electrolytes as a function of CO_2 purging time and (b) pH of KCl electrolytes with different initial pH as a function of CO_2 purging time.

D.3 Buffer capacity effect

In addition to the experiments in Figure D.2, we previously performed online HPLC experiments in phosphate buffers with three different buffer capacities for CO_2RR on immobilized InPP. As shown in Figure B.10 in Appendix B, higher buffer capacity leads to higher current density throughout the whole potential range, but not necessarily to higher HCOOH formation. The increase in current density is therefore mainly the result of enhanced HER, in agreement with Figure D.2d.

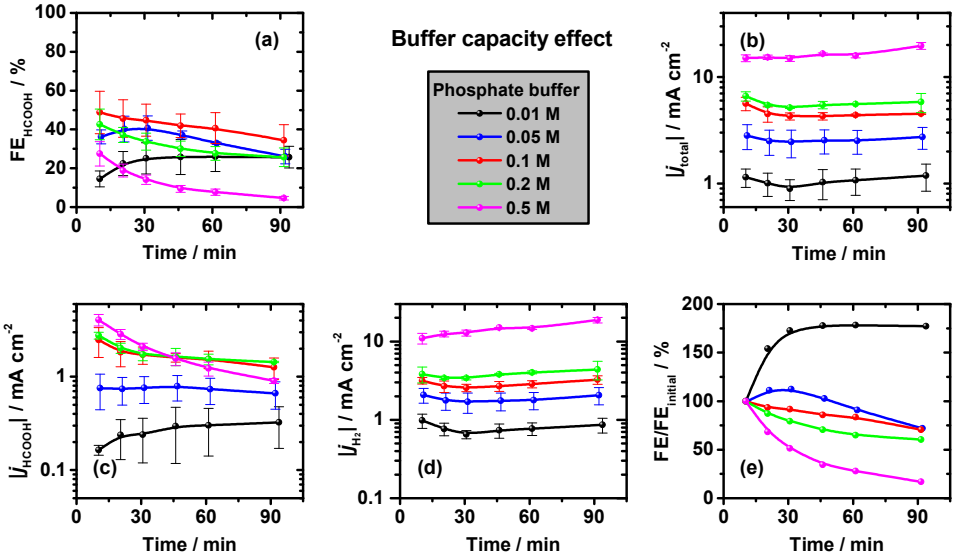

Figure D.2 (a) Faradaic efficiency toward HCOOH, (b) absolute total current density, (c) absolute partial current density for HCOOH, (d) absolute partial current density for H_2, (e) stability during CO_2 reduction on immobilized InPP on PG in phosphate buffers (initial pH $\approx$ 9.6) with different buffer capacity. Lines to guide the eye.

D.4 Effect of Ionic species

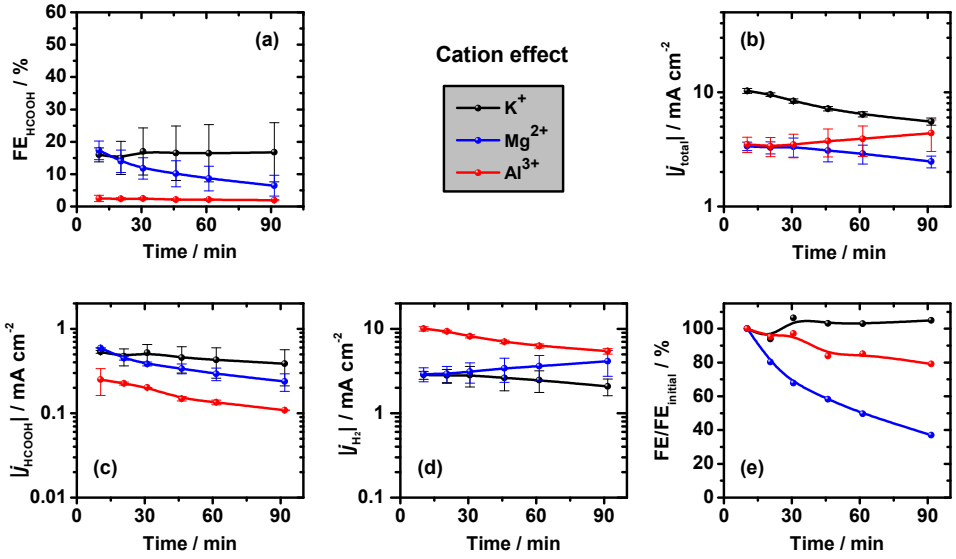

Figure D.3 (a) Faradaic efficiency toward HCOOH, (b) absolute total current density, (c) absolute partial current density for HCOOH, (d) absolute partial current density for H_2, (e) stability during CO_2 reduction on immobilized InPP on PG in 0.001 M HClO4 (pH $\approx$ 3) with 0.099 M K^+, Mg^{2+} and Al^{3+}. Lines to guide the eye.

To investigate the influence of Mg^{2+} and Al^{3+}, a $HClO_4$ electrolyte was used. It can be seen that these cations in solution worsen the selectivity, reactivity and stability of CO_2RR. The total and partial current densities corresponding to the experiments in Figure 7.4a and Figure 7.4b are given in respectively Figures D.4 and Figure D.5.

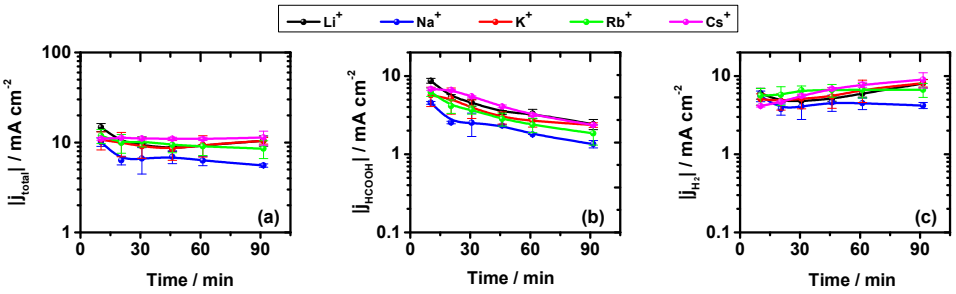

Figure D.4 (a) absolute total current density, (b) absolute partial current density for HCOOH, (c) absolute partial current density for H_2 during CO_2 reduction on immobilized InPP on PG in phosphate buffer (pH 9.6) with 25 μM alkali cations in solution. Lines to guide the eye.

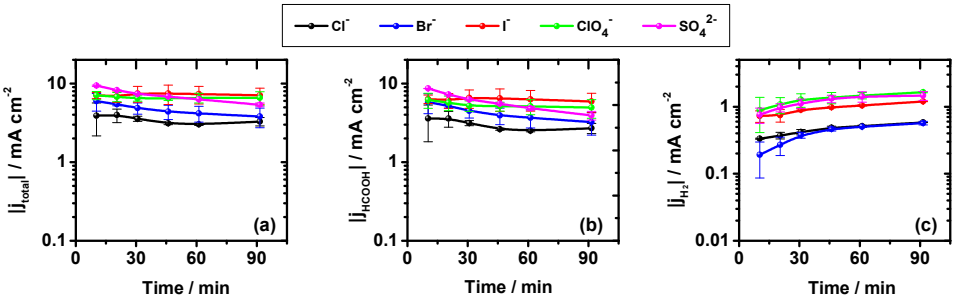

Figure D.5 (a) absolute total current density, (b) absolute partial current density for HCOOH, (c) absolute partial current density for H_2 during CO_2 reduction on immobilized InPP on PG in 0.1 M KX electrolyte brought to pH $\approx$ 9.6, where X stands for different anions. Lines to guide the eye.

D.5 References

[1] Y. Y. Birdja, J. Shen, M. T. M. Koper, *Catal. Today* **2017**, *288*, 37–47.

[2] Y. Y. Birdja, R. E. Vos, T. A. Wezendonk, L. Jiang, F. Kapteijn, M. T. M. Koper, *ACS Catal.* **under revision**.

[3] Y. Kwon, M. T. M. Koper, *Anal. Chem.* **2010**, *82*, 5420–5424.

List of publications

This thesis is based on the following publications:

Chapter 2

Yuvraj Y. Birdja, Elena Pérez-Gallent, Marta C. Figueiredo, Adrien Göttle, Federico Calle-Vallejo and Marc T. M. Koper
Advances and Challenges in the Electrocatalytic conversion of Carbon Dioxide to Fuels
Nat. Energy, **in preparation**

Chapter 3

Yuvraj Y. Birdja and Marc T. M. Koper
The Importance of Cannizzaro-type Reactions during Electrocatalytic Reduction of Carbon Dioxide
J. Am. Chem. Soc., **2017**, 139, 2030 - 2034

Highlighted as Editors' Choice in Science by Phil Szuromi (Febr. 23, 2017)
CO_2 reduction off base
Science, **355** (6327), 809-810

Chapter 5

Yuvraj Y. Birdja, Jing Shen and Marc T. M. Koper
Influence of the metal center of metalloprotoporphyrins on the electrocatalytic CO_2 reduction to formic acid
Catal. Today, **2017**, 288, 37 - 47

Chapter 6

Yuvraj Y. Birdja, Rafaël E. Vos, Tim A. Wezendonk, Lin Jiang, Freek Kapteijn and Marc T. M. Koper
Effects of Substrate and Polymer encapsulation on CO_2 Electroreduction by Immobilized Indium(III) protoporphyrin
ACS Catal., **under revision**

Chapter 7

Yuvraj Y. Birdja, Olha Nahorna and Marc T. M. Koper
Optimization of Electrolyte Composition for CO_2 Electroreduction on Immobilized Indium(III) protoporphyrin
Manuscript in preparation

Other publications:

Lin Jiang, Wangyang Fu, Yuvraj Y. Birdja, Marc T. M. Koper, Grégory F. Schneider
Quantum and electrochemical interplays in hydrogenated graphene
Nat. Commun., **2018**, in press

Amanda C. Garcia, Yuvraj Y. Birdja, Germano Tremiliosi-Filho and Marc T. M. Koper
Glycerol electro-oxidation on bismuth-modified platinum single crystals
J. Catal., **2017**, 346, 117-124

Amanda C. Garcia, Manuel J. Kolb, Chris van Nierop y Sanches, Jan Vos, Yuvraj Y. Birdja, Youngkook Kwon, Germano Tremiliosi-Filho and Marc T. M. Koper
Strong Impact of Platinum Surface Structure on Primary and Secondary Alcohol Oxidation during Electro-Oxidation of Glycerol
ACS Catal., **2016**, 6, 4491-4500

Jing Shen, Ruud Kortlever, Recep Kas, Yuvraj Y. Birdja, Oscar Diaz-Morales, Youngkook Kwon, Isis Ledezma-Yanez, Klaas Jan P. Schouten, Guido Mul and Marc T. M. Koper
Electrocatalytic reduction of carbon dioxide to carbon monoxide and methane at an immobilized cobalt protoporphyrin
Nat. Commun., **2015**, 6, 8177

Jing Shen, Yuvraj Y. Birdja and Marc T. M. Koper
Electrocatalytic Nitrate Reduction by a Cobalt Protoporphyrin Immobilized on a Pyrolytic Graphite Electrode
Langmuir, **2015**, 31, 8495-8501

Youngkook Kwon, Yuvraj Y. Birdja, Saeed Raoufmoghaddam and Marc T. M. Koper
Electrocatalytic Hydrogenation of 5-Hydroxymethylfurfural in Acidic Solution
ChemSusChem, **2015**, 8, 1745-1751

Y. Y. Birdja, J. Yang and M.T.M. Koper
Electrocatalytic Reduction of Nitrate on Tin-modified Palladium
Electrochim. Acta, **2014**, 140, 518-524

Youngkook Kwon, Yuvraj Birdja, Ioannis Spanos, Paramaconi Rodriguez, Marc T. M. Koper
Highly Selective Electro-Oxidation of Glycerol to Dihydroxyacetone on Platinum in the Presence of Bismuth
ACS Catal., **2012**, 2, 759-764

Curriculum Vitae

Yuvraj Birdja was born in Voorburg, the Netherlands and grew up in Paramaribo, Suriname, where he attended the Algemene Middelbare School (AMS). After graduation from the AMS as nationwide most succesful student in 2006, Yuvraj came to the Netherlands for his higher education, and started with the bachelor program Mechanical Engineering at the TU Delft. Due to his interest in chemistry, but the absence hereof in the Mechanical Engineering curriculum, Yuvraj decided to start with the bachelor program Molecular Science & Technology at TU Delft and Leiden University in 2007. Throughout this period as bachelor student, Yuvraj was a member of TopTrack (Honours program community of the faculty 3mE, TU Delft).

After obtaining the Bachelor of Science degree in Mechanical Engineering and Molecular Science & Technology, Yuvraj continued with the respective master programs Mechanical Engineering at the TU Delft, and Chemistry at the Leiden University. As part of the master curriculum Chemistry, Yuvraj did a research internship in the Electrochemical Energy Lab at Massachusetts Institute of Technology, USA, where he worked on lithium-air batteries under supervision of prof. Yang Shao-Horn. Back in the Netherlands, he started his M.Sc. thesis project Mechanical Engineering under supervision of prof. dr. ir. Christian Poelma and prof. dr. ir. Jerry Westerweel at the Laboratory for Aero- and Hydrodynamics, TU Delft. In 2012, Yuvraj graduated as mechanical engineer from TU Delft after he succesfully defended his thesis *Laminar to Turbulent Transition in Pulsatile Flow of non-Newtonian Fluids*. Yuvraj was selected by the TU Delft, and afterwards nominated by the jury, for the ECHO award, which is an award for succesfull students with non-western roots, who distinguish themselves by excellent performance and social involvement. After finishing the master mechanical engineering at TU Delft, Yuvraj started his master thesis project in the group Catalysis and Surface Chemistry of prof. dr. Marc Koper, under supervision of dr. Jian Yang, entitled *Electrocatalytic Nitrate Reduction on Tin-modified Palladium Electrodes*. After finishing the master program chemistry, Yuvraj pursued his PhD with prof. dr. Marc Koper as supervisor, where he worked on the electrocatalytic reduction of carbon dioxide. The results of this work are presented in this dissertation.

During his time as PhD candidate, Yuvraj did a research internship in the group of prof. dr. Marc Robert at the Laboratoire d'Electrochimie Moléculaire,

Université Paris Diderot, France, where he expanded his knowledge on experimental molecular electrocatalysis of CO_2 reduction, particularly in aprotic solvents. Moreover, Yuvraj collaborated with Lin Jiang, M.Sc. and dr. Grégory Schneider on the electrochemistry of graphene. Yuvraj supervised several bachelor students, one master student, practical chemistry courses (PBV - 1^{st} year bachelor) and chemistry working classes (FCK - 2^{nd} year bachelor). He has presented (parts of) his work at several (inter)national conferences and summer schools:

- Annual Meeting of the International Society of Electrochemistry, 2017, Providence, USA - *oral and poster presentation (the poster presentation was awarded the best poster prize of symposium "physical & interfacial electrochemistry")*
- the Netherlands' Catalysis and Chemistry Conference, 2017, Noordwijkerhout, the Netherlands - *oral presentation*
- International Summer School on CO_2 conversion; From fundamentals towards Applications, 2016, Switzerland - *poster presentation*
- Annual Meeting of the International Society of Electrochemistry 2016, The Hague, The Netherlands - *2 poster presentations*
- Summer school: Reactivity of nanoparticles for more efficient and sustainable energy conversion III; rising technologies, 2014, Denmark - *poster presentation*
- Summer school: Advanced Metal-Organic Chemistry and Catalysis, 2014, Deurne, the Netherlands - *poster presentation*